REPORT NO.
UCD/CGM-94/02

CENTER FOR GEOTECHNICAL MODELING

THREE-DIMENSIONAL DYNAMIC RESPONSE ANALYSES OF COGSWELL DAM DURING THE 1991 SIERRA MADRE AND 1987 WHITTIER NARROWS EARTHQUAKES

BY

ROSS W. BOULANGER
SCOTT M. MERRY
JONATHAN D. BRAY
LELIO H. MEJIA

The contents of this report were developed under contract No. 1091-352 from the California Department of Conservation, Division of Mines and Geology, Strong Motion Instrumentation Program. However, these contents do not necessarily represent the policy of that agency nor endorsement by the State government.

DEPARTMENT OF CIVIL & ENVIRONMENTAL ENGINEERING
COLLEGE OF ENGINEERING
UNIVERSITY OF CALIFORNIA AT DAVIS

NOVEMBER 1994

THREE-DIMENSIONAL DYNAMIC RESPONSE ANALYSES OF COGSWELL DAM DURING THE 1991 SIERRA MADRE AND 1987 WHITTIER NARROWS EARTHQUAKES

by

Ross W. Boulanger, Scott M. Merry, Jonathan D. Bray, and Lelio H. Mejia

The contents of this report were developed under contract No. 1091-352 from the California Department of Conservation, Division of Mines and Geology, Strong Motion Instrumentation Program. However, these contents do not necessarily represent the policy of that agency nor endorsement by the State government.

Report No. UCD/CGM-94/04

Center for Geotechnical Modeling
Department of Civil & Environmental Engineering
University of California
Davis, California

November 1994

ABSTRACT

The recorded strong motions at Cogswell Dam during the 1991 Sierra Madre and 1987 Whittier Narrows earthquakes provide a valuable opportunity to evaluate the applicability of established engineering procedures for evaluating the dynamic response characteristics of dams with highly three-dimensional geometries. In addition, these records provide an opportunity to back-calculate the dynamic properties of the rockfill, which cannot easily be measured in the laboratory or insitu. Peak transverse crest accelerations of 0.15 g and 0.42 g were recorded during the Whittier Narrows and Sierra Madre earthquakes, respectively, and thus the records cover a range of induced shear strains.

The present study begins with a review of the dam's history, construction, materials, and response to past earthquake events. Two-dimensional (2-D) and three-dimensional (3-D) dynamic response analyses were performed using established engineering procedures. The calculated 2-D and 3-D dynamic responses were compared to the recorded responses, and to the results of prior 3-D dynamic response analysis studies. The influence of dam-canyon interaction and topographic effects on the seismic response of the dam are evaluated and discussed. The observed permanent deformations are compared to the results of seismically-induced permanent deformation analyses commonly used in engineering practice. Estimates of the dynamic rockfill properties are presented based on the comparisons of calculated and recorded responses. Conclusions are presented regarding the applicability of the dynamic response analysis procedures used in practice, and a recommendation is made for modifying the strong motion instrumentation at the dam.

ACKNOWLEDGEMENTS

This research project was supported by the California Department of Conservation, Division of Mines and Geology, Strong Motion Instrumentation Program, Contract 1091-352. However, these contents do not necessarily represent the policy of that agency nor endorsement by the Sate government. Additional financial support for this project was partially provided by Woodward-Clyde Consultants and the National Science Foundation under Grant No. BCS-9157083. The U. C. San Diego Supercomputer Center provided the computer time for this project. All of this support is greatly appreciated. The authors would like to thank Mr. Robert Kroll of the Los Angeles County Department of Public Works for his assistance and discussions regarding the history of the dam and its recent performance.

TABLE OF CONTENTS

1. INTRODUCTION

The recorded responses of earth and rockfill dams during earthquake loading provide field evidence against which the profession can check the applicability of the analytical procedures used to evaluate the seismic performance of these structures. In the case of rockfill dams, field response records are particularly valuable as they provide an opportunity to back-calculate the dynamic rockfill properties which unlike sands, cannot easily be measured in the laboratory or insitu. Thus, the recorded response of Cogswell Dam by the State of California, Strong Motion Instrumentation Program (SMIP) during the 1987 Whittier Narrows and 1991 Sierra Madre earthquakes provide a valuable opportunity to investigate the dynamic properties of rockfill and to evaluate the applicability of present engineering dynamic response analysis procedures.

Cogswell Dam is a concrete-faced, dumped rockfill dam founded on bedrock in a narrow V-shaped canyon. The dam has a maximum height above bedrock of about 85 m and a crest length of about 175 m, giving the dam a crest length-to-height ratio of only 2.1. Photos 1-1 and 1-2 show views of the upstream and downstream faces of the dam, respectively. The dam is located approximately 32 km north of Whittier, California, in the San Gabriel Mountains on the West Fork of the San Gabriel River (Fig. 1-1).

The strong motion records from the 1987 Whittier Narrows (M_L=5.9) and 1991 Sierra Madre (M_L=5.8) earthquakes indicate that maximum horizontal accelerations at the crest of the dam were about 0.15 g and 0.49 g for these two events, respectively. Records of the earthquake motions were obtained by seismographs located at the center and right side of the dam crest, and on the right abutment above the dam crest as indicated on the plan view in Fig. 1-2.

A previous study of the dynamic response of Cogswell Dam was performed using the strong motion data from the 1987 Whittier Narrows Earthquake (Seed et al., 1989; Boulanger et al., 1993). This previous study evaluated the applicability of two-dimensional (2-D) dynamic analysis

Photo 1-1: Upstream Face of Cogswell Dam

Photo 1-2: Downstream Face of Cogswell Dam

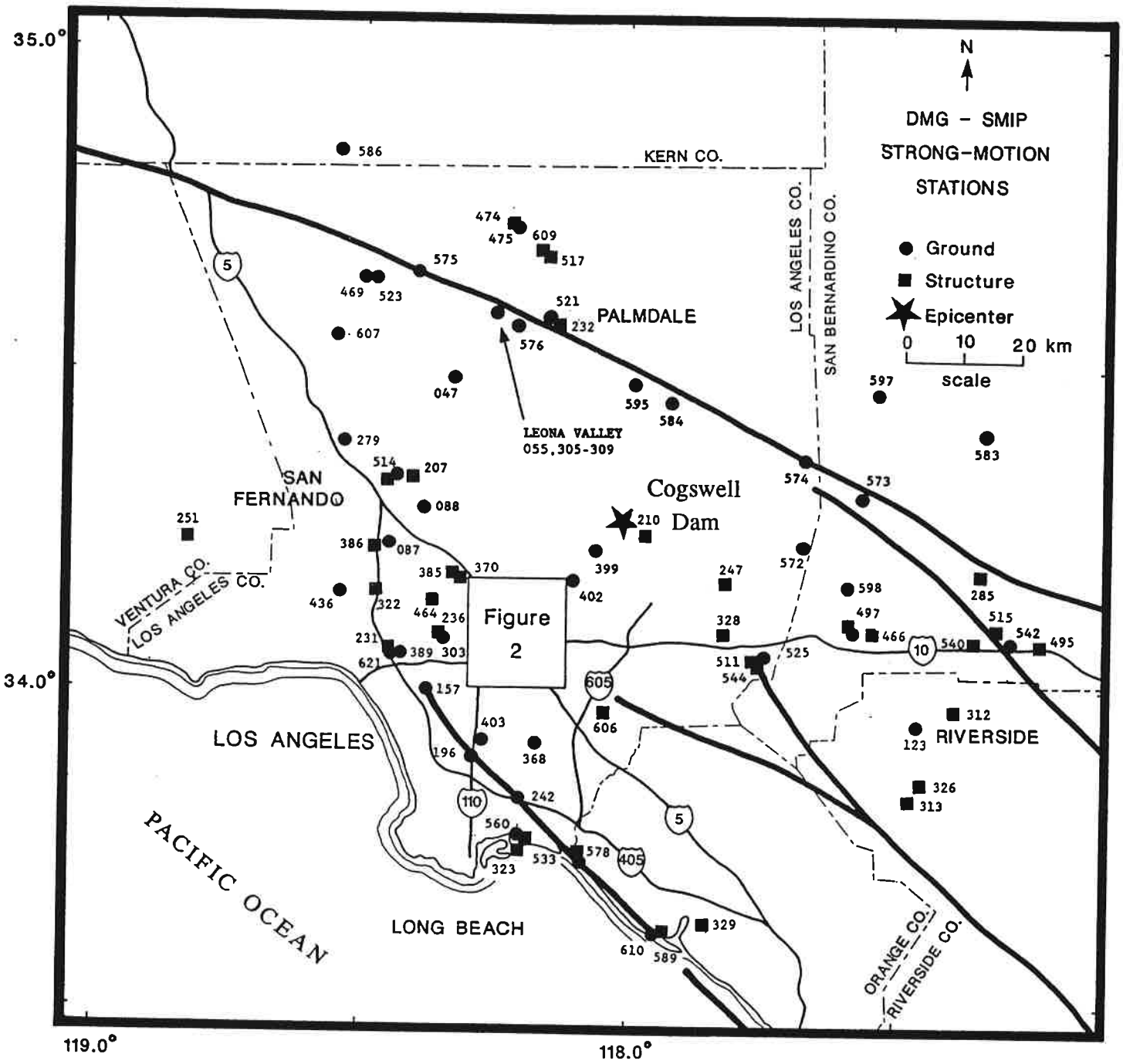

Fig. 1-1: Location of Cogswell Dam (SMIP Station 210) and Other SMIP Stations That Recorded the 1991 Sierra Madre Earthquake (after Huang et al. 1991)

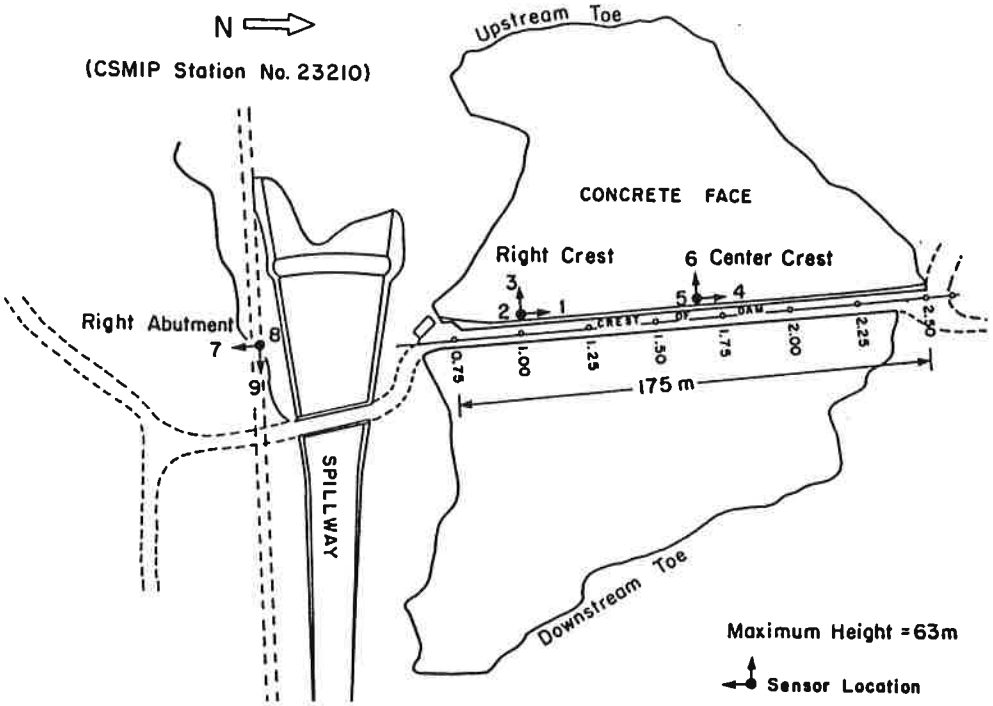

(a) Whittier Narrows Earthquake

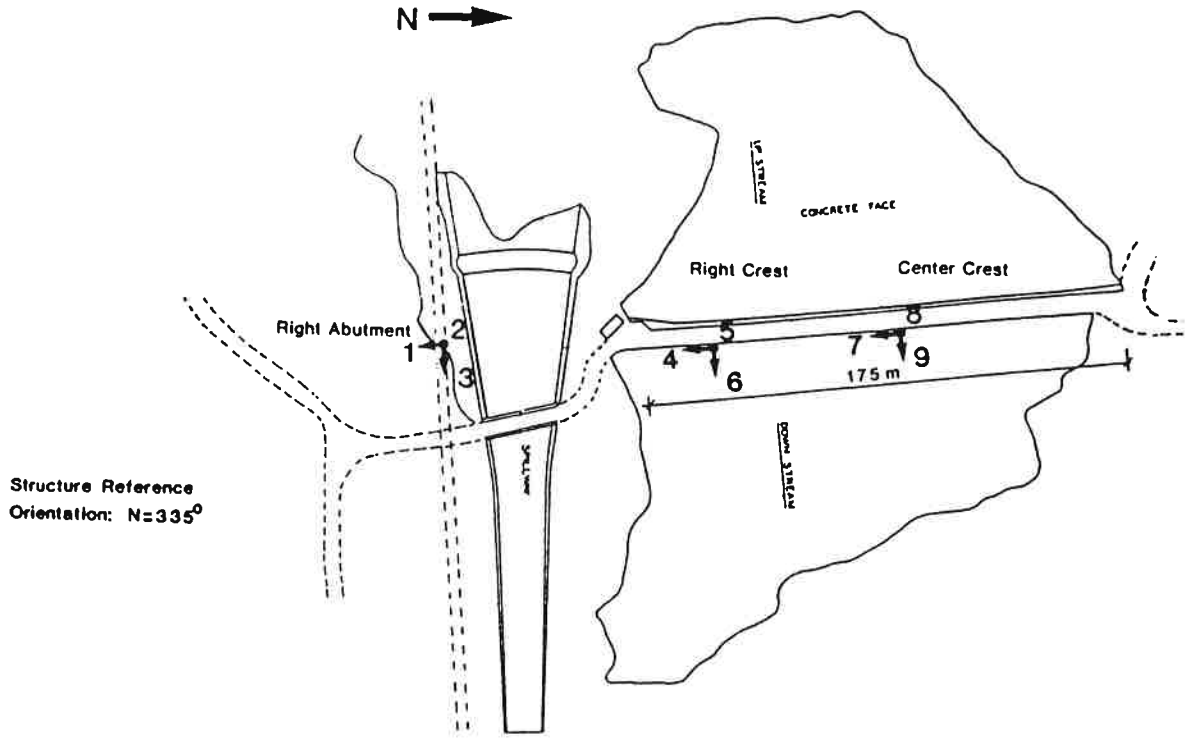

(b) Sierra Madre Earthquake

Fig. 1-2: Plan Views of Cogswell Dam Showing Instrument Locations and Station Numbering (after Huang et al. 1991)

procedures, and found that the 2-D dynamic analysis procedures consistently overestimated the observed response at the dam's crest. One of the possible explanations for the overestimation may have been the inherent difficulties in 2-D modeling of such a highly three-dimensional (3-D) dam geometry. In fact, this previous study relied on a correction for geometric effects (Mejia and Seed 1983) to estimate the insitu dynamic properties of the rockfill.

The recorded motions from the Sierra Madre Earthquake provide another opportunity to study the applicability of dynamic response procedures and investigate the dynamic properties of the rockfill. The present study, however, includes an evaluation of both 2-D and 3-D dynamic analysis procedures in view of the previous study's findings. Specifically, the present study attempts to evaluate the accuracy of established 2-D and 3-D dynamic analysis procedures by comparing the calculated and recorded dynamic responses, and to estimate the actual insitu dynamic properties of the rockfill over a range of earthquake-induced shear strains using both the 2-D and 3-D analysis results.

The observed permanent deformations during these earthquakes are compared to results obtained using common engineering procedures for estimating seismically-induced permanent deformations. The applicability of these permanent deformation analyses is discussed.

The present report is organized as follows. Chapter Two presents a description of Cogswell Dam and relevant aspects of its history. Chapter Three presents a description of the observed response of Cogswell Dam to earthquake loading, including a review of overall behavior and the processed strong motion data. Chapter Four presents a description of the dynamic response analysis procedures used and the results of the dynamic response analyses. Chapter Five presents the discussion and interpretation of the results of the dynamic response analyses. Chapter Six presents a discussion of the applicability of seismically-induced permanent deformation analyses. Chapter Seven summarizes the overall conclusions and recommendations of this study.

2. DESCRIPTION OF COGSWELL DAM

Information and data on the embankment and foundation materials were obtained from previous engineering studies, safety reviews, and construction records for the dam from the files maintained by the Division of Safety of Dams, State of California and from the Los Angeles County Flood Control District (LACFD), who owns and operates the dam. Recent summaries of these data are contained in reports by the LACFD (1980) and the State of California (1986).

Cogswell Dam, formerly San Gabriel Dam No. 2, is located approximately 32 km north of Whittier, California, in the San Gabriel Mountains on the West Fork of the San Gabriel River. The dam is a concrete-faced, dumped rockfill dam founded on bedrock in a narrow V-shaped canyon, as shown by the plan view in Fig. 1-2 and the cross-sections in Fig. 2-1. The dam has a maximum height above bedrock of 85 m and a crest length of 175 m, for a crest length-to-height ratio of only 2.1:1. The upstream face has a slope of 1.25:1 (H:V) near the crest, flattening slightly to 1.35:1 near the toe. The downstream face has a slightly flatter slope, beginning at 1.30:1 near the crest and flattening to 1.6:1 at the toe. The 5.5-m wide crest is covered by a recently completed (March 1991) reinforced concrete structure that includes a parapet wall with a uniform top elevation of 735.2 m (2412 feet) above mean sea level. The open ogee section spillway (crest elevation of 726.9 m) and outlet works are both located on the right abutment. The dam retains Cogswell Reservoir, with a capacity of about 12×10^6 m^3, for the purposes of flood control and water conservation. Construction of the dam was partially completed in April, 1934, and fully completed in 1948 when the permanent concrete facing was installed.

Cogswell Dam was constructed as a largely homogenous dumped-rockfill, with a total rockfill volume of about 0.8×10^6 m^3. Three classes of rockfill were specified in construction of the dam, as shown in Fig. 2-1. Class "A" rockfill comprises the main body of the dam and was a well graded mixture with the following specifications by weight: 40% from quarry chips to 450 kg; 30% between

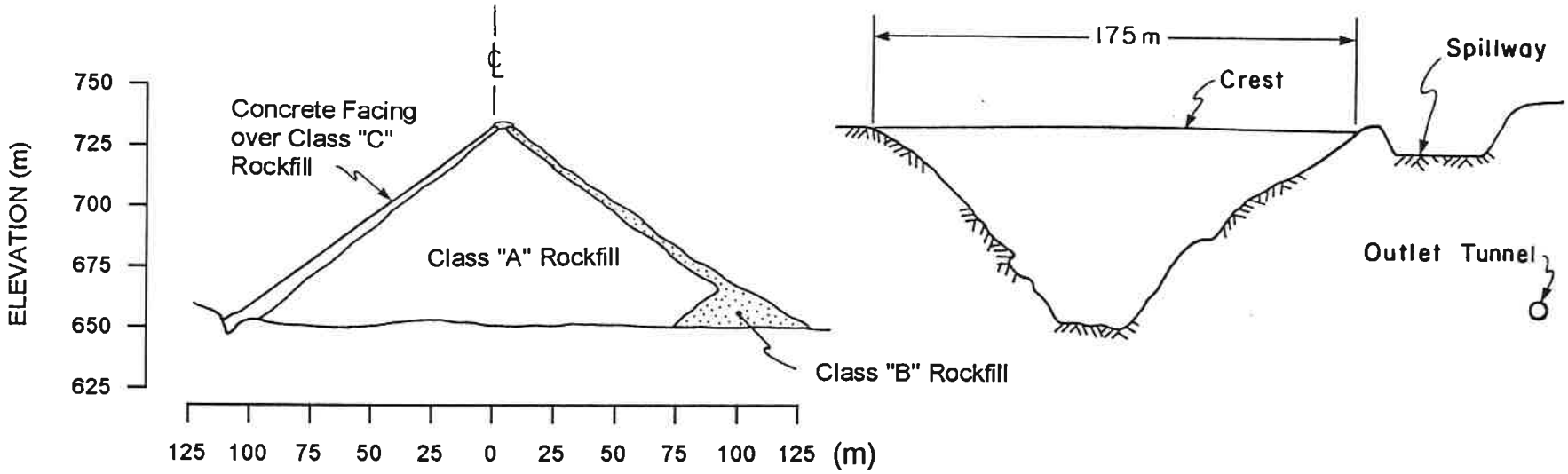

Figure 2-1: Transverse and Longitudinal Cross-Sections of Cogswell Dam

450 kg and 1,350 kg; 30% between 1,350 kg and 6,400 kg; and no more than 3% quarry dust. Class "B" rockfill was used to place both a 15-m high downstream toe and a downstream facing layer varying from 2.4-m thick at the crest to 3.7-m thick at the toe. Class "B" rockfill was a heavier specification, with one-half to exceed 6,400 kg in weight. Class "C" rockfill was used to place an upstream facing layer varying from 1.8-m thick at the crest to 4.6-m thick at the toe. Class "C" rockfill ranged from quarry chips to 6,400 kg and was to be derrick placed to the maximum possible density.

All rockfill material consisted of granitic rock obtained from a quarry located in Devil's Canyon, which is approximately 2.4 km upstream of the left abutment. The quarried rock was to be sound, hard, durable, and unaffected by air and moisture. Compression tests on 211 representative samples from the quarry indicated an average compressive strength of 45.7 Mpa (6,630 psi) and an average unit weight of 27.5 kN/m^3 for intact rock specimens. Very few specimens were cut due to the absence of a cutting machine. Rock Drop tests, developed for this project, performed on 132 samples indicated an average breakdown of 5.04%, slightly above the specified allowance of 5.00%. These data suggest that the rockfill may not be as hard or durable as might be expected for a hard granitic rockfill.

The design called for the excavation of the foundation to sound bedrock and the construction of a concrete cutoff wall along the contact between the foundation and the upstream face of the dam. Preliminary excavation of both abutments was performed using a water cannon, but shattered material still remained over substantial portions of the exposed abutments. The remaining abutment excavation was performed by small hand tools in 7.6-m lifts just ahead of the placement of the rockfill. Excavation of the cutoff wall preceded rockfill placement by 15 m, with mechanical equipment being approved for this purpose. The cutoff wall was excavated into sound bedrock with a width of 1.5 m to 3.0 m and a depth of 3.7 m to 16.5 m. Unacceptable rock conditions were

encountered in the cutoff wall trench on the right abutment between elevations 681 m and 707 m (54 m to 28 m below the dam crest), which delayed placement of rockfill against the right abutment. Eventually, concrete was placed in this portion of the cutoff wall to facilitate completion of the rockfill placement. A tunnel was later driven (spring 1935) under the right abutment cutoff wall, and additional excavation with concrete replacement was performed to attain a satisfactory bedrock foundation.

A majority of the main body of the embankment was placed by dry dumping in 7.6-m lifts with no compaction or sluicing. The conventional practice of sluicing the rockfill was omitted due to the scarcity of water at the dam site. In response to the delays associated with the poor rock conditions encountered at roughly mid-height on the right abutment, rockfill placement continued against the left abutment until it was at the crest elevation. This left a roughly 50-m deep, notch-shaped, uncompleted portion of the rockfill against the right abutment. Subsequent placement of rockfill was performed by dry dumping from the completed crest level, resulting in a single lift of almost 50 m in thickness. Following completion of the entire rockfill section in the Fall of 1933, construction began on the upstream concrete facing with the intention of completing this work by the Spring of 1934.

Heavy rains in December 1933 through March 1934 wetted the fill and led to large settlements which disrupted the facing already constructed and caused significant deformations of the dam. During one particularly severe rainstorm on December 31, 1933, and January 1, 1934, 382 mm of rainfall was reported at the dam. This heavy rain effectively sluiced the rockfill and resulted in a maximum settlement of approximately 1.77 m near the right abutment, which appears to have coincided with the location of the 50 m-thick lift previously described. Throughout the following four months of rain, the total settlement of the crest was as much as 4.15 m (almost 5% of the dam's maximum height) with downstream movements of as much as 1.43 m. Prior to subsequent reshaping of the dam and construction of a temporary upstream timber facing, sluicing of the rockfill was

performed which resulted in up to 0.90 m of additional vertical settlement and 0.18 m of upstream movement. The temporary timber facing was left in place for about 10 years until settlements had essentially ceased, at which time it was replaced by a reinforced concrete panel facing consisting of a single layer of 9.14-m square slabs ranging in thickness from 0.20 m near the crest to about 0.61 m at the toe. The dam continues to settle at a progressively slower rate, with current rates being less than 5 mm per year.

The foundation rock of Cogswell Dam is predominantly light-colored (augen) gneiss intruded by numerous dikes of andesite porphyry and hornblende amphibolite and dike-like masses of granophyric granite. The largest dike was roughly 10 m thick and passes through the right abutment. Surficial weathering has reduced exposed portions of these rocks to relatively incompetent materials. During construction preparation of the dam foundation, the weakest rock was removed. The rock within the prepared dam foundation is described as significantly jointed and sheared, moderately to strongly weathered, moderately hard and moderately strong. During dam construction, the foundation was treated with 241 grout holes beneath the upstream concrete cutoff wall. Grout holes were 3 m to 45 m deep, spaced about 1.5 m apart, and had grout takes ranging from almost zero to over three sacks-per-foot, which are not very large takes given the fractured condition of the foundation. Additional grouting beneath the cutoff wall on both abutments was performed in 1962, 1964, and 1966 to reduce seepage under the dam. The borings indicate that highly fractured, moderately to strongly weathered, and locally friable rocks often extended to depths greater than 30 m, although more competent rock was encountered in two boreholes located on the mid-left abutment. Three of these borings were located in the spillway and appear to coincide with a major, subvertical shear zone which, as shown by construction records, comprises much of the spillway foundation.

3. OBSERVED RESPONSE OF COGSWELL DAM

3.1 Instrumentation and Seismic Performance

The instrumentation at Cogswell Dam includes 6 piezometers, 23 survey monuments, seven leakage measurement points, and 9 strong-motion accelerographs. The strong-motion accelerographs were installed in recent years by the State of California SMIP. As shown in Fig. 1-2, the accelerographs record transverse, vertical, and longitudinal motions at the crest center, on the right abutment, and at a point on the crest between the crest center and the right abutment. The right abutment instrument is located behind the control house situated at the top of the vertical cut slope extending up from the right side of the spillway channel. It should be noted that the accelerographs on the dam crest were temporarily removed during recent construction of a reinforced concrete parapet wall along the dam crest and upon re-installation (prior to the Sierra Madre Earthquake), were renumbered differently from the time of the Whittier Narrows Earthquake.

The only prior earthquake to produce any damage to the dam was a magnitude 5.0 earthquake on August 23, 1952 with an epicenter 37 km from the dam. This earthquake is estimated to have produced a peak ground acceleration of about 0.03 g at the dam site. This earthquake resulted in a crack in a metal expansion joint and a subsequent increase in leakage through the dam until it was repaired. The greatest prior shaking felt by Cogswell Dam is thought to be from the San Fernando (moment magnitude of 6.6) earthquake of February 9, 1971, with an epicenter 43 km west of the dam, which was estimated to have produced a peak ground acceleration of about 0.15 g at the dam site. No damage was reported and less than 8 mm of crest displacement was attributed to this event.

Since installation of the strong motion accelerographs, the strongest motions recorded at the dam were obtained during the 1987 Whittier Narrows (M_L=5.9) and 1991 Sierra Madre (M_L=5.8) earthquakes. The epicenter of the Whittier Narrows Earthquake was 29 km southwest of the dam and the epicenter of the Sierra Madre Earthquake was 4 km northwest of the dam. The piezometer

and drainage system discharge data indicate no significant effects as a result of the Whittier Narrows or Sierra Madre earthquakes. However, the reservoir was only at about elevation 691 m (43 m below the crest) at the time of the Whittier Narrows Earthquake and was nearly empty for silt removal at the time of the Sierra Madre Earthquake. Survey monument data indicates that deformations of the crest of the dam were insignificant as a result of the Whittier Narrows Earthquake and attained maximum values of 41 mm vertically and 16 mm horizontally (downstream) as a result of the Sierra Madre Earthquake. The Whittier Narrows Earthquake was not reported to have caused any damage to the dam.

The Sierra Madre Earthquake was initially reported to have only caused minor transverse hairline cracks in the crest pavement and cracks along vertical joints in the parapet wall at three locations. Subsequent detailed inspections indicated that the earthquake caused cracking of the upstream concrete facing near its juncture with the concrete cutoff walls along both abutments. The observed zones of cracking ranged from 0.6 m to 2.4 m wide and extended from just below the parapet wall to about 11 m down (vertically) on the right abutment and 5 m down on the left abutment. Maximum crack widths of 13 mm were reported while more typical crack widths were less than about 6 mm.

3.2 Recorded Motions for Whittier Narrows Earthquake

The Whittier Narrows Earthquake produced transverse peak ground accelerations at the right abutment, right crest and center crest (locations shown on Fig. 1-2) of 0.06 g, 0.10 g, and 0.15 g, respectively. The recorded acceleration time histories are presented in Figs. 3-1 through 3-3 for each of the three instrument locations. Acceleration response spectra are presented for the transverse motions in Fig. 3-4, and for the longitudinal motions in Fig. 3-5. Fourier amplification ratios from the abutment to center crest and abutment to right crest, for transverse motions, are presented in Fig. 3-6. As expected, the crest motions indicate amplification of abutment ground motions and a

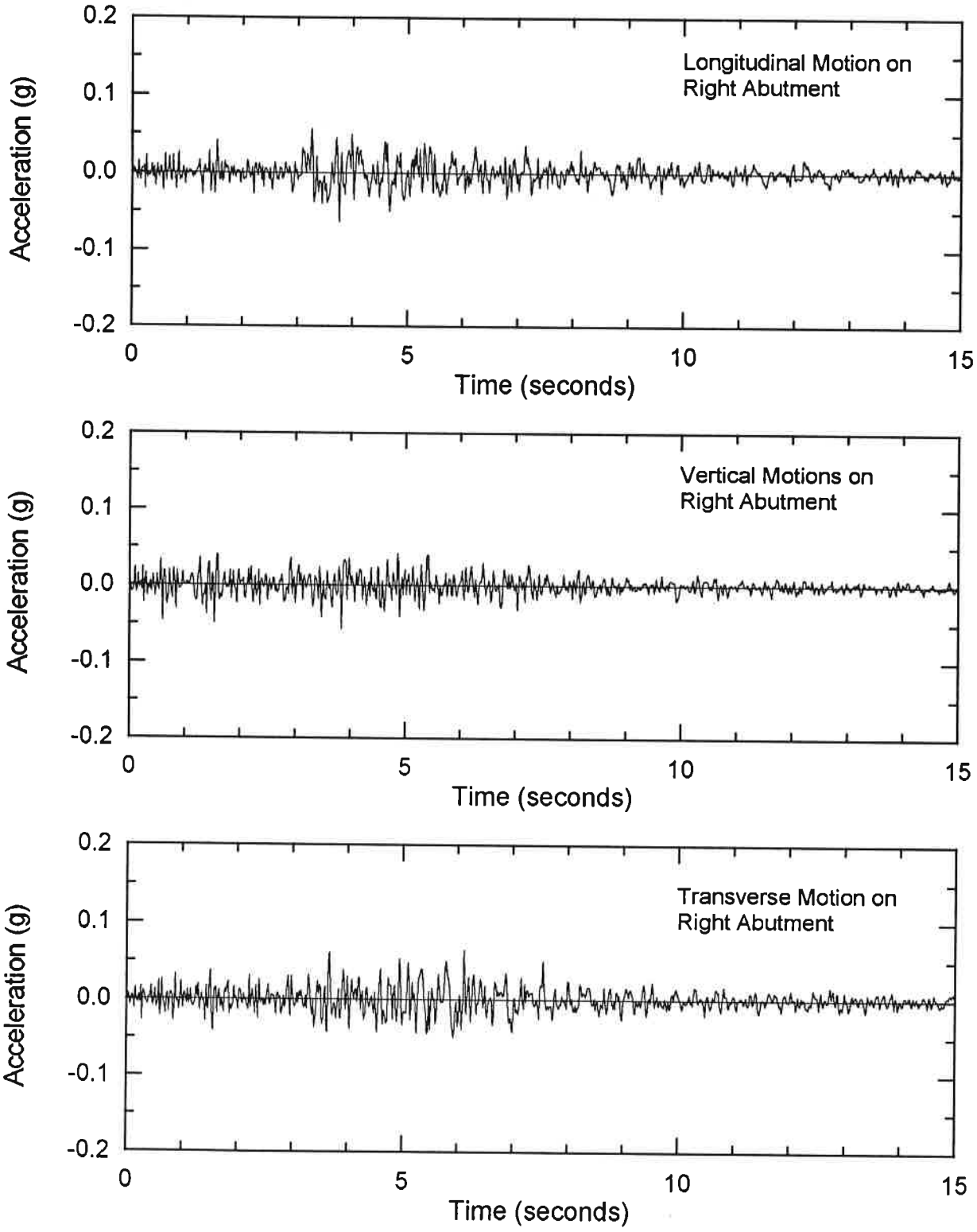

Figure 3-1: Acceleration Time Histories at the Right Abutment - Whittier Narrows Earthquake

WN789TH.GRF

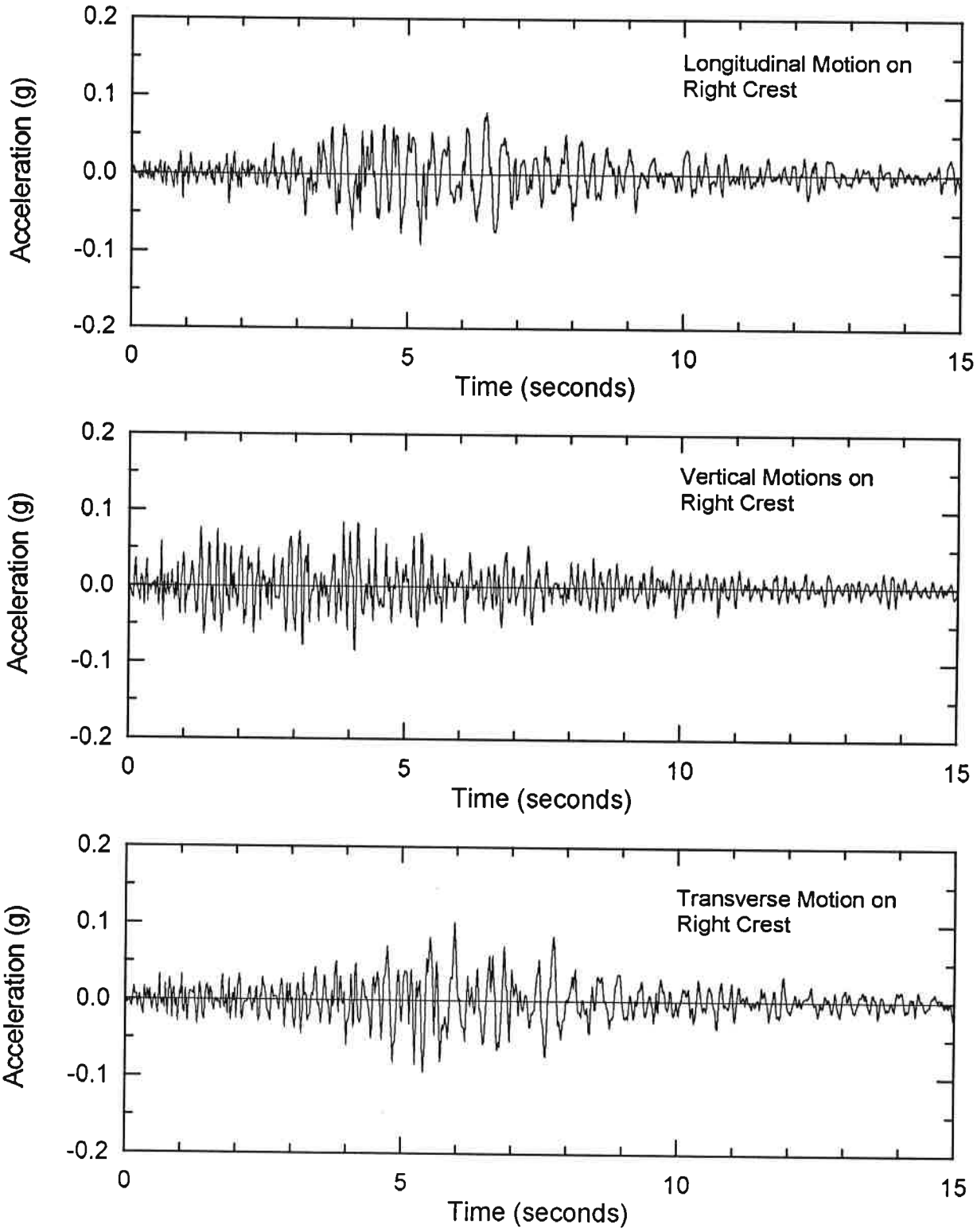

Figure 3-2: Acceleration Time Histories at the Right Crest - Whittier Narrows Earthquake

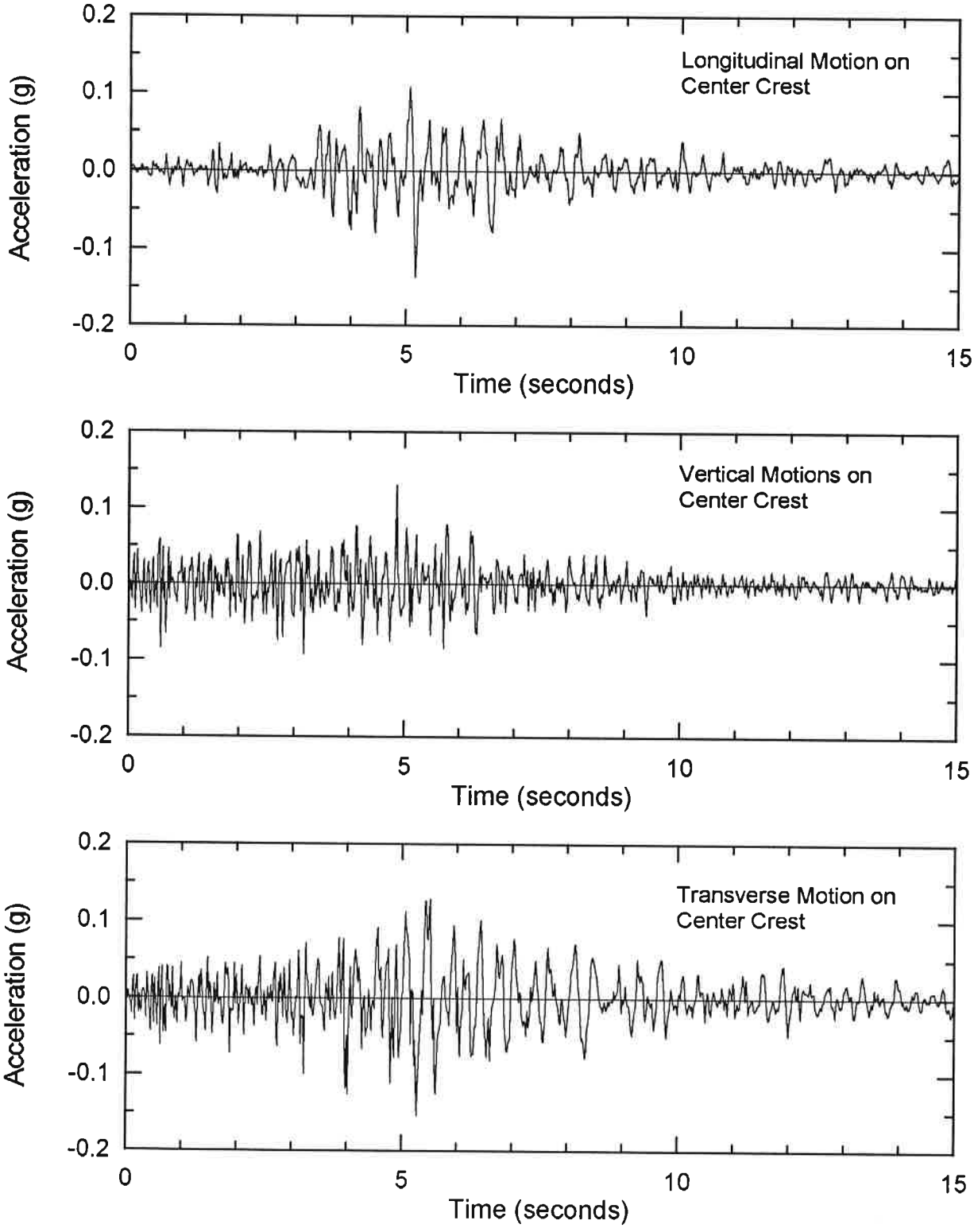

Figure 3-3: Acceleration Time Histories at the Center Crest - Whittier Narrows Earthquake

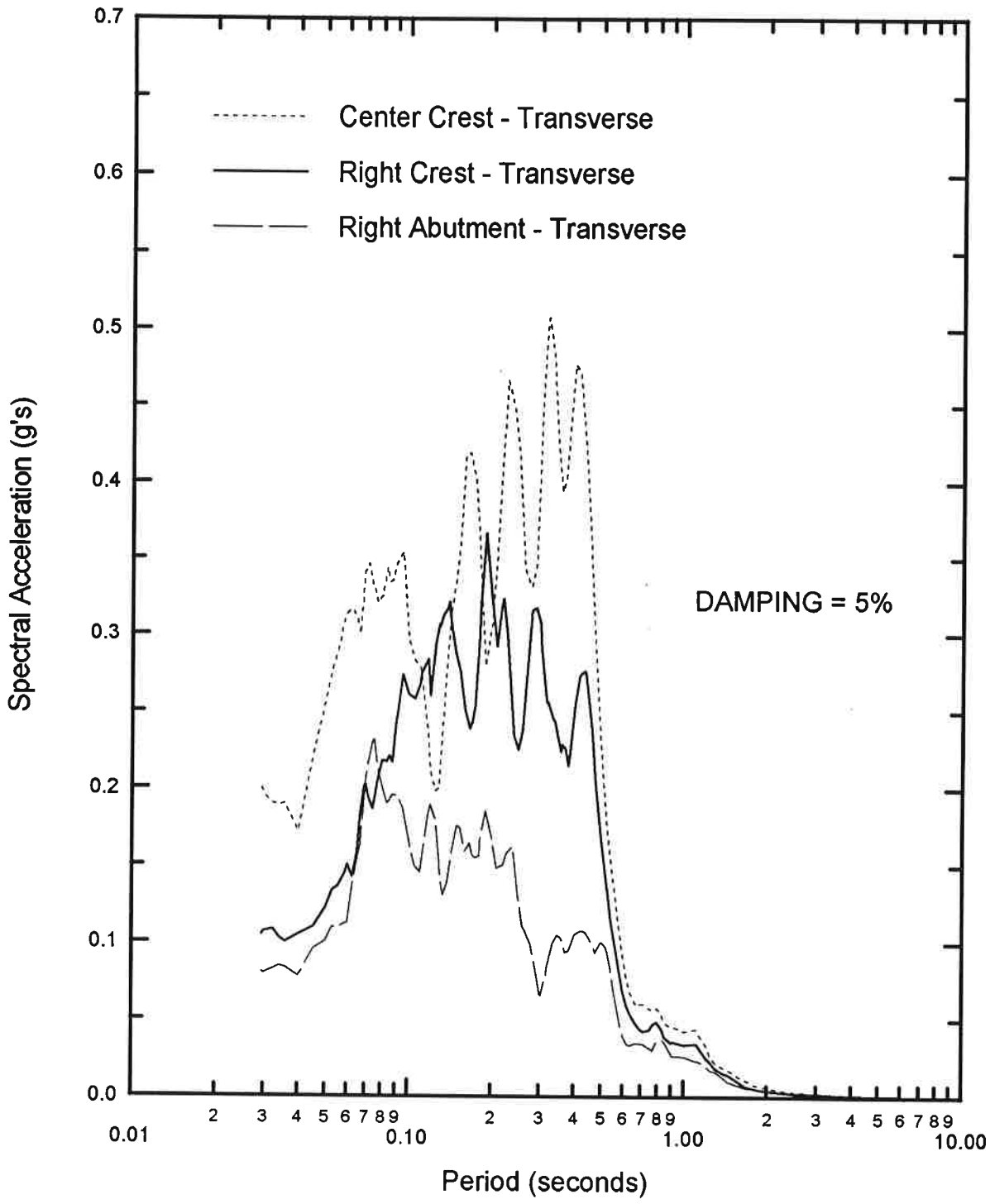

Figure 3-4: Recorded Response Spectra for Transverse Motions: Whittier Narrows Earthquake

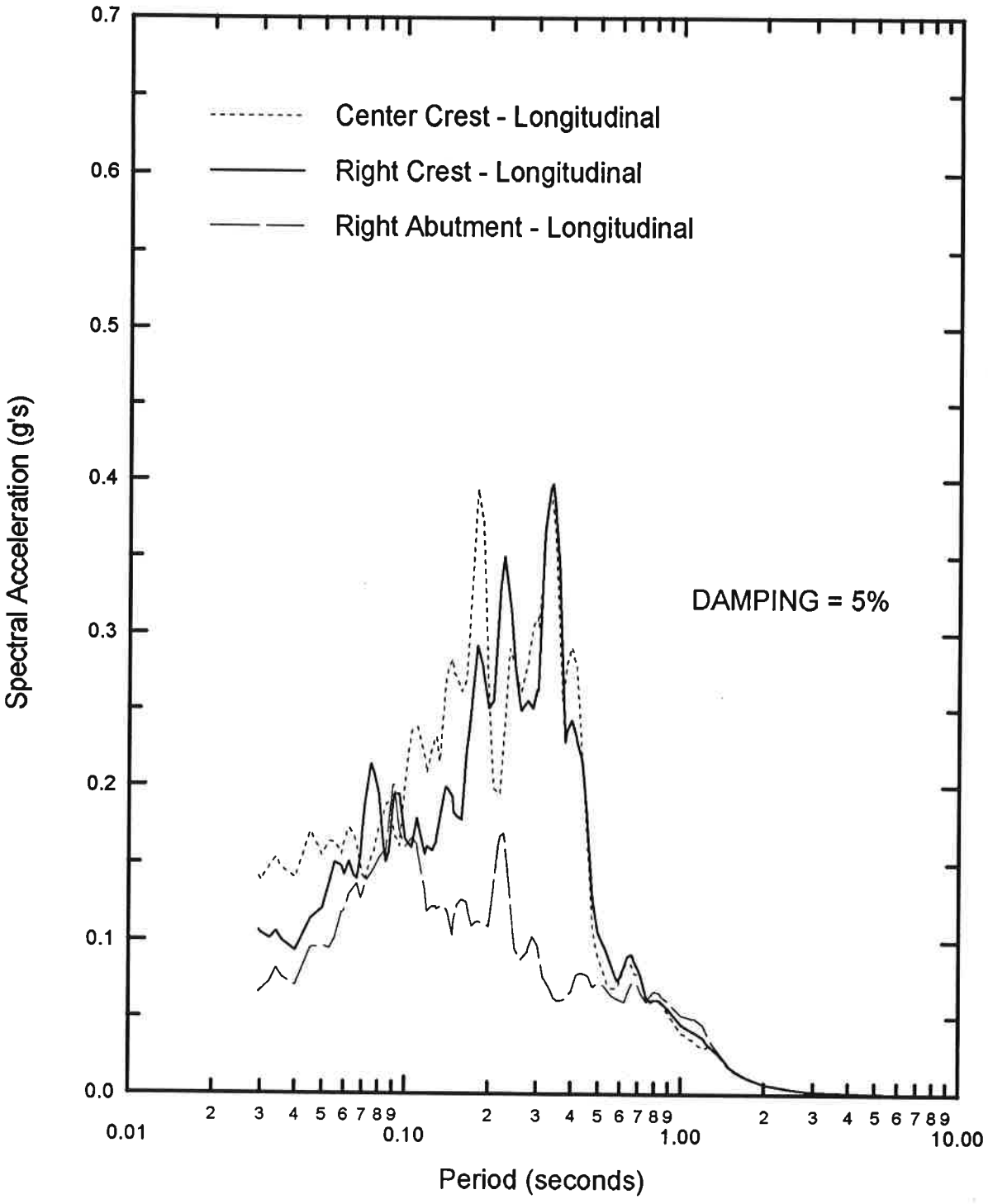

Figure 3-5: Recorded Response Spectra for Longitudinal Motions: Whittier Narrows Earthquake

SPEC147.GRF

lengthening of the motion's predominant period. A summary of the recorded maximum surface accelerations and the calculated maximum spectral accelerations is given in Table 3-1.

The observed 3-D fundamental period of the dam during the Whittier Narrows Earthquake was estimated to be between 0.37 and 0.42 seconds. A fundamental period of 0.42 seconds was indicated by the first peak in the Fourier amplification ratios from the right abutment to the center crest and right crest (Fig. 3-6). Larger Fourier amplification ratios occur at longer periods possibly because of the instruments' positions relative to the dam's mode shapes. The acceleration response spectra for the recorded crest motions (Fig. 3-4) provide a secondary check on the above estimated fundamental period in that a strong spectral acceleration would be expected near the fundamental period of the dam. Referring to Fig. 3-4, the response spectra for the recorded center crest motion has its strongest peak at 0.32 seconds with a slightly smaller peak at 0.40 seconds. As a further check, response spectra were calculated for select sections of the crest motion representing the initial period of decay, as shown in Fig. 3-7, which showed predominant peaks at about 0.37 seconds. Thus, the fundamental period of the dam during the Whittier Narrows Earthquake appears to have been between about 0.37 and 0.42 seconds.

3.3 Recorded Motions for Sierra Madre Earthquake

The Sierra Madre Earthquake produced transverse peak ground accelerations at the right abutment, right crest, and center crest of 0.26 g, 0.32 g, and 0.42 g, respectively. The recorded acceleration time histories are presented in Figs. 3-8 through 3-10 for each of the three instrument locations shown on Fig. 1-2. Response spectra are presented for the transverse motions in Fig. 3-11, and for the longitudinal motions in Fig. 3-12. Fourier amplification ratios from the abutment to center crest and abutment to right crest, for transverse motions, are presented in Fig. 3-13. As expected, the crest motions indicate amplification of abutment ground motions and a lengthening of the motion's predominant period. A summary of the recorded maximum surface accelerations and the calculated

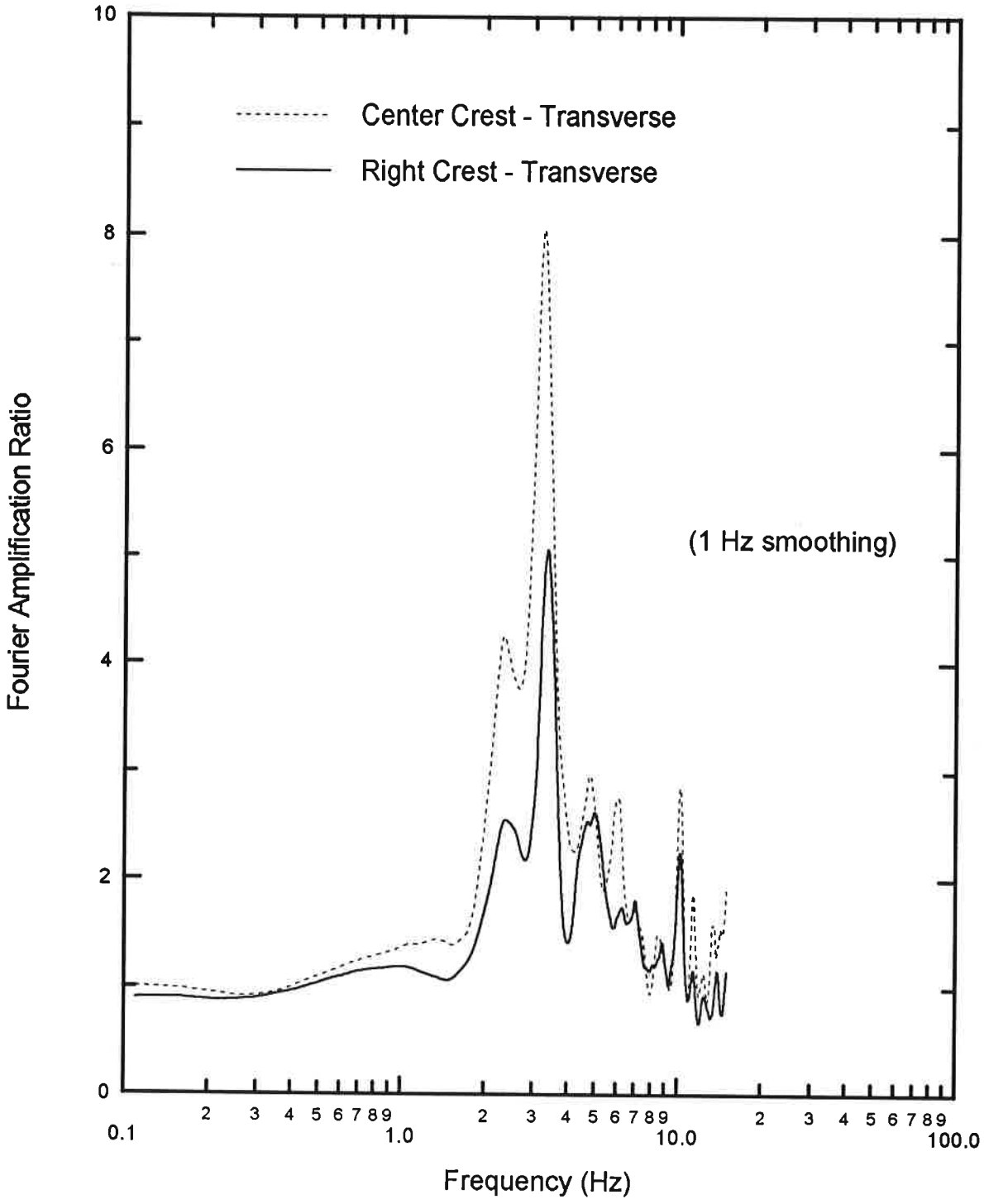

Figure 3-6: Fourier Amplification Ratios for Transverse Motions: Whittier Narrows Earthquake

samp10hz.GRF

TABLE 1. Characteristics of Earthquake Motions

Accelerograph	Component	Whittier Narrows			Sierra Madre		
		Peak Ground Accel.[1] (g)	Max. Spectral Accel.[1] (g)	Period at Max. Spectral Accel. (sec)	Peak Ground Accel.[1] (g)	Max. Spectral Accel.[1] (g)	Period at Max. Spectral Accel. (sec)
Abutment	Transverse	0.064	0.200	0.075	0.264	0.838	0.080
Right Crest	Transverse	0.100	0.367	0.190	0.318	1.082	0.227
Center Crest	Transverse	0.151	0.507	0.320	0.421	1.031	0.138
Abutment	Longitudinal	0.061	0.175	0.225	0.302	0.980	0.250
Right Crest	Longtiduinal	0.087	0.391	0.325	0.376	1.775	0.420
Center Crest	Longitudinal	0.137	0.385	0.320	0.486	1.647	0.435
Abutment	Vertical	0.06	--	--	0.227	--	--
Right Crest	Vertical	0.11	--	--	0.386	--	--
Center Crest	Vertical	0.14	--	--	0.484	--	--

[1]After baseline and instrument correction of accelerogram records.

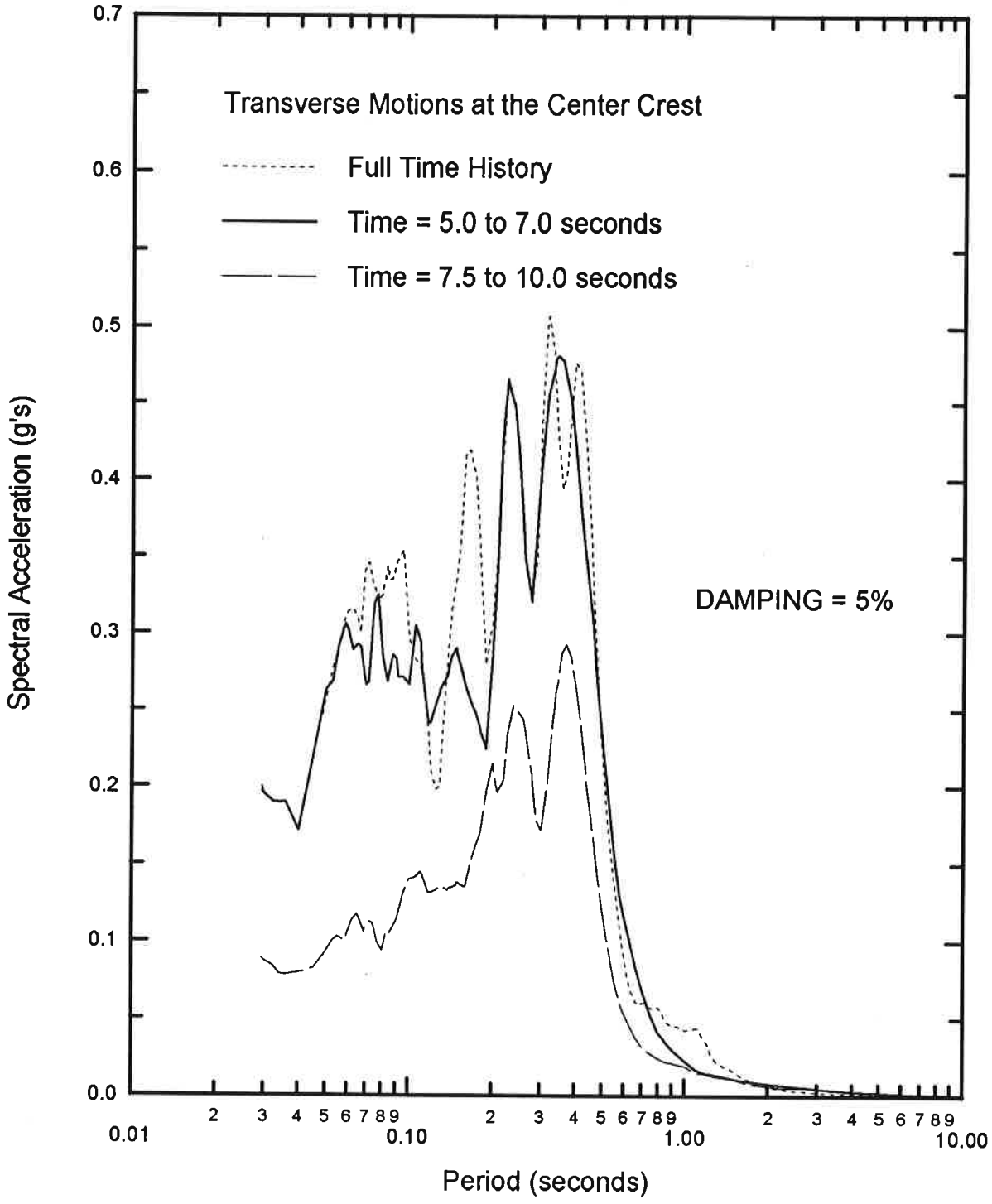

Figure 3-7: Recorded Response Spectra for Select Time Windows in the Center Crest Transverse Motions: Whittier Narrows Earthquake

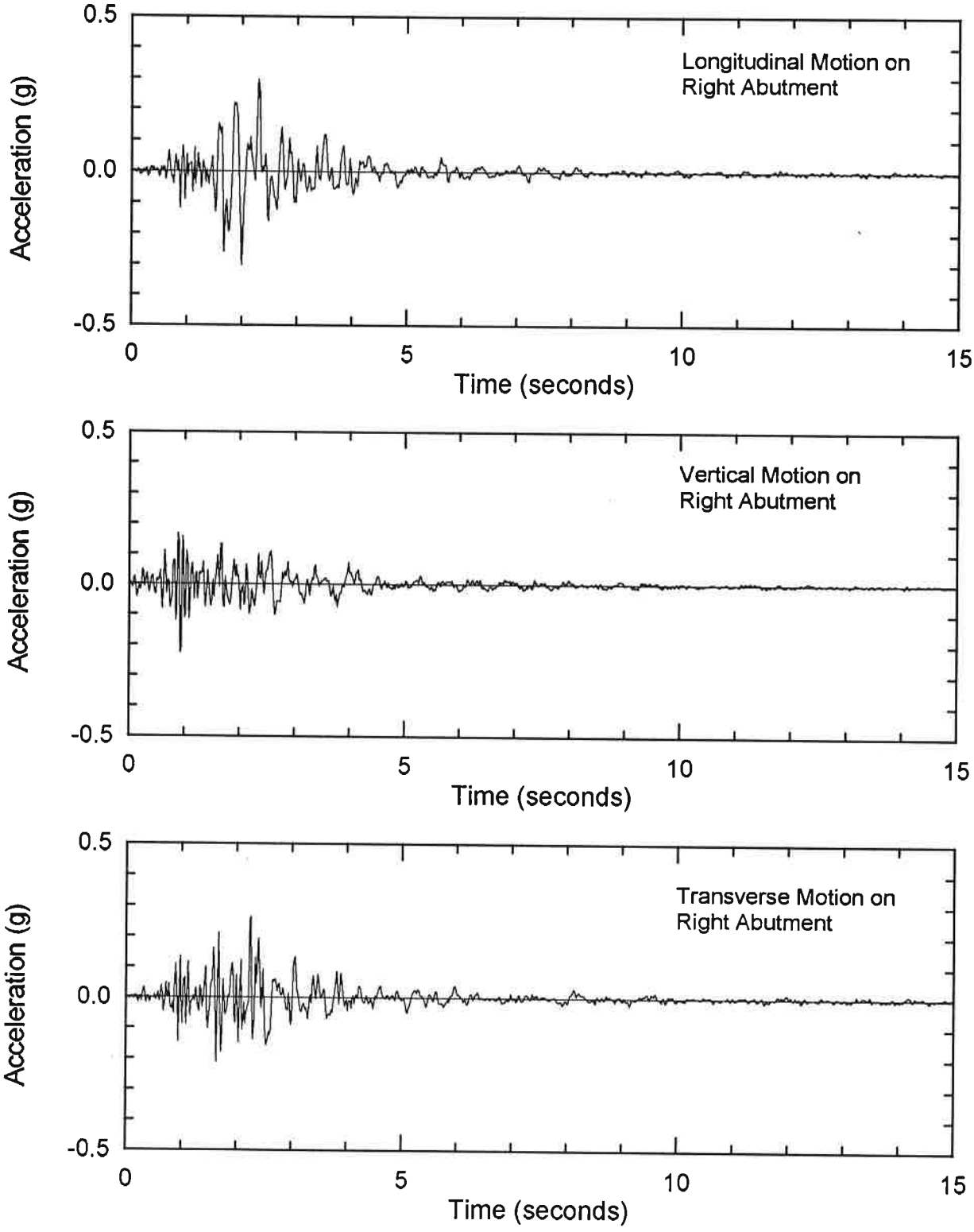

Figure 3-8: Acceleration Time Histories at the Right Abutment - Sierra Madre Earthquake

SM123TH.GRF

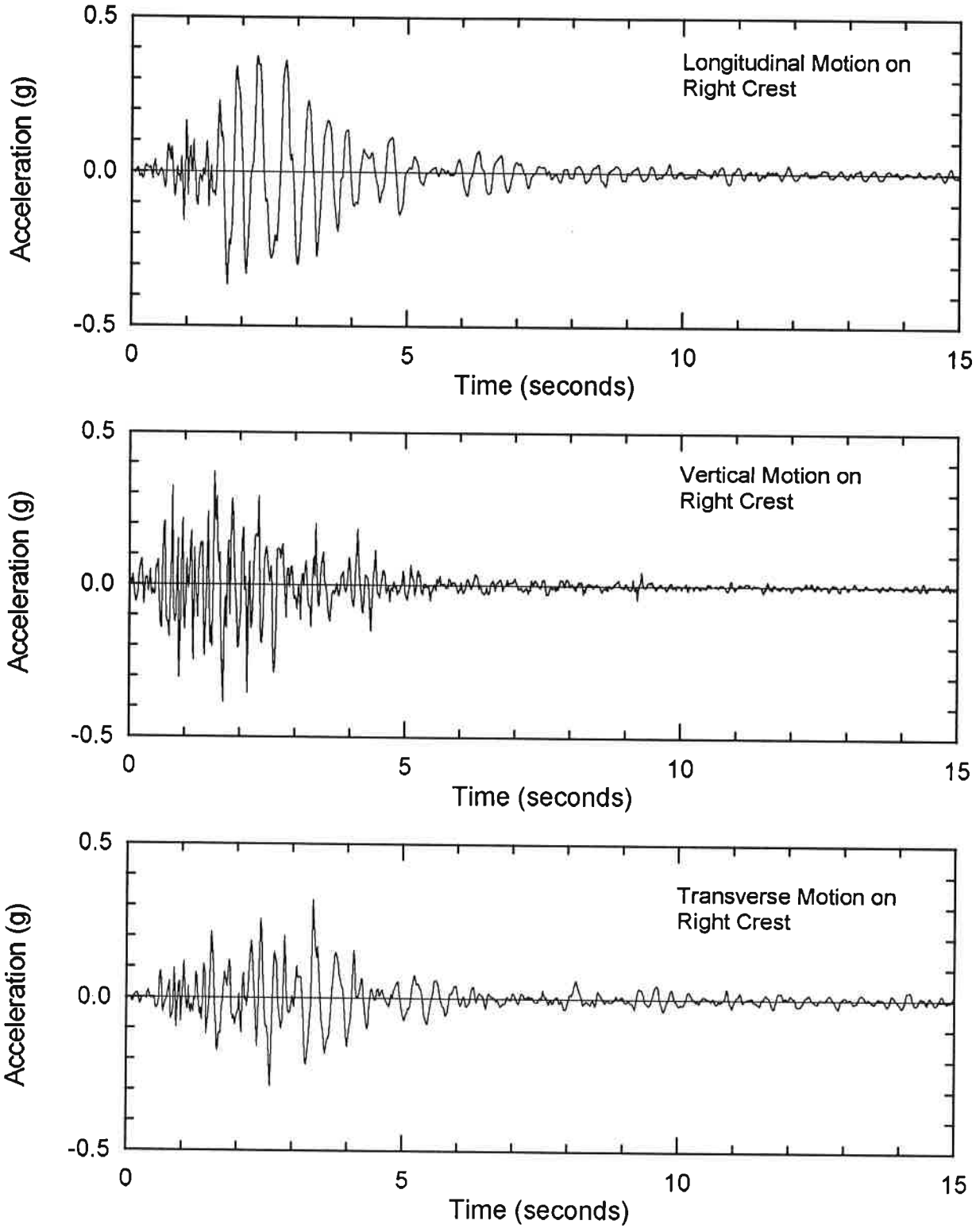

Figure 3-9: Acceleration Time Histories at the Right Crest - Sierra Madre Earthquake

SM456TH.GRF

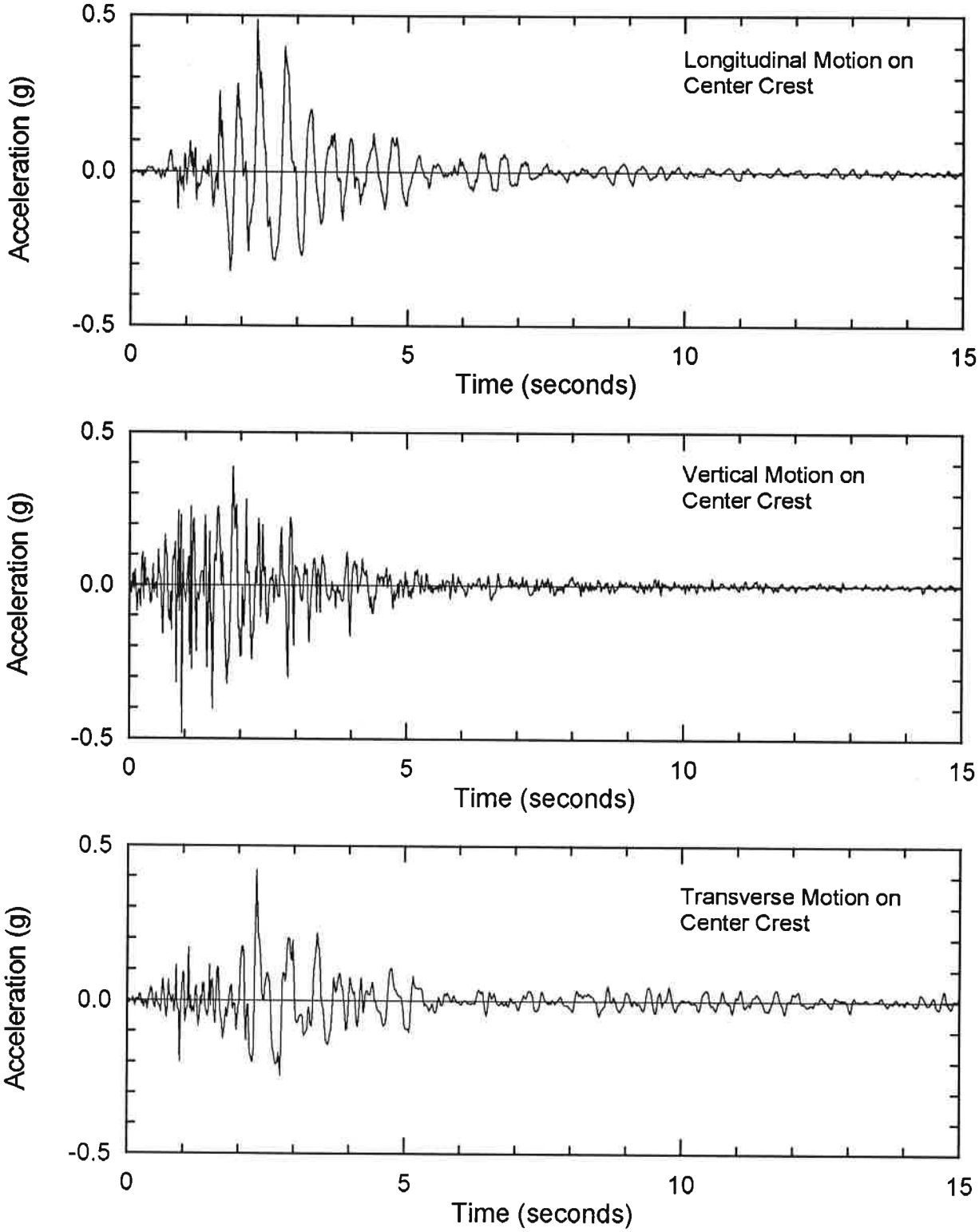

Figure 3-10: Acceleration Time Histories at the Center Crest - Sierra Madre Earthquake

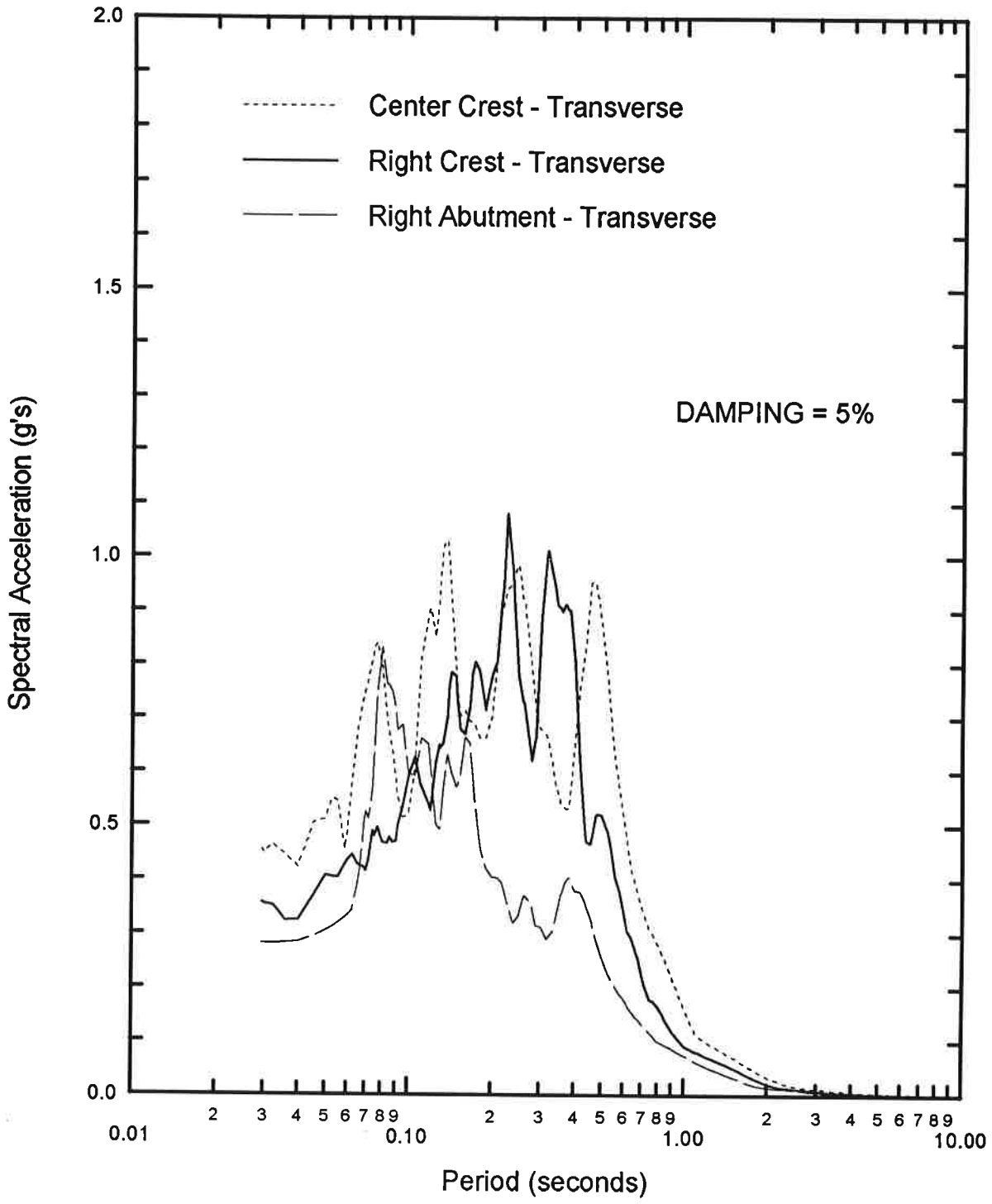

Figure 3-11: Recorded Response Spectra for Transverse Motions: Sierra Madre Earthquake

SPEC963.GRF

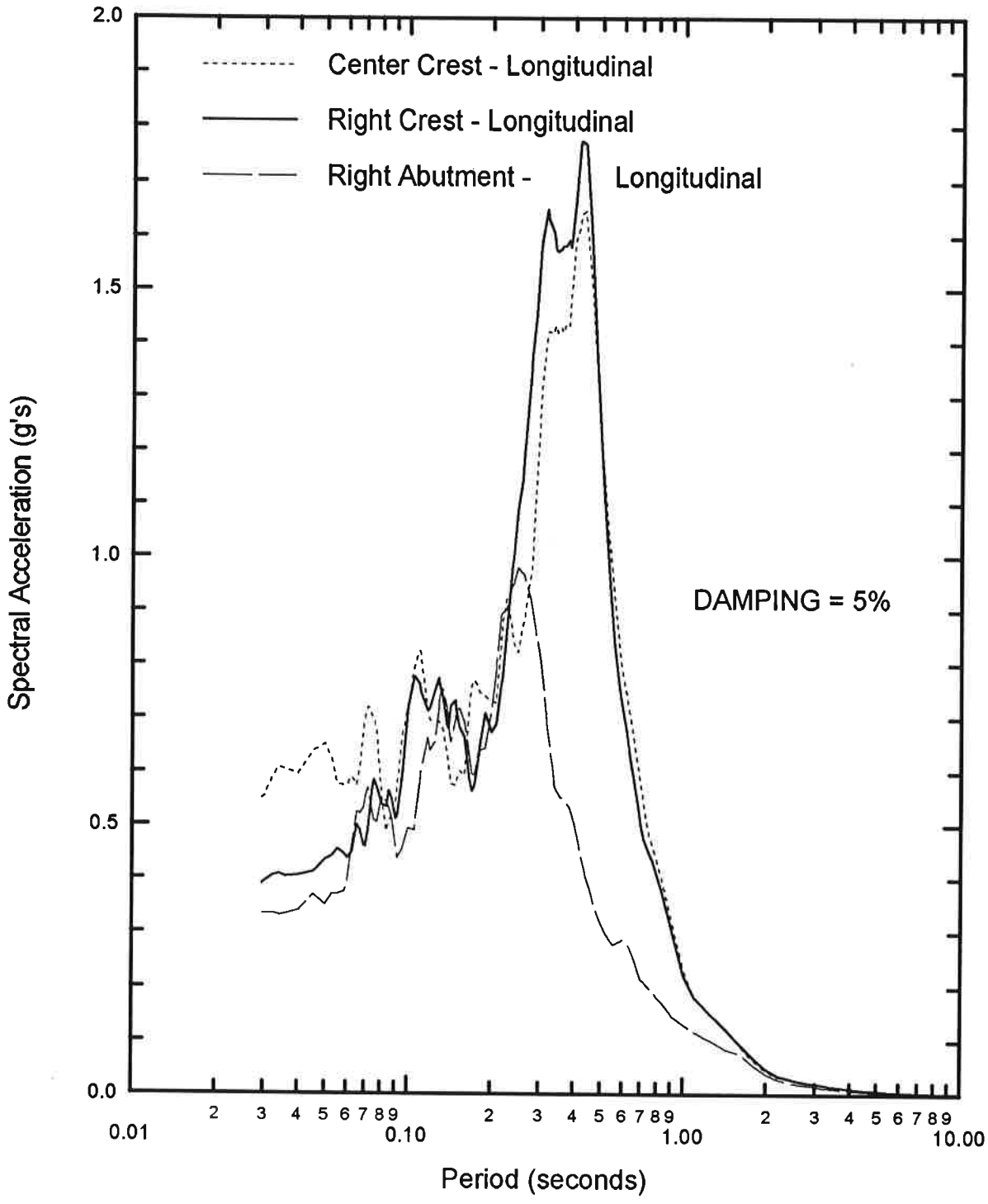

Figure 3-12: Recorded Response Spectra for Longitudinal Motions: Sierra Madre Earthquake

SPEC147.GRF

maximum spectral accelerations is given in Table 3-1.

The observed 3-D fundamental period of the dam during the Sierra Madre Earthquake was estimated to be between 0.45 and 0.48 seconds based on: (1) Fourier amplification ratios from the right abutment to the center crest and right crest (Fig. 3-13) indicate that the recorded motion's predominant period was about 0.48 seconds; and (2) the response spectra for the recorded center crest and right crest transverse motions suggest that the motion's predominant period was about 0.45 seconds (Fig. 3-11).

3.4 Comparison of Recorded Motions

The two earthquakes excited Cogswell Dam at significantly different levels. The Whittier Narrows Earthquake produced transverse peak ground accelerations at the right abutment, right crest and center crest of 0.06 g, 0.10 g, and 0.15 g, respectively. The Sierra Madre Earthquake produced higher transverse peak ground accelerations at these locations of 0.26 g, 0.32 g and 0.42 g, respectively. The observed crest center to abutment amplification ratio for the Whittier Narrows event was roughly 2.4; whereas, for the Sierra Madre event this ratio was 1.6. These crest center to abutment amplification ratios, and the observed decrease in the amplification ratio resulting from stronger earthquake shaking agree with the findings of previous case studies (e.g., Harder 1991).

The fundamental period of Cogswell Dam was found to be slightly longer during the Sierra Madre Earthquake ($T_p \approx 0.45$-0.48 seconds) than during the Whittier Narrows Earthquake ($T_p \approx 0.37$-0.42 seconds). The longer fundamental period of the dam during the stronger shaking of the Sierra Madre Earthquake is consistent with the expectation that the rockfill's stiffness would degrade under stronger earthquake excitation (i.e., greater induced shear strain). It should be noted that the term "fundamental period" may not be strictly appropriate for a nonlinear system, but is commonly used to indicate the "apparent" or "effective" fundamental period for a given level of loading.

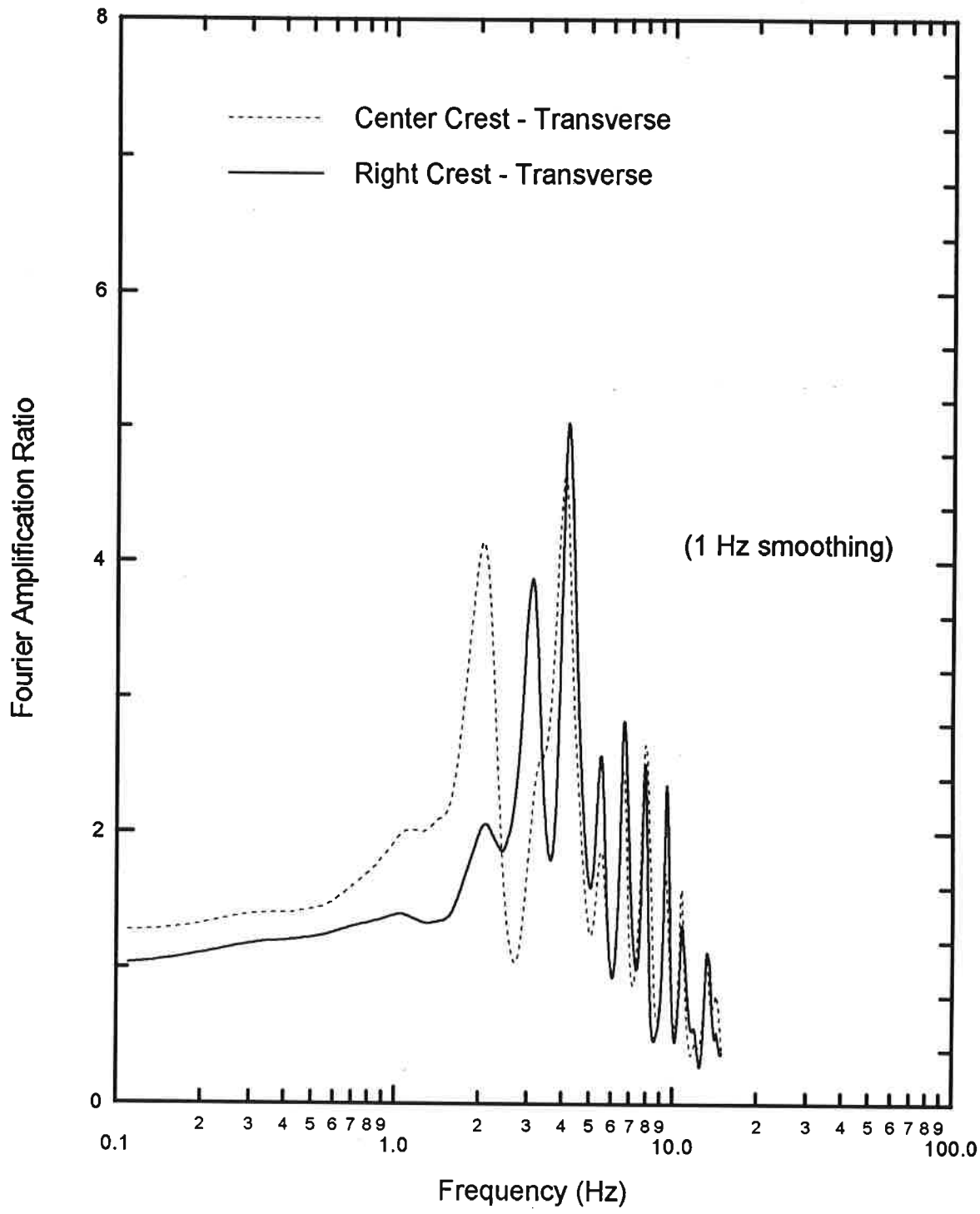

Figure 3-13: Fourier Amplification Ratios for Transverse Motions: Sierra Madre Earthquake

samp10hz.GRF

4. DYNAMIC RESPONSE ANALYSES

4.1 Finite Element Models

Analyses of the initial static stresses in the dam (required for determining dynamic properties) were performed using the finite element method (FEM) program SSCOMPPC (Boulanger et al. 1991). SSCOMPPC is a 2-D plane-strain program that employs the Duncan et al. (1980) hyperbolic soil model to represent the nonlinear stress-dependant stress-strain and volumetric strain response of the rockfill. The finite element mesh for the two-dimensional analyses of the maximum cross-section through the dam is shown in Fig. 4-1.

The two-dimensional (2-D) dynamic FEM analyses were performed using the computer program FLUSH (Lysmer et al. 1975). FLUSH uses the method of complex response to solve the equations of motion of a soil-structure system in the frequency domain. The nonlinear dynamic behavior of soils is modeled using the equivalent-linear method as proposed by Seed and Idriss (1970). The effective shear strain for individual elements is taken as a set ratio (65% in this study) of the maximum shear strain computed in the time domain. Elements are 4-node isoparametric quadrilaterals. The normalized mass matrix was taken as the average of the consistent mass matrix and the lumped mass matrix. After node and element renumbering, the same finite element mesh used for the initial static stress analyses was utilized for the 2-D dynamic response analyses. Hydrodynamic effects were not included as they are generally considered to be of secondary importance due to the relatively flat slopes encountered in earth and rockfill dams.

The three-dimensional (3-D) dynamic FEM analyses were performed using a version of the computer program TLUSH (Kagawa et al. 1981) modified to run on the Cray C90 at the U. C. San Diego Supercomputer Center. The fully 3-D program TLUSH is similar to FLUSH in that it uses the method of complex response in the frequency domain and models soil behavior by the equivalent-linear method. Elements are 8-node isoparametric bricks. The normalized mass matrix was taken

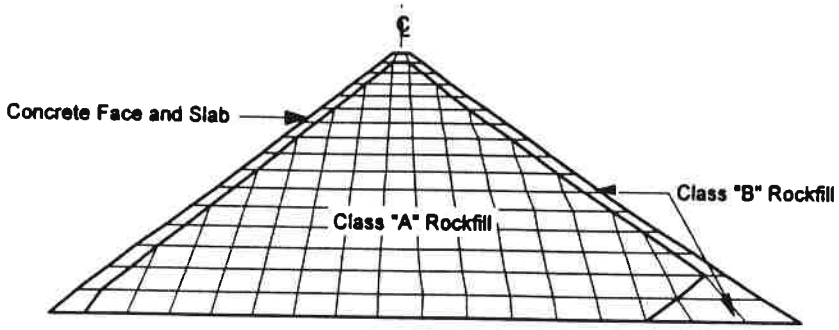

Fig. 4-1: Two-Dimensional Finite Element Mesh

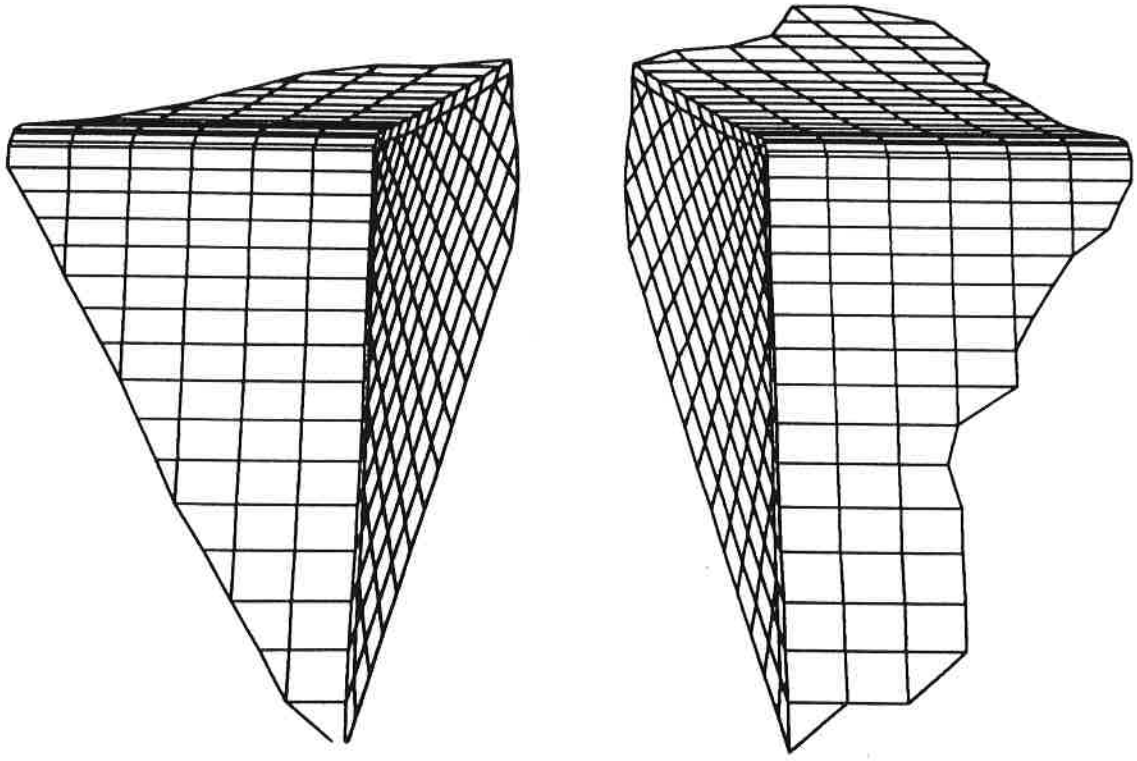

Fig. 4-2: Three-Dimensional Finite Element Mesh

as the average of the consistent mass matrix and the lumped mass matrix. The equivalent shear strain for individual elements is taken as a set ratio (65% in this study) of the maximum shear strain computed in the time domain. The finite element mesh for the 3-D dynamic response analyses is shown in Fig. 4-2. The maximum section in the 3-D mesh differs slightly from the 2-D mesh due to the irregularity of the bedrock foundation, particularly near the downstream toe. A full 3-D mesh was used due to several asymmetrical features in the dam.

4.2 Dynamic Rockfill Properties

The dynamic properties of rockfill materials are not well documented or understood. For rockfill materials that are too large to test in the laboratory, it is customary to assume that the material behaves similar to gravel or sand in terms of modulus degradation and damping characteristics. Based on that assumption, the parameters defining the maximum (low strain) shear modulus of large rockfills have been back-calculated based on comparisons of calculated and recorded dynamic response analyses of prototype dams. Lai (1985) used the upper bound damping and median modulus degradation relationships for sand presented by Seed et al. (1984) in analyses of El Infiernillo and La Villita Dams. Similar analyses of these dams were also performed by Romo et al. (1980). Mejia et al. (1991), however, found that the modulus degradation relationship for gravel presented by Seed et al. (1984) combined with estimates of maximum shear modulus based on insitu shear wave velocity measurements provided a reasonable analytical representation of the recorded response of Ririe Dam during the 1983 Mt. Borah Earthquake.

Recent laboratory test data appear to indicate that modulus degradation relationships for many gravels and smaller rockfill materials are closer to the median and upper-bound sand curves presented by Seed and Idriss (1970) than to the gravel curves presented by Seed et al. (1984). Fig. 4-3 summarizes the modulus degradation and damping relationships presented by Yasuda and Matsumoto (1993) along with those of earlier investigators. Yasuda and Matsumoto's (1993) data was for a

quartz andesite with a maximum particle size of 38 mm. Fig. 4-4 compares select relationships with the relationships presented by Kono et al. (1993) based on large-scale field tests and laboratory tests on a dense gravel having a maximum particle size of 150 mm. Upon review of Figs. 4-3 and 4-4, it is clear that the median modulus degradation relationship for gravel presented by Seed et al. (1984) is essentially a lower bound on the more recent data of other investigators, and that the median modulus degradation relationship for sand presented by Seed et al. (1984) better represents these more recent data. Furthermore, it appears that the modulus degradation relationships for sand and gravel may be more similar than previously thought. While the appropriate relationship for large-sized rockfill cannot be directly evaluated based on the above data, one might reasonably expect rockfill to behave similar to sand and gravel. Thus, a modulus degradation relationship must be assumed, and then any subsequently back-calculated maximum shear modulus parameters must be qualified as only being appropriate for the assumed modulus degradation curve. However, it will be shown later in Section 5 that equivalent combinations of maximum shear modulus and modulus degradation relationships can be readily estimated. The median damping relationship for gravel presented by Seed et al. (1984) is within the range of the more recent data of other investigators, while the upper bound damping relationship for gravel presented by Seed et al. (1984) would appear to represent a reasonable upper bound to the more recent data.

The dynamic analyses for this study were completed using the median modulus degradation relationship and the upper bound damping relationship presented for gravel by Seed et al. (1984). The results of the analyses are also interpreted for the modulus degradation relationship presented for sand by Seed and Idriss (1970). The effect of using the median damping relationship for sand (Seed et al. 1970) was also investigated in a few sensitivity analyses.

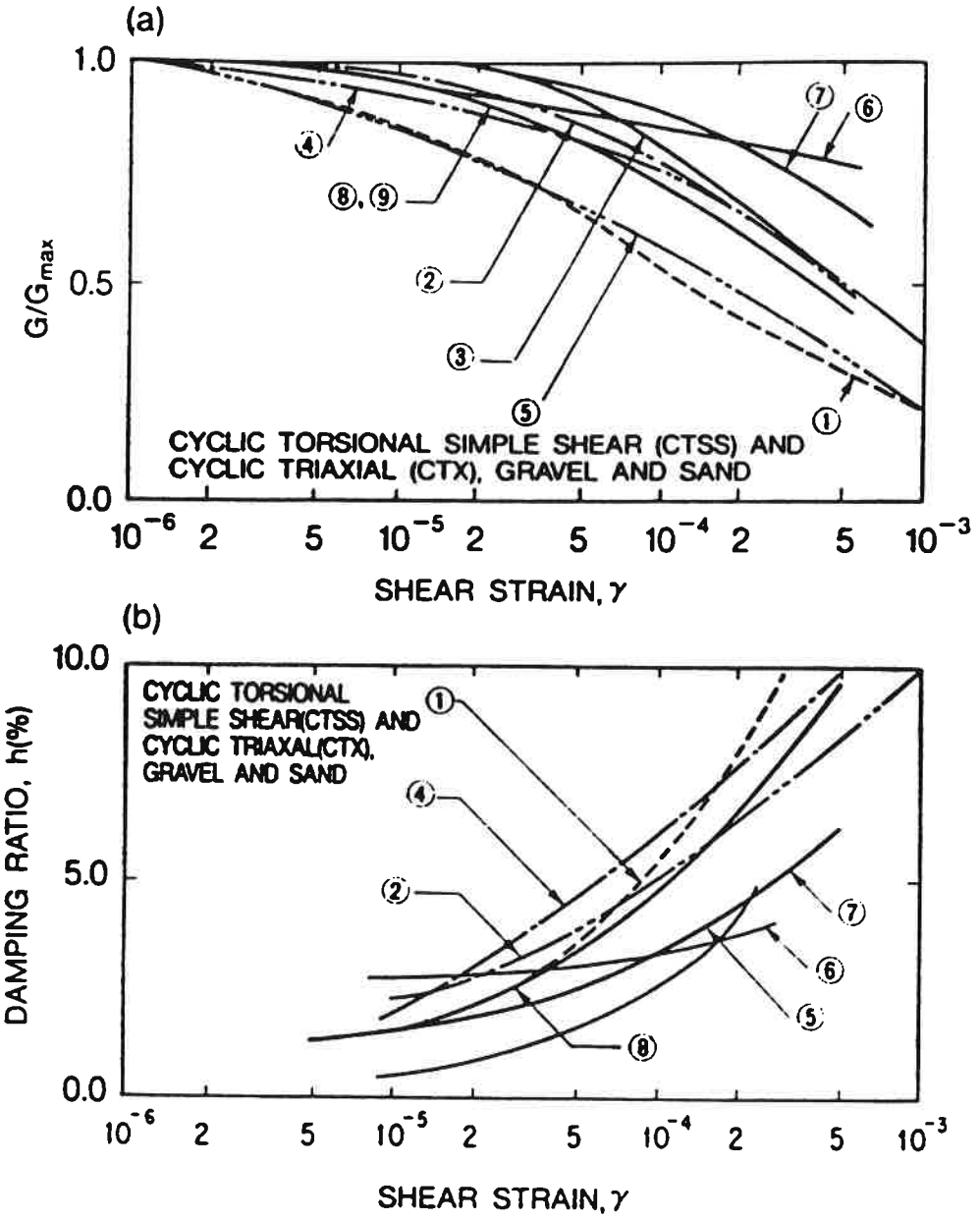

FIG4-3.GRF

No.	References	Diameter (cm)	Height (cm)	Material	D_{max}	Remarks
1	Seed et al. (1984)	30.5	73.7	Gravel	50.8	CTX
2	Matsumoto et al. (1985)	30	60	Rockfill	63.5	CTX
3	Shamoto et al. (1986)	30	60	Gravel	—	CTX
4	Hatanaka et al. (1988)	30	60	Gravel	90.0	CTX
5	Hynes et al. (1988)	38.1	97.8	Rockfill	76.2	CTX
6	Shibuya et al. (1990)	30	60	Gravel	6.65 (D_{50})	CTX
7	This study	80 (outer), 40 (inner)	80	Sand	—	CTSS
8	This study	80 (outer), 40 (inner)	80	Rockfill	38.1	CTSS
9	This study	40	80	Rockfill	38.1	CTX

NOTE: D_{max} = maximum particle size; D_{50} = average particle size.

Figure 4-3: (a) G/G_{max} and (b) Damping Ratios Versus Shear Strain Relationships of Rockfill and Gravelly Soils (after Yasuda and Motsumoto, 1993)

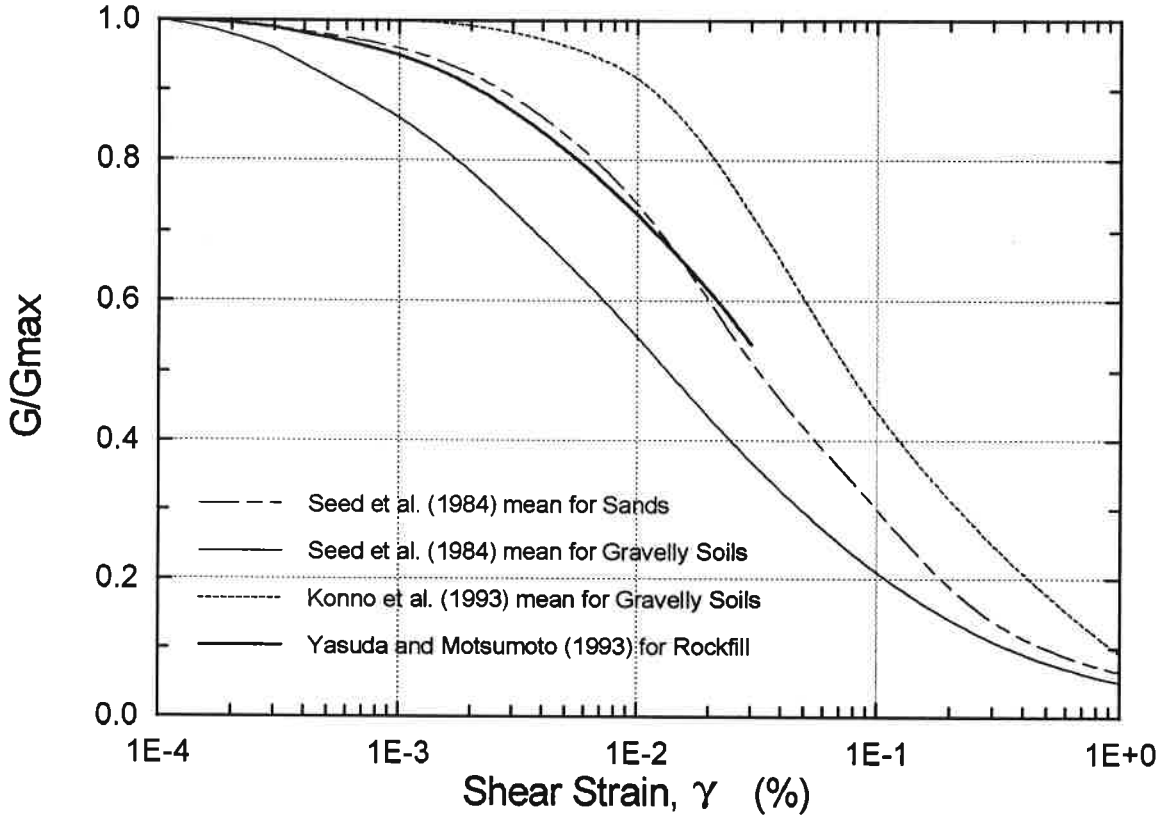

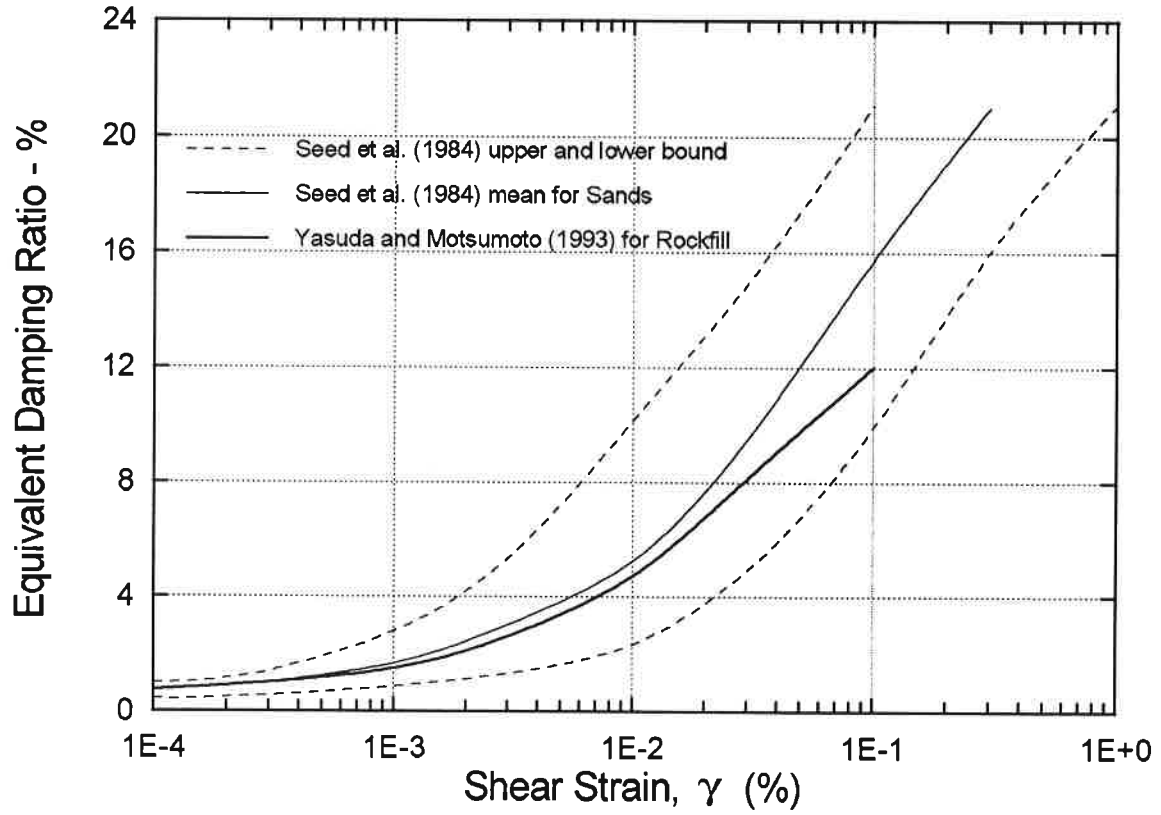

ROCKFILL.GRF

Figure 4-4: Comparison of Dynamic Properties With Recent Literature

It then remains to select a value for the parameter $K_{2,max}$ which establishes the maximum shear modulus (G_{max}) as:

$$G_{max} = 219\ K_{2max}\ (\sigma'_m)^{1/2} \qquad (1)$$

where G_{max} and the mean effective confining stress (σ_m') are in units of kPa. The value of σ_m' was taken as the average of the three principal stresses, of which two are obtained from the initial static stress analyses described in the next section. Since the 2-D static stress analyses do not provide the intermediate principal stress (σ_2'), it was estimated for each element as:

$$\sigma'_2 = \nu\ (\sigma'_1+\sigma'_3) \geq \sigma'_3 \qquad (2)$$

The above guideline expression is based on elastic theory for an isotropic material with a Poisson's ratio of υ, but subject to the limitation that the out-of-plane principal stress be intermediate to the in-plane principal stresses. A Poisson's ratio of 0.35 for the rockfill was used in Eqtn. (2) for estimating intermediate principal stresses and in the dynamic response analyses. The value of K_{2max} for the Class "B" and "C" rockfill zones were taken as 1/3 greater than the value assigned to the body of the dam (Class "A") in all analyses; thus, only the $K_{2,max}$ value for the body of the dam is referred to hereafter.

4.3 Initial Static Stress Analyses

The initial static stress analyses were calculated for the maximum cross-section of the dam, and were performed in steps to incrementally model the placement of the rockfill and the subsequent loads produced against the upstream face by the reservoir (elevation set to the value reported at the time of each earthquake). Model parameters were the same as presented by Boulanger et al. (1990). Additional parameter studies showed that the calculated mean confining stresses were not sensitive to the model parameters, which is reasonable given the homogenous cross-section of the dam. The initial stress distribution shown in Fig. 4-5 corresponds to conditions at the time of the Whittier

Narrows Earthquake; the stress distribution was only slightly affected by the different reservoir water levels at the times of the two earthquakes.

The results of the 2-D static stress analysis were then corrected to account for the effects of canyon shape using data presented by Lefebvre and Duncan (1971). For a triangular shaped canyon, Lefebvre and Duncan showed that a dam with a crest length (L) to height (H) ratio of 2:1, a 2-D analysis of the maximum cross-section can overestimate the static stresses in the lower third of the dam by as much as 40%, as shown in Fig. 4-6. Consequently, the mean confining stresses obtained from the 2-D analyses were reduced by an amount that varied linearly with elevation from 0% at the lower 1/3-point of the dam to 30% at the base of the dam. Since the same maximum cross-sectional mesh geometry was used for the static and dynamic FEM analyses, the calculated mean confining stresses corresponded directly to individual elements in the 2-D dynamic mesh and were projected longitudinally into the 3-D dynamic mesh.

4.4 Two-Dimensional Dynamic Response Analyses

The 2-D (plane-strain) dynamic response of the dam was computed using the recorded transverse abutment motions as the input motion to the rigid base. A maximum frequency of 12 Hz was used in the analyses. Analyses were performed with values for the soil model parameter K_{2max} of 80, 100, 120, 140, 160, and 180 with the median modulus degradation relationship for gravel proposed by Seed et al. (1984). Sensitivity analyses included the use of upper bound and median relationships for the damping ratio versus shear strain relationship. The computed response of the dam crest was compared to the recorded response at the crest center in terms of acceleration response spectra, Fourier amplification ratios, and acceleration time histories at the dam crest. The results of selected analyses are summarized in Table 4-1, including the typical range of induced shear strains within the FE models. The response spectra and Fourier amplification ratios calculated for a K_{2max} value of 120 and both earthquake motions are presented in Figs. 4-7 through 4-10.

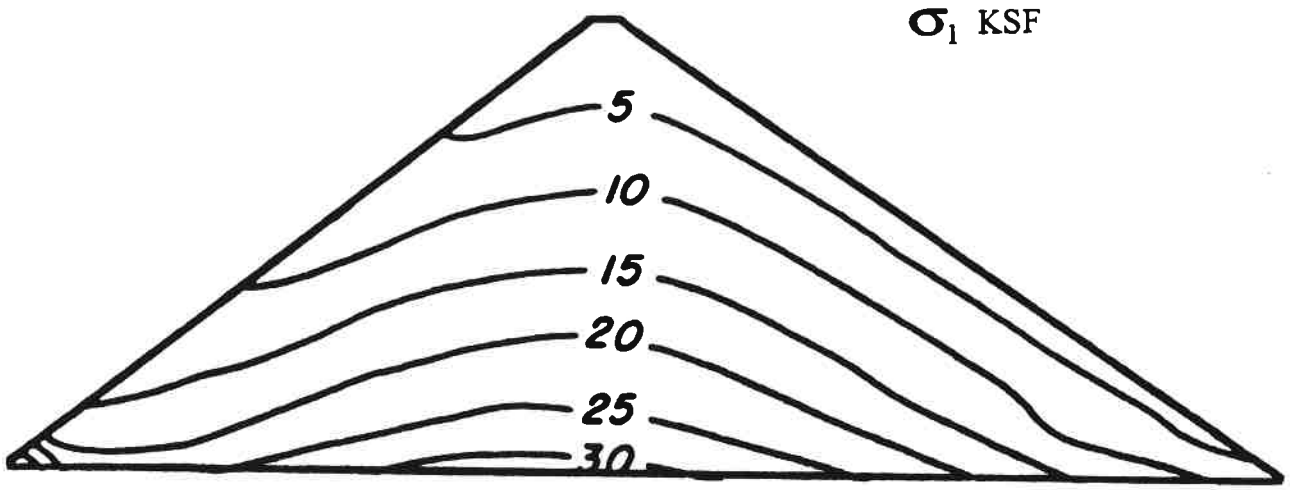

(a) Major Principal Effective Stress (σ_1)

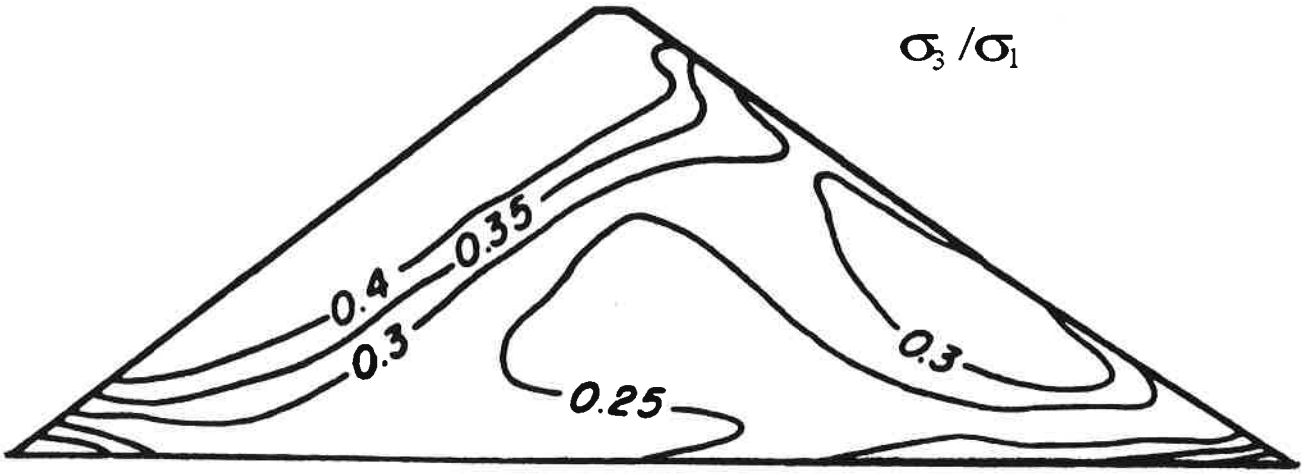

FIG#4 GRF

(b) Effective Principal Stress Ratio (σ_3/σ_1)

Figure 4-5: Contours of Static Effective Stresses in Dam Prior to Allowance For 3-D Effects

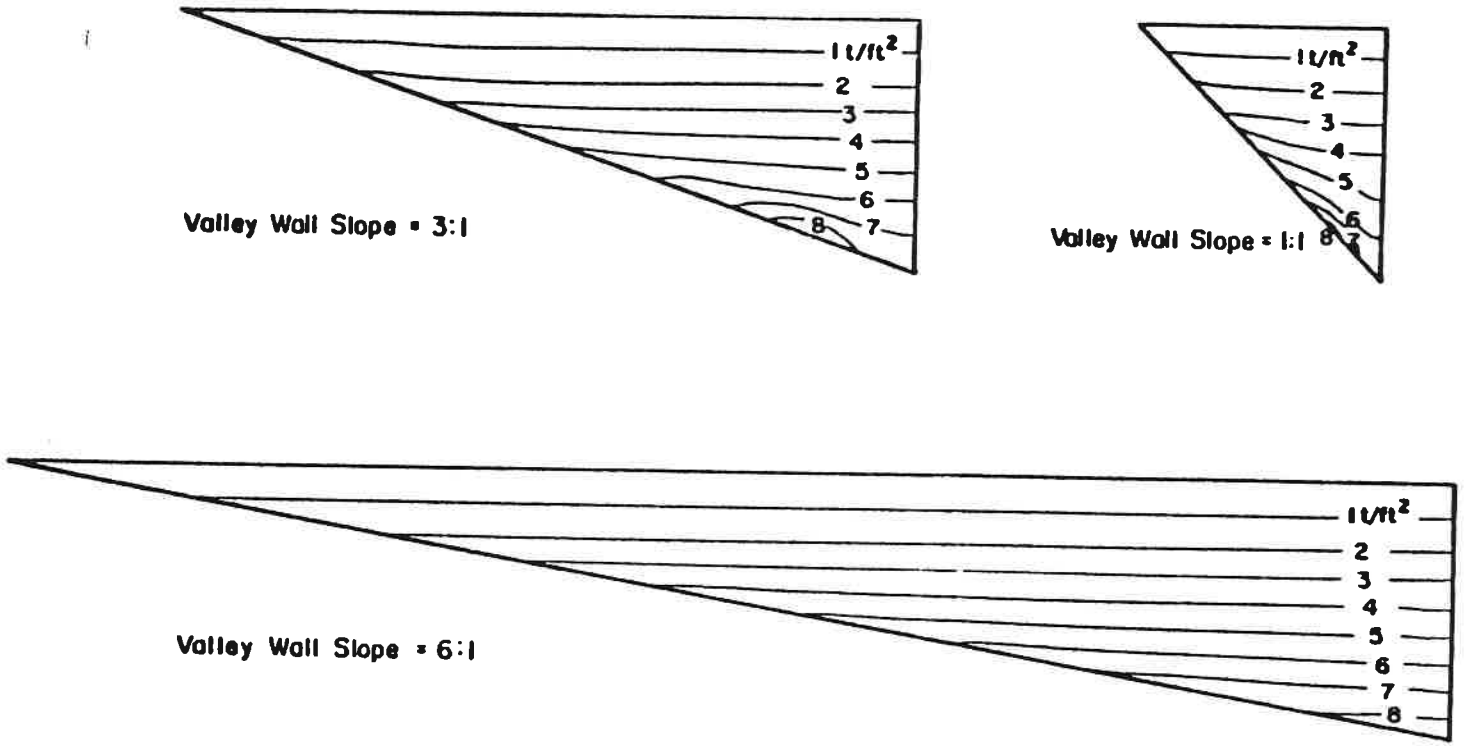

Figure 4-6: Contours of Values of Major Principal Stress σ_1 In Longitudinal Section Calculated Using Three-Dimensional Analyses With Three Different Valley Wall Slopes (after Lefebvre et al. 1973)

TABLE 4-1(a): Results of 2-D Dynamic Response Analyses for Sierra Madre Earthquake

K-2,max for Class A Rockfill	Input Motion	Modulus Degradation Relationship	Damping Relationship	Representative Effective Strain (2) Average (Range) (%)	Typical Ratio of G/Gmax	Typical Damping (%)	Fundamental Period (1) (sec)	Maximum Peak Acceleration at Crest
Recorded	0.26	n/a	n/a	n/a	n/a	n/a	0.45 - 0.48	0.42
100	Abutment	Gravel	Upper	0.027 (.010-.042)	0.40	14.3	0.87	0.36
120	Abutment	Gravel	Upper	0.026 (.01-.046)	0.40	14.1	0.77	0.45
140	Abutment	Gravel	Upper	0.025 (.009-.046)	0.41	13.9	0.72	0.51
160	Abutment	Gravel	Upper	0.024 (.008-.043)	0.42	13.6	0.66	0.55
180	Abutment	Gravel	Upper	0.022 (.007-.038)	0.43	13.3	0.62	0.56

1. From maximum fourier amplification ratios between crest nodal points and model base.
2. Range of shear strains is representative of the maximum section. Effective strain is taken as 65% of peak shear strain.

TABLE 4-1(b): Results of 2-D Dynamic Response Analyses for Whittier Narrows Earthquake

K-2,max for Class A Rockfill	Input Motion	Modulus Degradation Relationship	Damping Relationship	Representative Effective Strain (2) Average (Range) (%)	Typical Ratio of G/Gmax	Typical Damping (%)	Fundamental Period (1) (sec)	Maximum Peak Acceleration at Crest
Recorded	0.064	n/a	n/a	n/a	n/a	n/a	0.37-0.42	0.15
100	Abutment	Gravel	Upper	0.007 (.003-.014)	0.61	8.6	0.69	0.20
120	Abutment	Gravel	Upper	0.006 (.002-.012)	0.63	8.2	0.62	0.19
140	Abutment	Gravel	Upper	0.006 (.002-.010)	0.62	8.3	0.59	0.19
160	Abutment	Gravel	Upper	0.006 (.002-.009)	0.63	8.3	0.55	0.18
180	Abutment	Gravel	Upper	0.008 (.002-.009)	0.62	8.3	0.52	0.21

1. From maximum fourier amplification ratios between crest nodal points and model base.
2. Range of shear strains is representative of the maximum section. Effective strain is taken as 65% of peak shear strain.

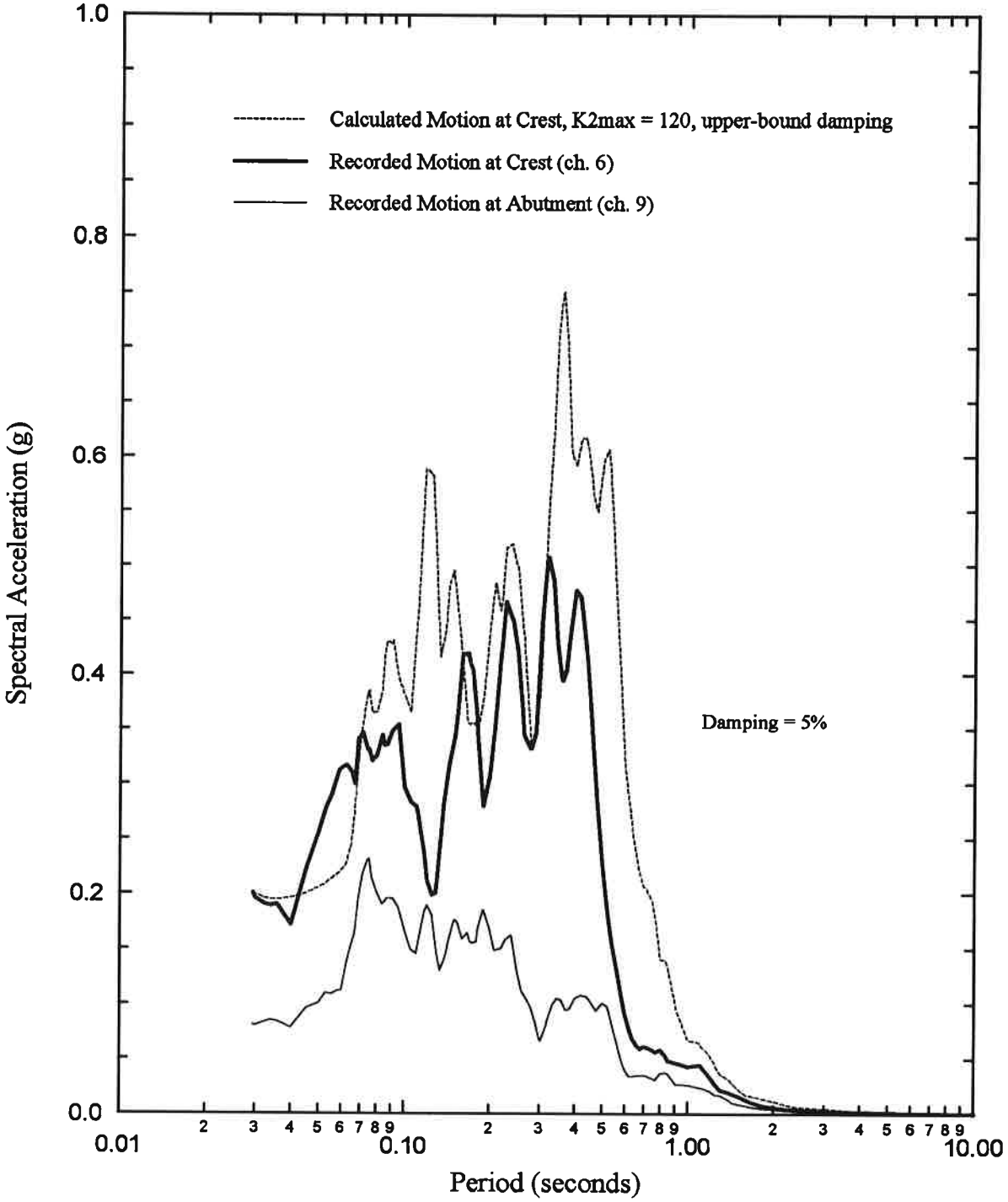

120WNRSP.GRF

Figure 4-7: Calculated 2-D Dynamic Response Spectra
Whittier Narrows Earthquake

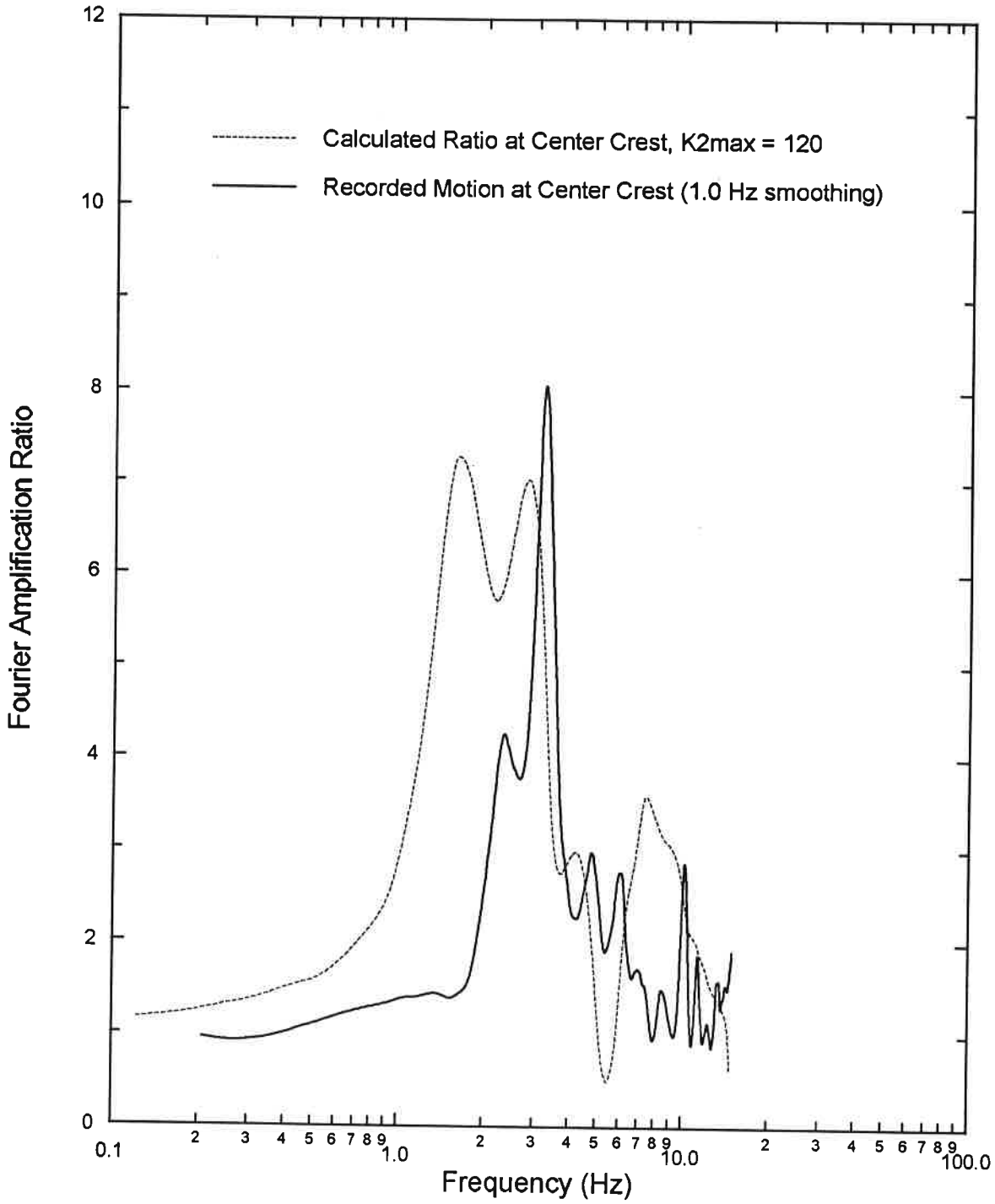

120WDRAT.GRF

Figure 4-8: 2-D Fourier Amplification Ratios
Whittier Narrows Earthquake

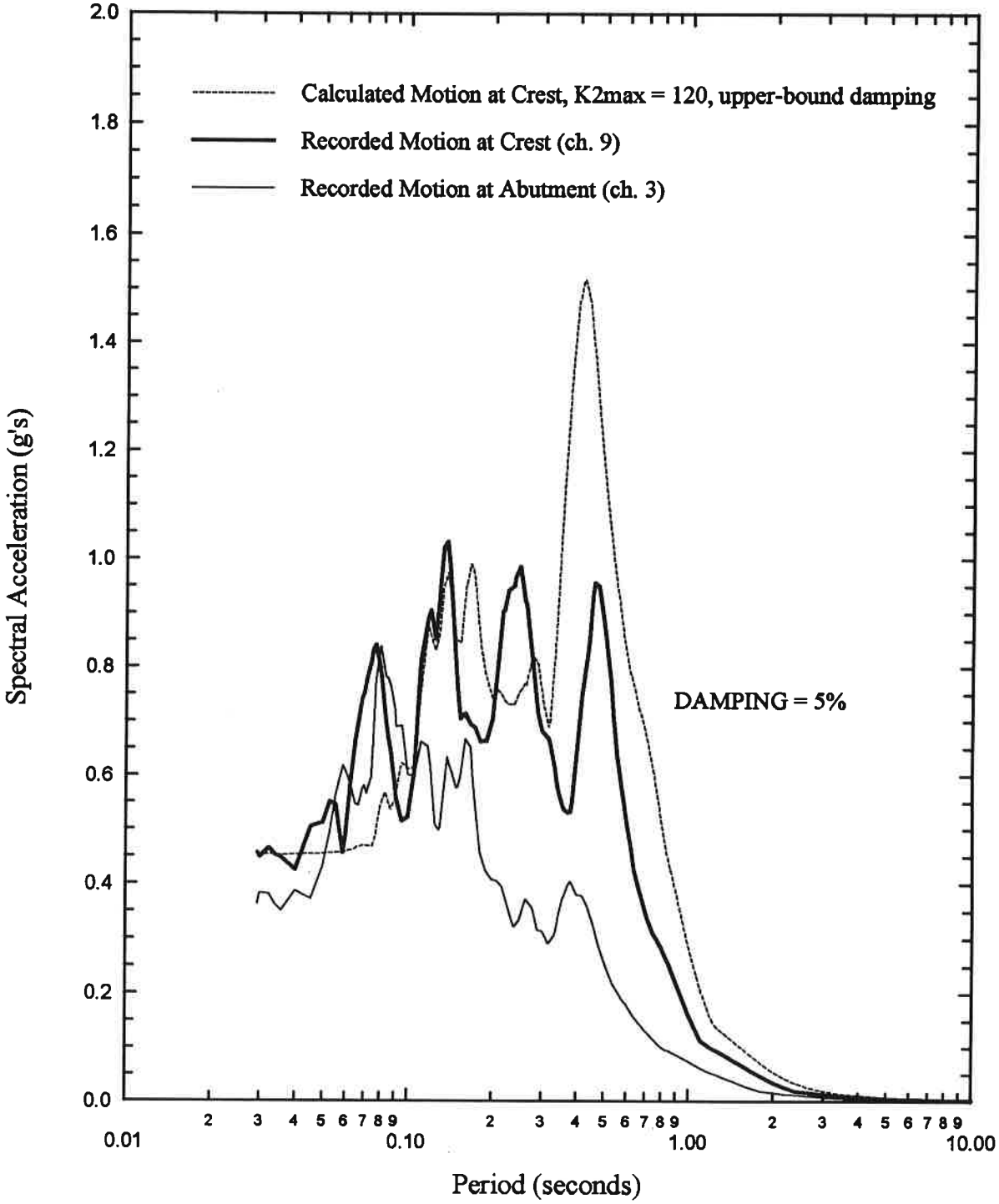

K2SMRESP.GRF

Figure 4-9: Calculated 2-D Dynamic Response Spectra
Sierra Madre Earthquake

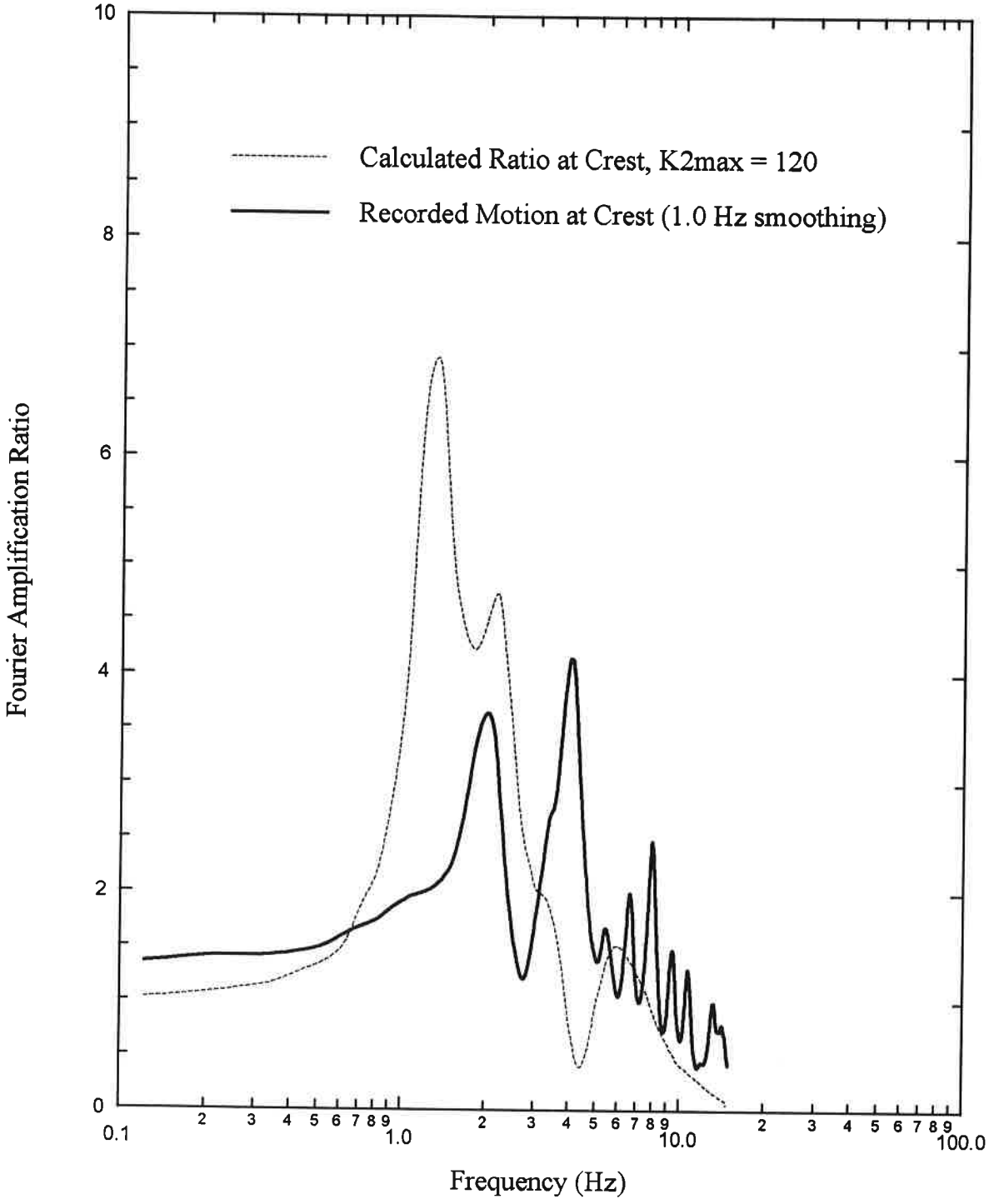

AMP2SMD.GRF

Figure 4-10: 2-D Fourier Amplification Ratios
Sierra Madre Earthquake

In general, the 2-D dynamic response analyses using realistic $K_{2,max}$ values (considered to be 100 to 140) were not able to capture all aspects of the recorded responses at the crest center. As expected, the calculated Fourier amplification ratios exhibit their greatest value at their longest period (corresponding to the first mode of vibration for the 2-D model) followed by progressively smaller amplification ratios at higher modes of vibration. In contrast, the Fourier amplification ratios for the recorded motions at the crest center exhibit a lower peak ratio at their first mode of vibration than is produced at the second mode of vibration, possibly reflecting asymmetrical dam motions or the relative positioning of the accelerograph with respect to the 3-D modal shapes. The difference between the calculated and recorded Fourier amplification ratios is reflected in the differences between the calculated and recorded acceleration response spectra. The calculated response spectra generally over-predict the recorded response spectra by a factor of roughly 1.5 to 1.9 and do not accurately reproduce the same "shape" because the 2-D model is amplifying the input motions in a significantly different way than the recorded motions indicate was the case. Similarly, the peak ground accelerations at the crest are generally over-predicted by a factor of roughly 1.1 to 1.3.

The $K_{2,max}$ value input into a 2-D analysis is sometimes artificially increased to a value that "stiffens" the 2-D model to a fundamental frequency that matches the prototype's 3-D geometry. For Cogswell Dam, $K_{2,max}$ values in the range of 200 to 240 would be necessary in a 2-D analysis to compensate for the stiffening effects of the V-shaped valley it is located in. When these larger values are used, the fundamental frequency of the FE model becomes closer to the predominant frequencies present in the input motions. Consequently, the FE model responds even more strongly in its first mode, and thus the over-prediction of the dynamic response of the dam is increased.

The use of the median damping relationship in any of the analyses resulted in poorer agreement between the calculated and recorded motions in terms of the magnitude of response but did not significantly affect the general shape of the response spectra or Fourier amplification ratios.

4.5 Three-Dimensional Dynamic Response Analyses

The 3-D dynamic response of the dam was computed using the recorded transverse abutment motions as the input motion to the rigid base. Results were practically identical for frequency cutoffs of 10 or 12 Hz, so a cutoff frequency of 10 Hz was used in the remaining analyses. Analyses were performed with values for the soil model parameter $K_{2,max}$ of 80, 100, 120, 140, and 160. Sensitivity analyses included the use of upper bound and median damping relationships presented for sand by Seed and Idriss (1970). The computed response of the dam was compared to the recorded motions (node 291 vs. the crest center motions, and node 961 vs. the right crest motions) in terms of acceleration response spectra, Fourier amplification ratios, and acceleration time histories. The response spectra and Fourier amplification ratios calculated for a $K_{2,max}$ value of 120 are presented in Figs. 4-11 through 4-14 for the two earthquakes. The results of selected analyses are summarized in Table 4-2 (the results obtained for a scaled down abutment motion will be discussed later).

The computed variations of peak transverse acceleration along the crest of the dam, based on the 3-D dynamic response analyses, are shown in Fig. 4-15 for the two earthquakes. Peak accelerations are somewhat asymmetrical about the center of the dam crest because of the asymmetrical features in the FEM mesh. Also shown on Fig. 4-15 are the recorded peak transverse accelerations at the crest center and right crest instruments. These 3-D dynamic response analysis results suggest the greatest peak transverse accelerations during these earthquakes may have occurred at a point on the dam crest slightly to the right of the center crest instrument.

In general, the 3-D dynamic response analyses over-predicted the recorded dam response. The Fourier amplification ratios to the crest and the subsequently affected peak crest accelerations are generally over-predicted by factors of roughly 1.6 to 2.3 for the two earthquakes. The calculated acceleration response spectra at the crest are generally over-predicted by factors of roughly 1.7 to 2.6. The use of the median damping relationship resulted in a slightly greater over-prediction of the

recorded response but did not significantly affect the general shapes of the Fourier amplification ratios or response spectra.

TABLE 4-2(a): Results of 3-D Dynamic Response Analyses for Sierra Madre Earthquake

K-2,max for Class A Rockfill	Input Motion	Modulus Degradation Relationship	Damping Relationship	Representative Effective Strain (2) Average (Range) (%)	Typical Ratio of G/Gmax	Typical Damping (%)	Fundamental Period (1) (sec)	Maximum Peak Accelerations (g)		Comparison to 2-D Results, Same K-2,max (3)		
								Center Crest Node 291	Right Crest Node 961	Ratio Tp-2d to Tp-3d	Typ. Ratio of 2D/3D Strains	Typ. Ratio of 2D/3D G/Gmax ratio
Recorded	0.26	n/a	n/a	n/a	n/a	n/a	0.45 - 0.48	0.42	0.32	-	-	-
120	Abutment	Gravel	Upper	0.032 (0.014-0.057)	0.37	15.3	0.539	0.67	0.44	1.43	0.81	1.08
140	Abutment	Gravel	Upper	0.034 (0.012-0.050)	0.36	15.7	0.488	0.74	0.48	1.48	0.74	1.14
160	Abutment	Gravel	Upper	0.028 (0.012-0.046)	0.40	14.5	0.450	0.81	0.51	1.47	0.86	1.05
120	Abut*0.5	Gravel	Upper	0.016 (0.007-0.028)	0.47	12.1	0.488	0.46	0.25			
140	Abut*0.5	Gravel	Upper	0.015 (0.007-0.027)	0.48	11.8	0.450	0.50	0.30			

1. From maximum fourier amplification ratios between crest nodal points and model base.
2. Range of shear strains is representative of the maximum section. Effective strain is taken as 65% of peak shear strain.
3. For elements in the maximum cross-section.

TABLE 4-2(b): Results of 3-D Dynamic Response Analyses for Whittier Narrows Earthquake

K-2,max for Class A Rockfill	Input Motion	Modulus Degradation Relationship	Damping Relationship	Representative Effective Strain (2) Average (Range) (%)	Typical Ratio of G/Gmax	Typical Damping (%)	Fundamental Period (1) (sec)	Maximum Peak Accelerations (g)		Comparison to 2-D Results, Same K-2,max (3)		
								Center Crest Node 291	Right Crest Node 961	Ratio Tp-2d to Tp-3d	Typ. Ratio of 2D/3D Strains	Typ. Ratio of 2D/3D G/Gmax ratio
Recorded	0.064	n/a	n/a	n/a	n/a	n/a	0.37-0.42	0.15	0.10	-	-	-
120	Abutment	Gravel	Upper	0.009 (.004-.016)	0.40	14.6	0.455	0.31	0.19	1.36	0.67	1.58
140	Abutment	Gravel	Upper	0.008 (.003-.015)	0.43	13.6	0.418	0.35	0.22	1.41	0.75	1.44
120	Abut*0.5	Gravel	Upper	0.005 (.002-.009)	0.65	7.5	0.418	0.20	0.11			
140	Abut*0.5	Gravel	Upper	0.004 (.001-.008)	0.68	6.6	0.379	0.23	0.13			

1. From maximum fourier amplification ratios between crest nodal points and model base.
2. Range of shear strains is representative of the maximum section. Effective strain is taken as 65% of peak shear strain.
3. For elements in the maximum cross-section.

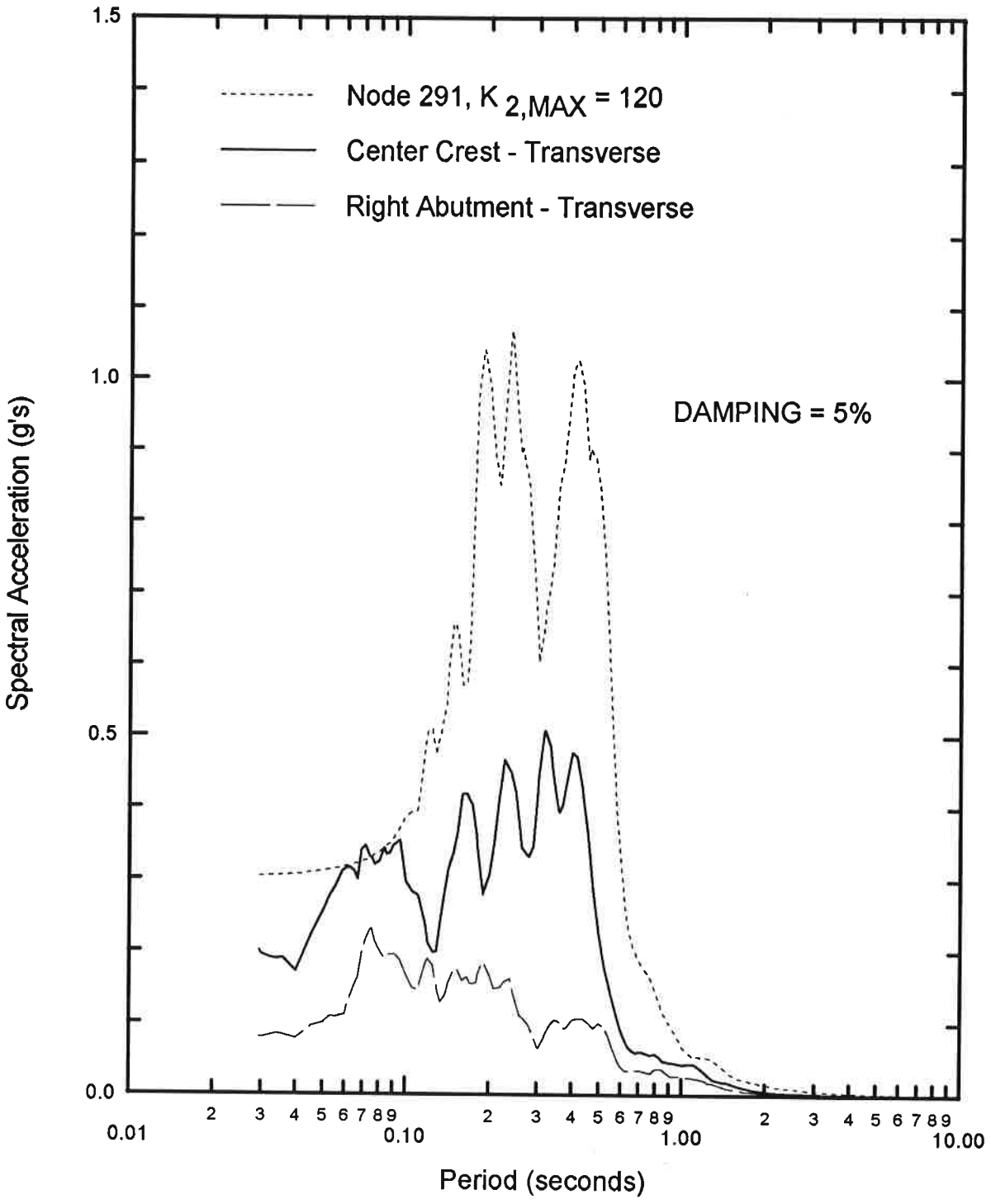

(a) Transverse Motions at the Center Crest

Figure 4-11: Calculated 3-D Dynamic Response Spectra: Whittier Narrows Earthquake

QN291RS.GRF

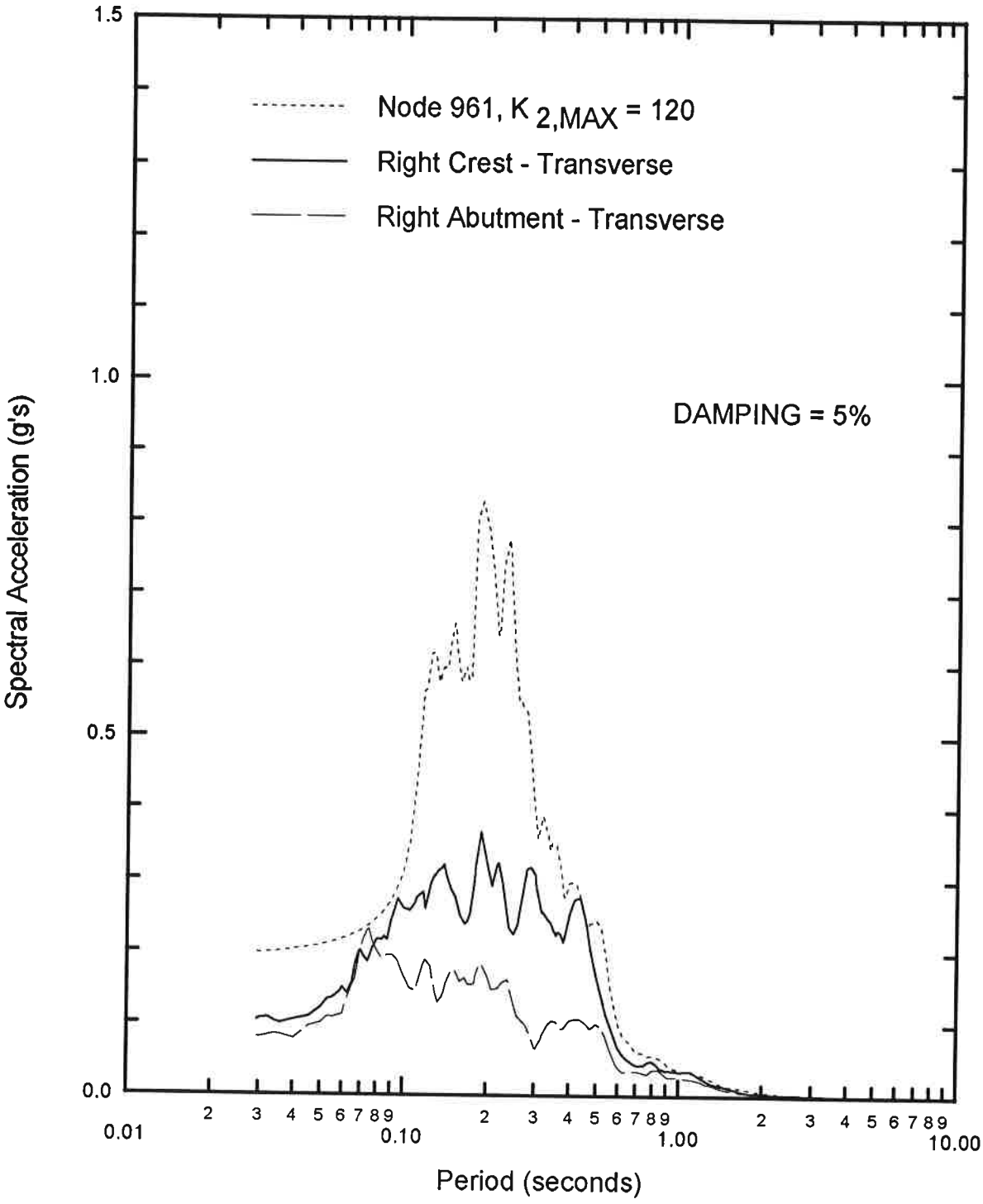

(b) Transverse Motions at the Right Crest

Figure 4-11: Calculated 3-D Dynamic Response Spectra: Whittier Narrows Earthquake

QN961RS.GRF

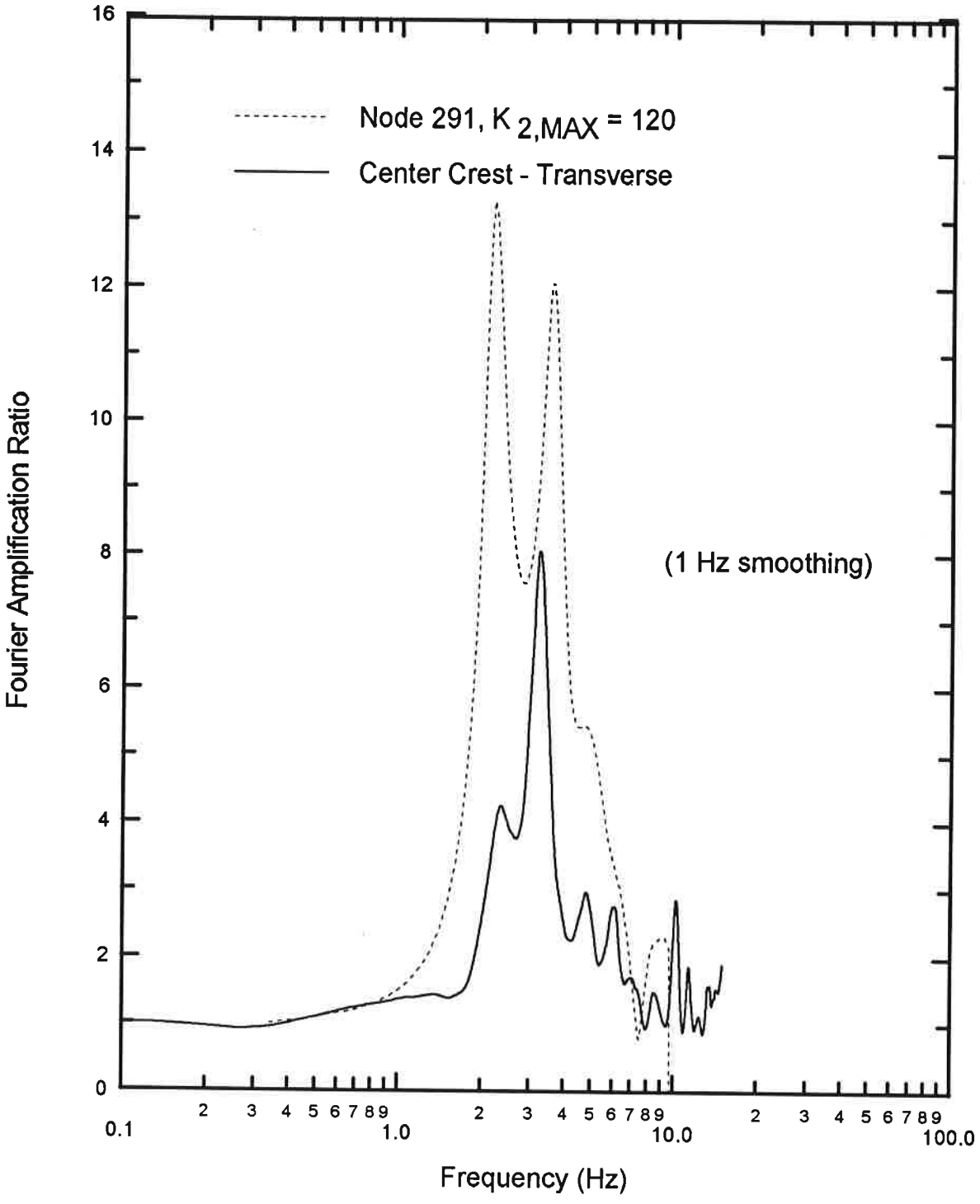

(a) Transverse Motions at the Center Crest

Figure 4-12: Calculated 3-D Fourier Amplification Ratios: Whittier Narrows Earthquake

QNAMP291.GRF

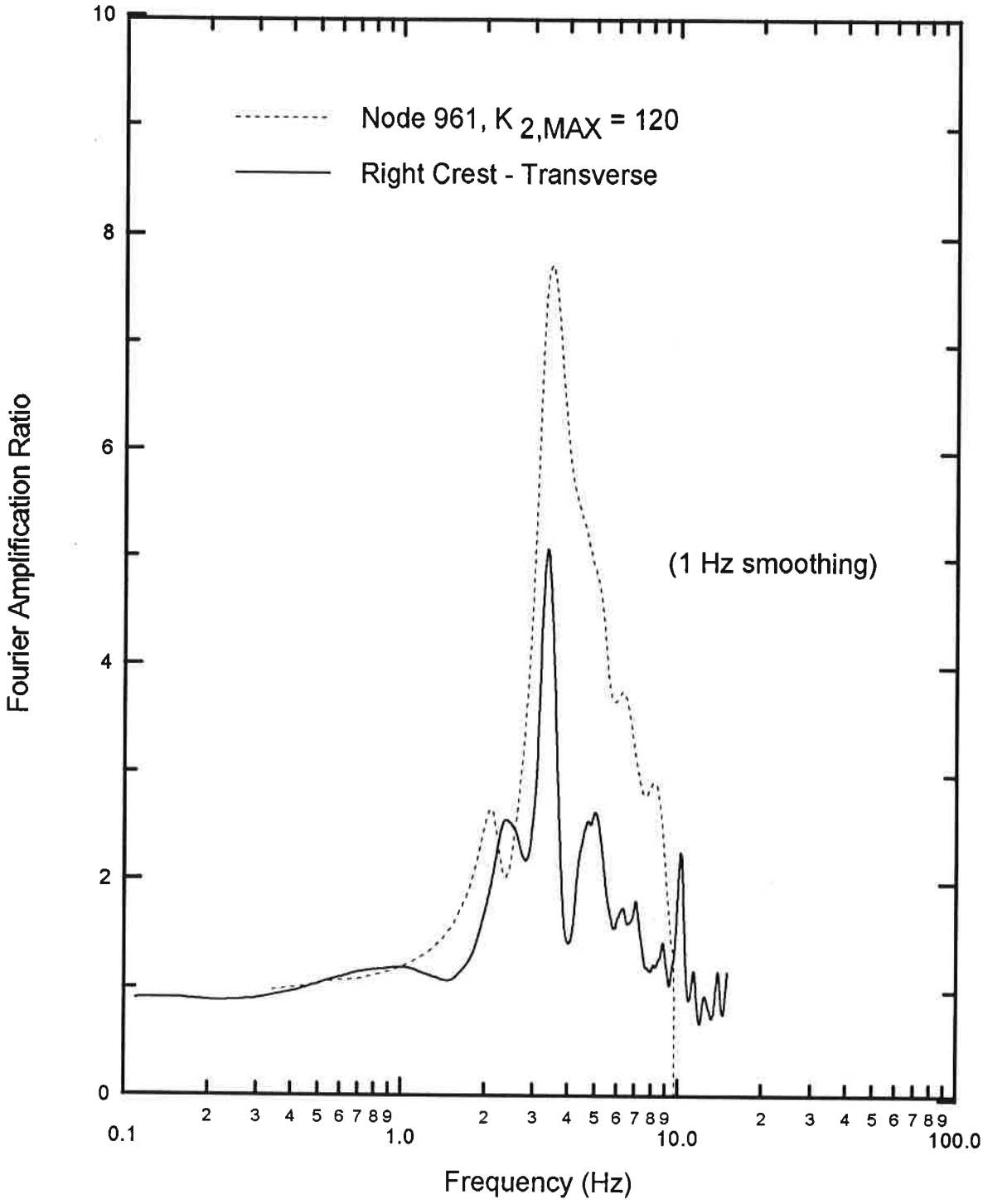

(b) Transverse Motions at the Right Crest

Figure 4-12: Calculated 3-D Fourier Amplification Ratios: Whittier Narrows Earthquake

QNAMP961.GRF

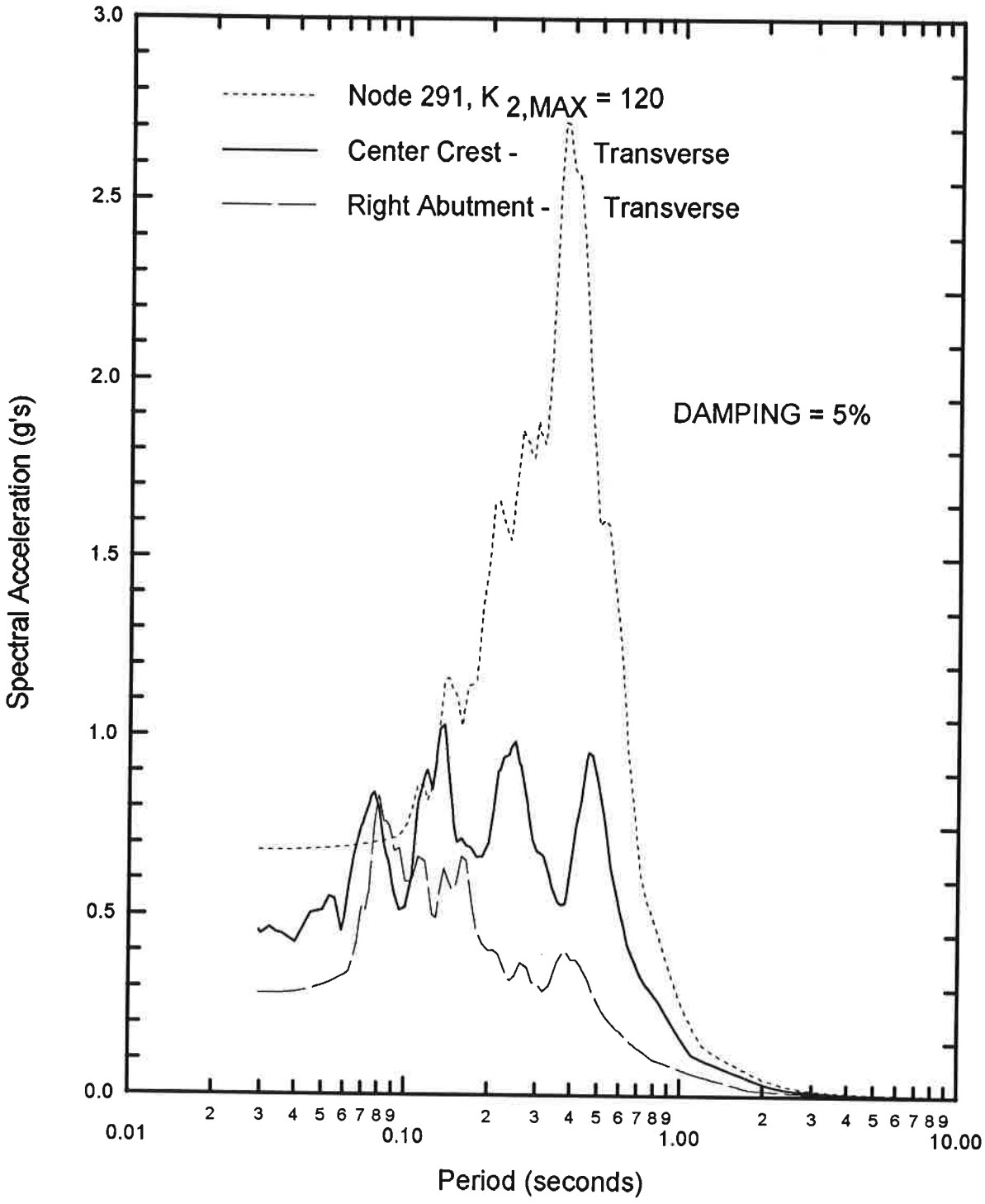

(a) Transverse Motions at the Center Crest

Figure 4-13: Calculated 3-D Dynamic Response Spectra: Sierra Madre Earthquake

LN291RS.GRF

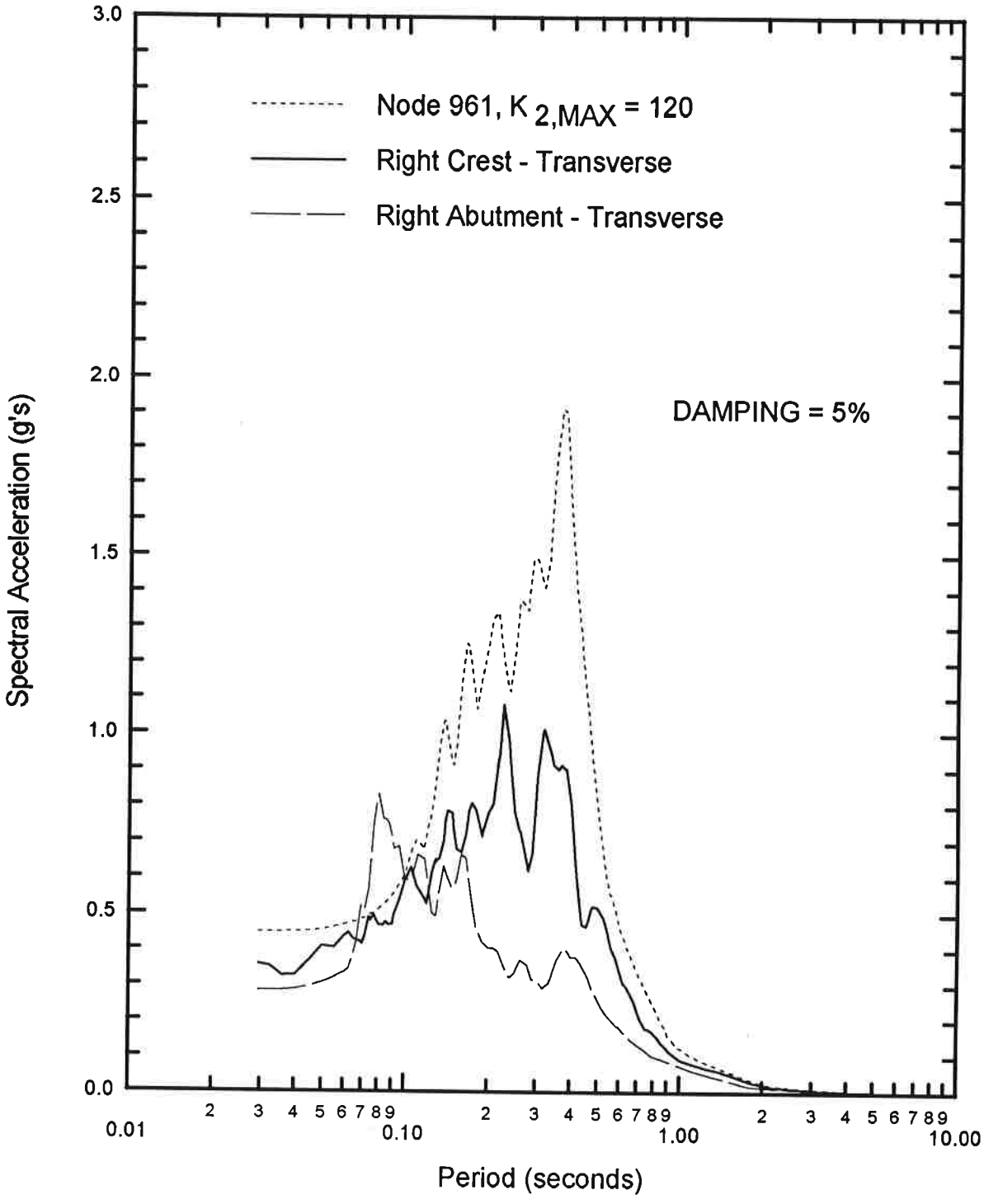

(b) Transverse Motions at the Right Crest

Figure 4-13: Calculated 3-D Dynamic Response Spectra:
Sierra Madre Earthquake

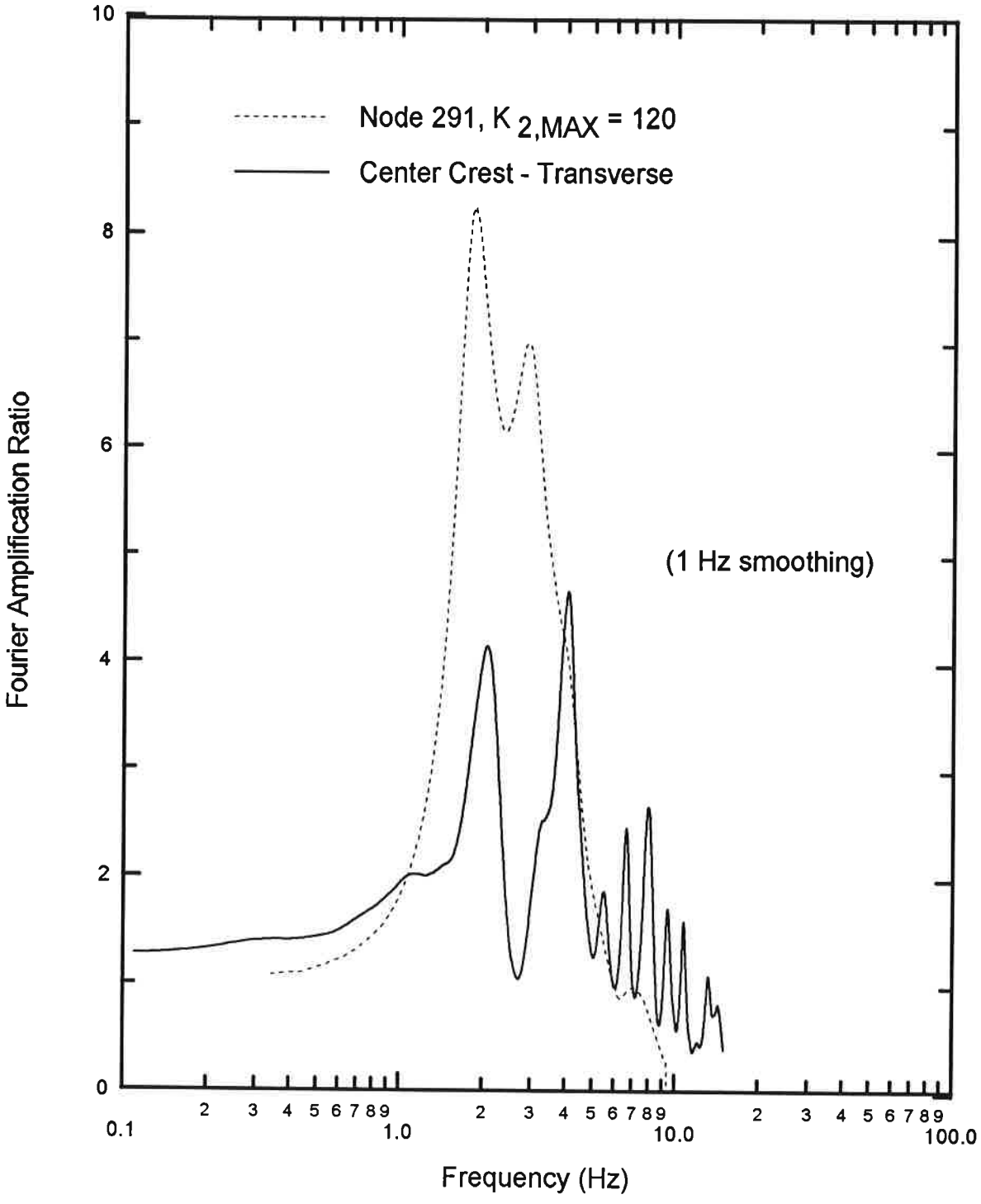

(a) Transverse Motions at the Center Crest

Figure 4-14: Calculated 3-D Fourier Amplification Ratios: Sierra Madre Earthquake

LNAMP291.GRF

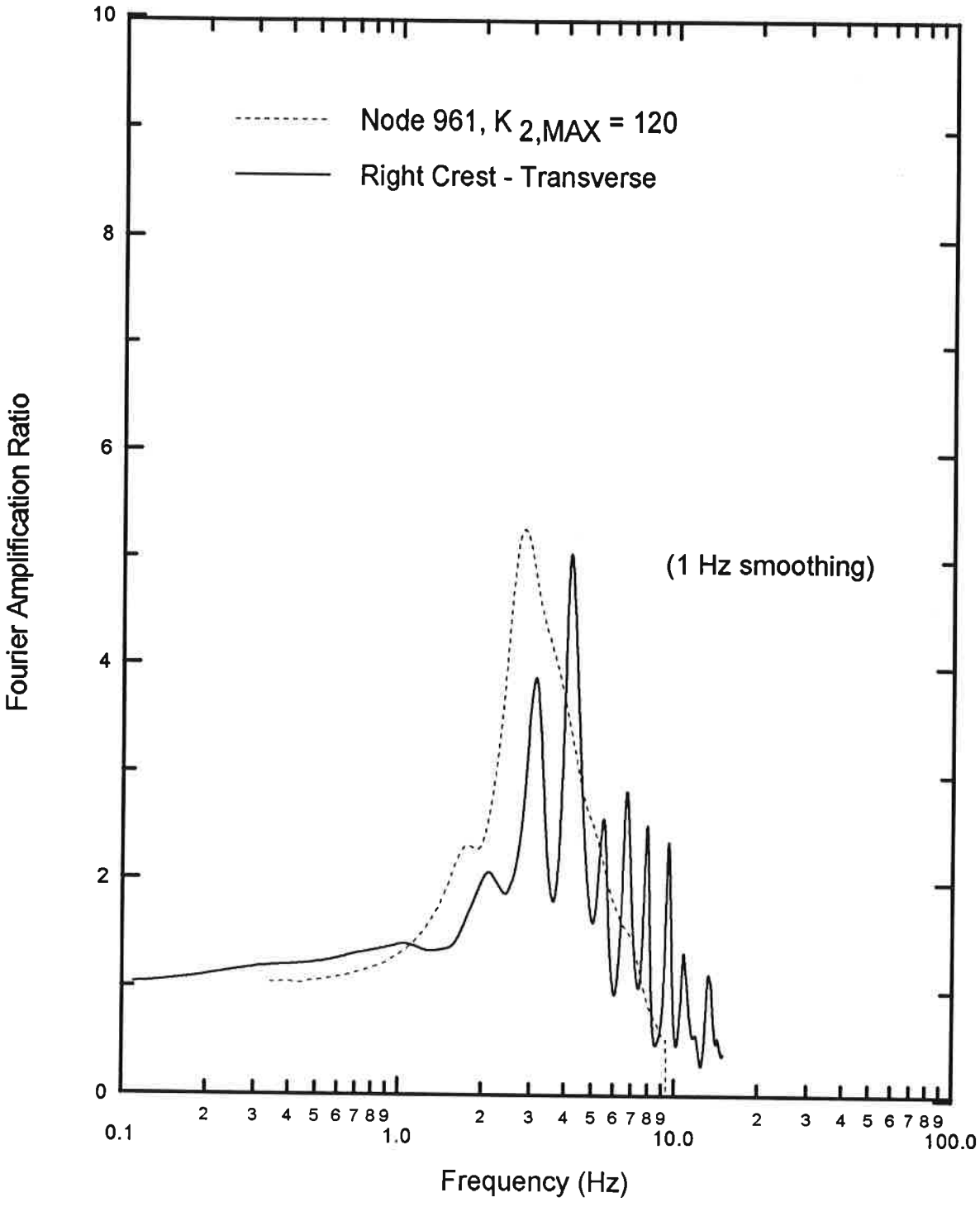

(b) Transverse Motions at the Right Crest

Figure 4-14: Calculated 3-D Fourier Amplification Ratios: Sierra Madre Earthquake

LNAMP961.GRF

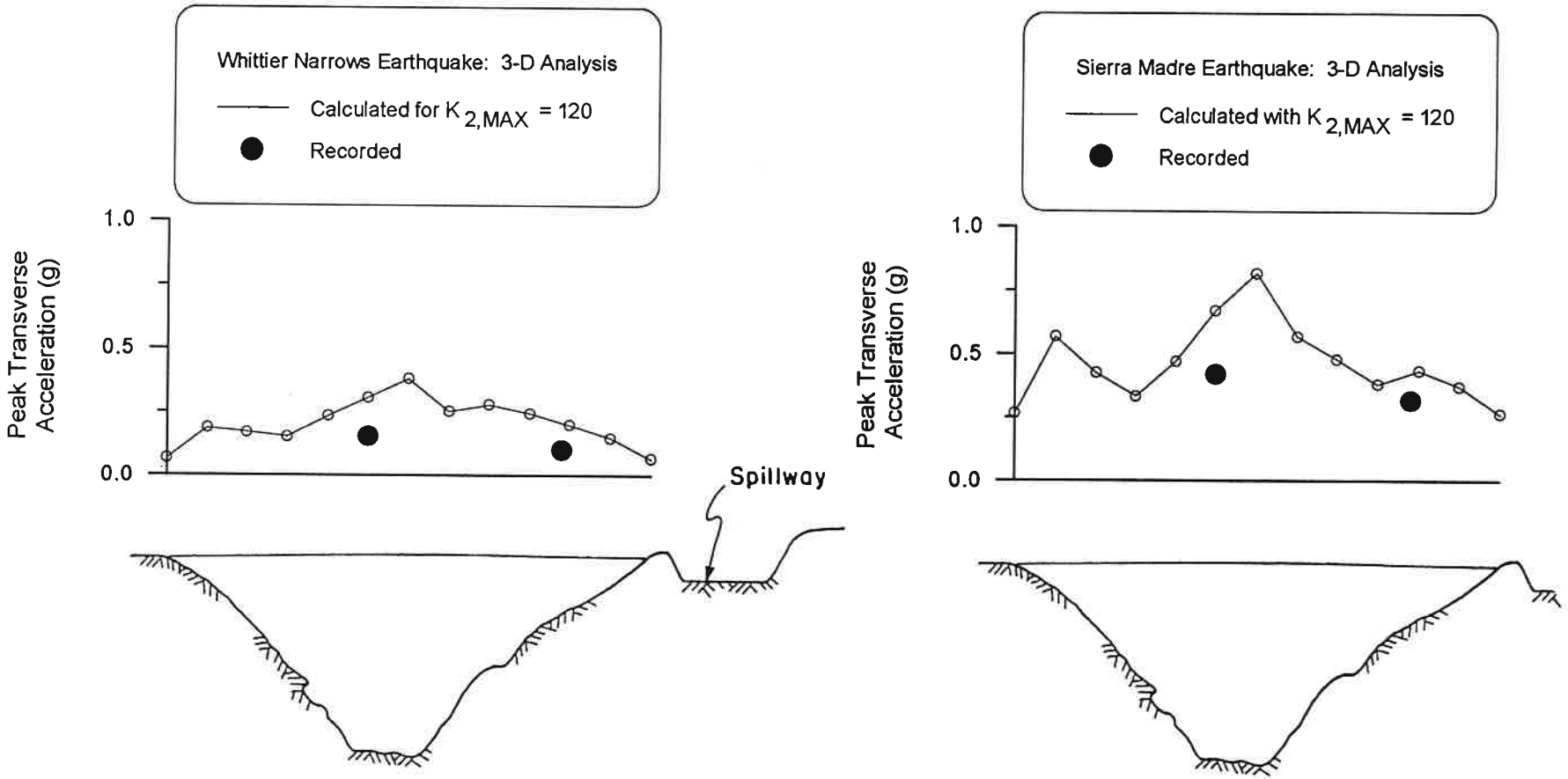

Figure 4-15: Peak Transverse Accelerations Computed From 3-D Analyses

5. DISCUSSION

5.1 Comparison of Calculated and Recorded Dynamic Response

In general, the 2-D and 3-D calculated dynamic responses of Cogswell Dam were greater than the recorded dynamic responses during both earthquakes. As discussed in Section 4, the 3-D analyses generally resulted in an overestimation of the crest's dynamic response characteristics by factors of about 1.6 to 2.6, and the 2-D analyses resulted in an overestimation of the crest's dynamic response characteristics by factors of about 1.1 to 1.9. The 2-D analyses using realistic $K_{2,max}$ values did show better agreement than the 3-D analyses in terms of peak crest accelerations, but this is attributed to the fact that the 2-D model is substantially softer than the 3-D model (or the prototype) and thus underestimates the contribution of the dam's first mode of response. Overall, the 3-D dynamic response analyses did no better than the 2-D dynamic response analyses in recreating the recorded response of the dam.

Possible explanations for the general over-prediction of dynamic response are the possible amplification of the abutment motions relative to those beneath the dam due to topographic effects, and the influence of dam-canyon interaction effects such as nonsynchronous foundation motions and radiation damping. These phenomena probably affect the dynamic response of dams in most cases, but to differing degrees. For example, it should be noted that the 2-D methods used in this study have been successful in providing good agreement between calculated and recorded dynamic responses for other dams (e.g., Bray et al. 1989; Mejia et al. 1991; Mejia et al. 1992; Mejia and Boulanger 1993).

The overestimation of the dam response during these earthquakes may be largely due to dam-canyon interaction effects. Dakoulas (1993) shed valuable insight on the role of dam-canyon interaction effects on the dynamic response using closed form solutions for the simplified condition condition of triangular dams in semi-cylindrical canyons (Fig. 5-1(a)). Dakoulas's analyses showed

that both radiation damping and spatial variability of motions had an increasingly important effect on dam response as the impedance ratio (IR) decreased. The impedance ratio is defined as:

$$IR = \frac{V_c}{V_d}\frac{\rho_c}{\rho_d}$$

where V_c and ρ_c are the shear wave velocity and density of the canyon material, respectively, and V_d and ρ_d are the shear wave velocity and density of the dam material, respectively. Fig. 5-1(b) shows the amplification ratio (AF on displacements) for IR values of 15, 10, 5, and 2.5. The amplification for IR=15 was essentially the same as for a perfectly rigid semi-cylindrical canyon, and show an AF of almost 10 at the first resonant frequency. The AF at the first resonant frequency decreased to about 6 at IR=5 and to about 3 at IR=2.5. The AF at the second resonant frequency decreases even more rapidly with decreasing IR than does the AF at the first resonant frequency. The reduction in amplification as IR decreases was attributed to increased radiation damping and increased destructive interference of nonsynchronous base motions (i.e., spatial variations in canyon response). Spatial variability of base motions increases: (1) for higher frequencies which correspond to shorter wave lengths; and (2) for smaller impedance ratios (IR) which correspond to smaller shear wave velocities in the canyon rock relative to that of the dam, and thus shorter wave lengths at a given natural frequency of the dam. The destructive interference of nonsynchronous base motions is reflected in Fig. 5-1 in that the reduction in AF with decreasing IR is especially important at higher frequencies.

The above results by Dakoulas can be qualitatively applied to Cogswell Dam by considering the expected approximate range of the impedance ratio (IR) insitu. The shear wave velocity in the foundation rock mass is roughly estimated to be between 1200 m/s and 1500 m/s based on the geologic data,the fact that the upstream concrete cutoff wall was excavated to depths of 4 m to 15

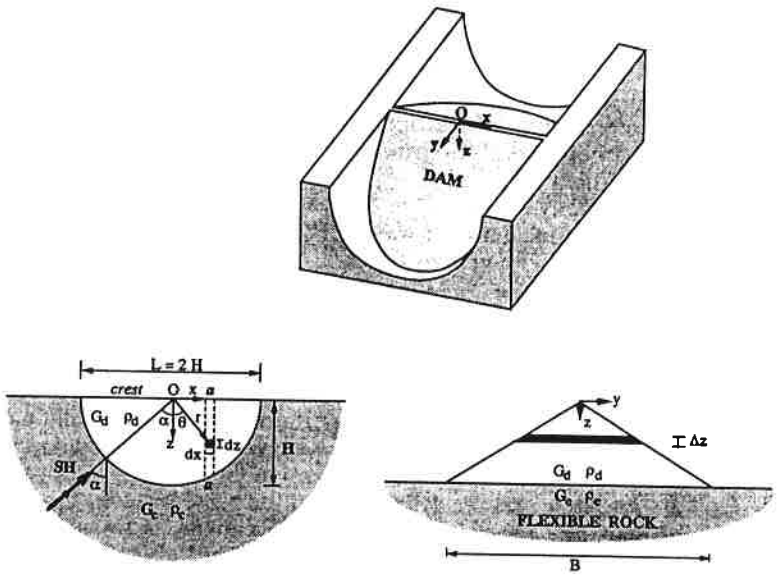

(a) Perspective View and Cross-Sections of Dam

Fig. 5-1: Effect of Impedance Ratio (IR) on Midcrest Amplifications of Dam in Semicylindrical Canyon and Plane-Strain Dam (Dakoulas 1993)

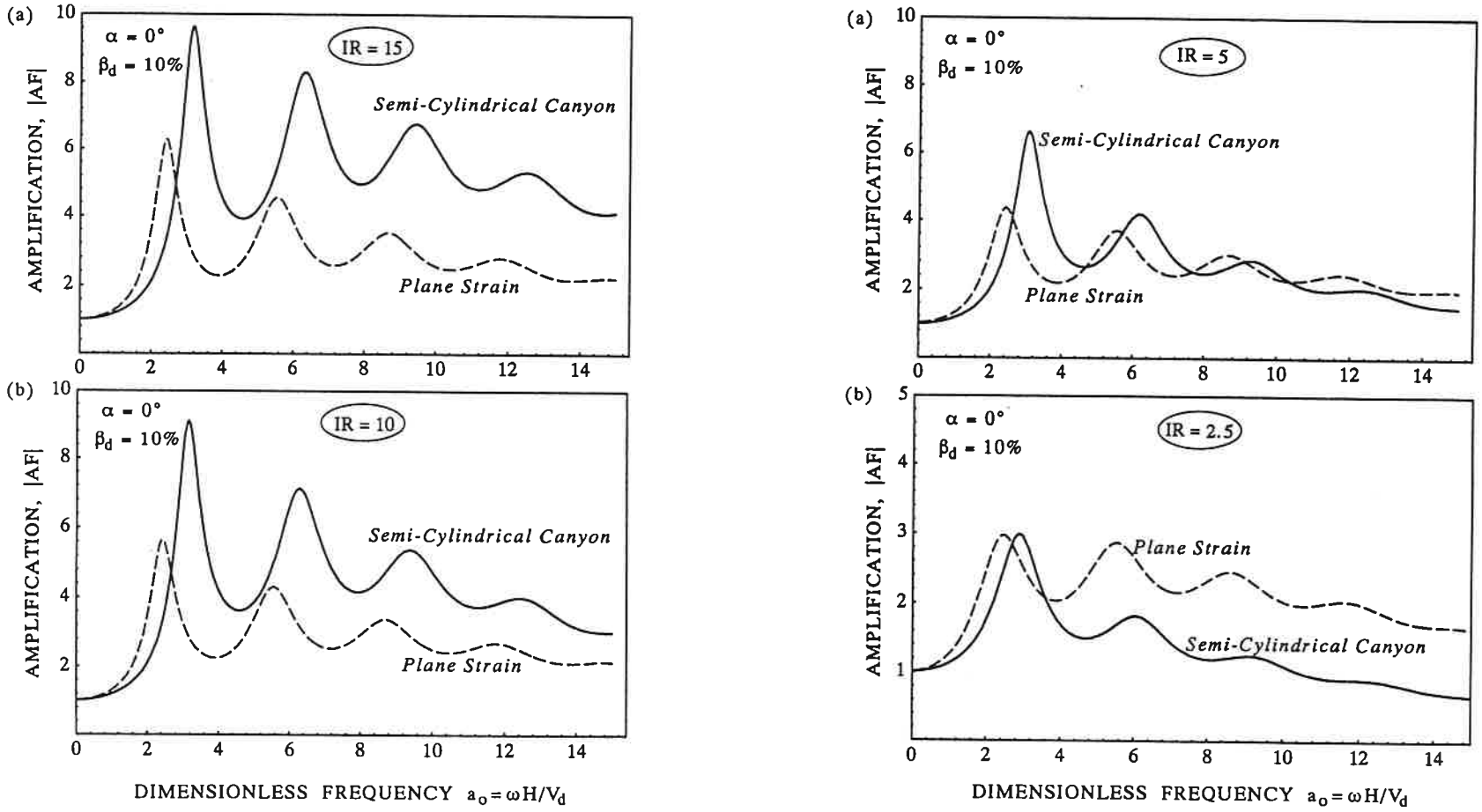

(b) Amplification Functions (AF) to Midcrest of the Dam Versus Dimensionless Frequency

Fig. 5-1: Effect of Impedance Ratio (IR) on Midcrest Amplifications of Dam in Semicylindrical Canyon and Plane-Strain Dam (Dakoulas 1993)

m using only mechanical equipment (no blasting was reported), and Caterpillar's (1991) guidelines for rippabillity versus shear wave velocity in igneous rocks. Since the shear wave velocity of the rockfill varies spatially and with the strength of shaking, a shear wave velocity in the rockfill near the foundation contact may be most appropriate for evaluating radiation damping effects, while an overall average shear wave velocity may be more appropriate for evaluating nonsynchronous motion effects. For the Sierra Madre Earthquake, the 3-D analyses suggest representative shear wave velocities in the rockfill of about 365 m/s near the foundation contact and about 290 m/s as an overall "average." Thus, the value of IR would be between 4.7 and 5.8 for radiation damping and between 5.9 and 7.3 for nonsynchronous motion. Using Dakoulas's results as guidelines and assuming that the first and second modes of response contribute equally to the overall dam response (as roughly indicated by the recorded motions), one would expect the FEM analyses (synchronous motion, no radiation damping) to over-predict the amplification ratios by about 50% to 90% for the Sierra Madre Earthquake. For the Whittier Narrows Earthquake, the 3-D analyses suggest representative shear wave velocities in the rockfill of about 425 m/s near the foundation contact and about 340 m/s as an overall "average." Thus, the value of IR would be between 4.0 and 5.0 for radiation damping and between 5.0 and 6.2 for nonsynchronous motion. Again, using Dakoulas's results as guidelines, one would expect the FEM analyses to overpredict the amplification ratios by about 70% to 140% for the Whittier Narrows Earthquake. The amount of over-prediction is expected to be greater for the Whittier Narrows Earthquake than for the Sierra Madre Earthquake because of the lower shaking levels and thus higher effective shear moduli and lower impedance ratios. This expected pattern is observed in the results of the 3-D dynamic analyses for which the peak center crest transverse accelerations were over-predicted by 100-140% for the Whittier Narrows Earthquake and by 60-80% for the Sierra Madre Earthquake. These qualitative estimates are in reasonably good agreement with the comparisons of calculated and recorded dynamic responses in this study, and thus it is reasonable

to conclude that radiation damping and nonsynchronous motions probably played major roles in the dynamic response of the dam.

Other topographic effects may also have contributed to amplification of the abutment motions relative to those beneath the dam, or possibly changes in the frequency content of the right abutment motion. The right abutment instrument is located behind the control house situated at the top of the vertical cut slope extending up from the right side of the spillway channel. At this point, the instrument is separated from the dam's right abutment contact by the spillway which is largely founded on a large shear zone (see Section 2). The positioning of the instrument seems conducive to differences between the recorded abutment motions and the dam's foundation.

5.2 Comparison of 2-D and 3-D Dynamic Response Analyses

Dynamic response analyses of embankments are most often concerned with estimating dynamic shear stresses and strains in order to predict deformations within the embankment: the preceding analyses, however, focused on the motion characteristics because this enabled a comparison of calculated and recorded dynamic responses. The differences between dynamic shear stresses predicted by 2-D and 3-D dynamic response analyses were found to be significant by Mejia and Seed (1983) for highly 3-D geometries. Fig. 5-2 shows how the difference was less than about 20% for a dam with length to height ratio of 6.8:1, but much greater for a dam with a length to height ratio of only 2:1 (particularly near the base of the dam). Similar comparisons were made in this study to confirm the general observations made by Mejia and Seed (1983).

Fig. 5-3 presents the ratio of the peak, dynamic, horizontal shear stresses in the transverse direction predicted in a 2-D analysis ($\tau_{xy,2D}$) to that predicted at the maximum cross-section in a 3-D analysis ($\tau_{xy,3D}$) using a $K_{2,max}$ value of 120 and the Siera Madre Earthquake. The maximum cross-section in the 3-D mesh matches the 2-D mesh except for the absence of a few elements near the downstream toe in the 3-D mesh. The 2-D analyses predict greater dynamic shear stresses near the

FIG5-2.GRF

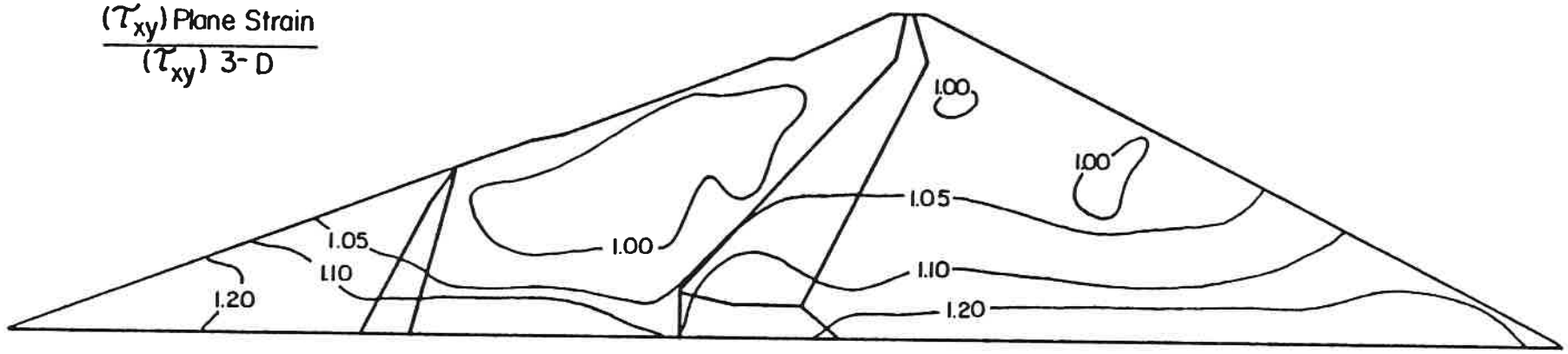

Figure 5-2 (a): Ratio of τ_{xy2D}/τ_{xy3D} Computed For Maximum Section of Oroville Dam With Length to Height Ratio of 6.8 (after Mejia and Seed, 1981)

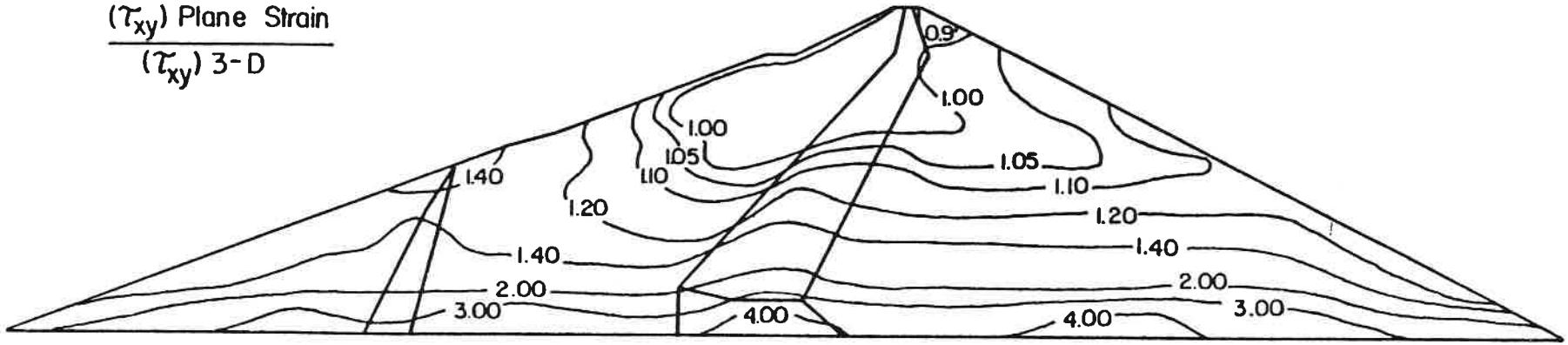

Figure 5-2 (b): Ratio of τ_{xy2D}/τ_{xy3D} Computed For Maximum Section of Dam With Valley Wall Slopes of 1:1 (after Mejia and Seed, 1981)

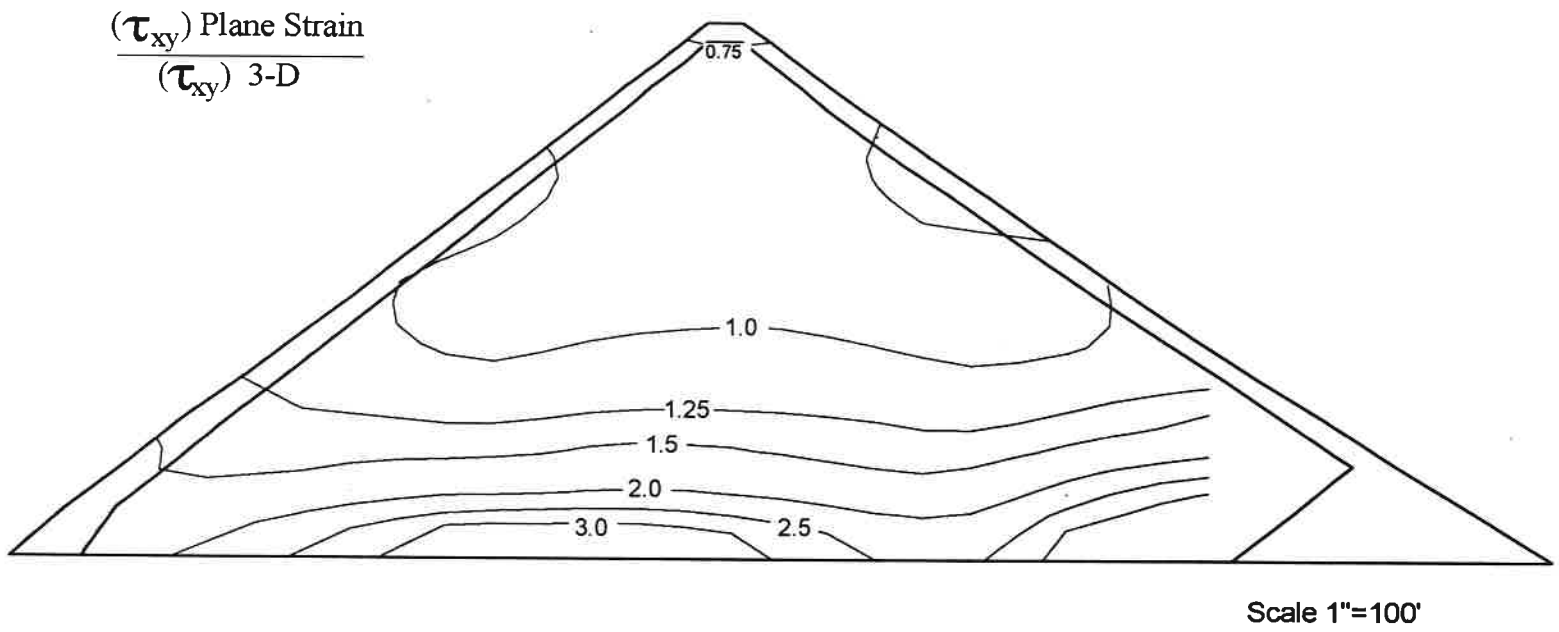

Figure 5-3: Ratio $\tau_{xy2D} / \tau_{xy3D}$ Computed For the Maximum Section of Cogswell Dam: $K_{2,max} = 120$, Sierra Madre Earthquake

base of the dam than do the 3-D analyses, with the ratio being about 3.0 along the lowest row of elements. The dynamic shear stresses in the 3-D elements near the base are probably reduced relative to the 2-D model by the constraining effects of the nearby, rigid foundation nodes. The ratio $\tau_{xy,2D}/\tau_{xy,3D}$ decreases towards the crest of the dam, where it becomes only about 0.75. The dynamic shear stresses in the 3-D elements at the crest are greater than in the 2-D model, which is consistent with the greater peak crest accelerations predicted by the 3-D models relative to the 2-D models.

Fig. 5-4 presents the ratio of the longitudinal to transverse peak, dynamic, horizontal shear stresses at the maximum cross-section in the 3-D analysis with a $K_{2,max}$ value of 120 for the Sierra Madre Earthquake. This ratio is less than 0.40 throughout most of the maximum cross-section, but does become larger near the base and crest of the dam. The longitudinal shear stresses are significant for this highly 3-D dam geometry, especially since the analysis only considers excitation in the transverse direction.

Fig. 5-5 presents the ratio of the transverse peak, dynamic, horizontal shear stress ($\tau_{xy,3D}$) to the maximum, peak, dynamic shear stress ($\tau_{max,3-D}$) at the maximum cross-section in the same 3-D analysis. This ratio is between 0.90 and 1.0 throughout most of the cross-section, but decreases to about 0.70 near the base and crest of the dam. These results are in good agreement with those of Mejia and Seed (1983) as shown in Fig. 5-6. Comparing Figs. 5-4 and 5-5, it appears that the difference between the transverse peak, dynamic, horizontal shear stress ($\tau_{xy,3D}$) and the maximum, peak, dynamic shear stress ($\tau_{max,3-D}$) corresponds closely to the influence of the longitudinal peak, dynamic, horizontal shear stress ($\tau_{xz,3D}$). This aspect of dynamic response is not captured by 2-D analyses and needs to be incorporated using appropriate judgement.

In general, the observations and recommendations made by Mejia and Seed (1983) regarding 2-D and 3-D dynamic response analyses were supported by the results of this study.

TXZDTXY.GRF

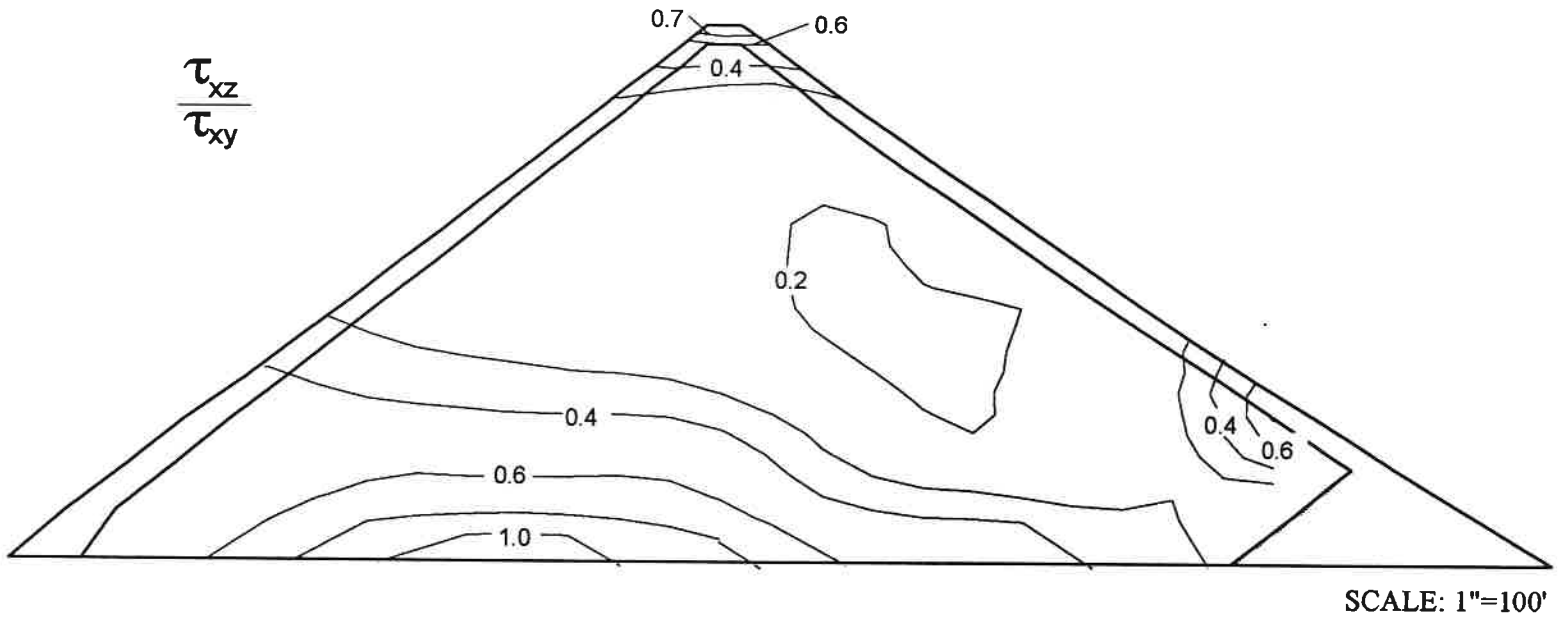

Figure 5-4: Ratio of τ_{xz}/τ_{xy} Computed for the Maximum Section of Cogswell Dam: $K_{2,max}$ = 120, Sierra Madre Earthquake

TXYDTMX.GRF

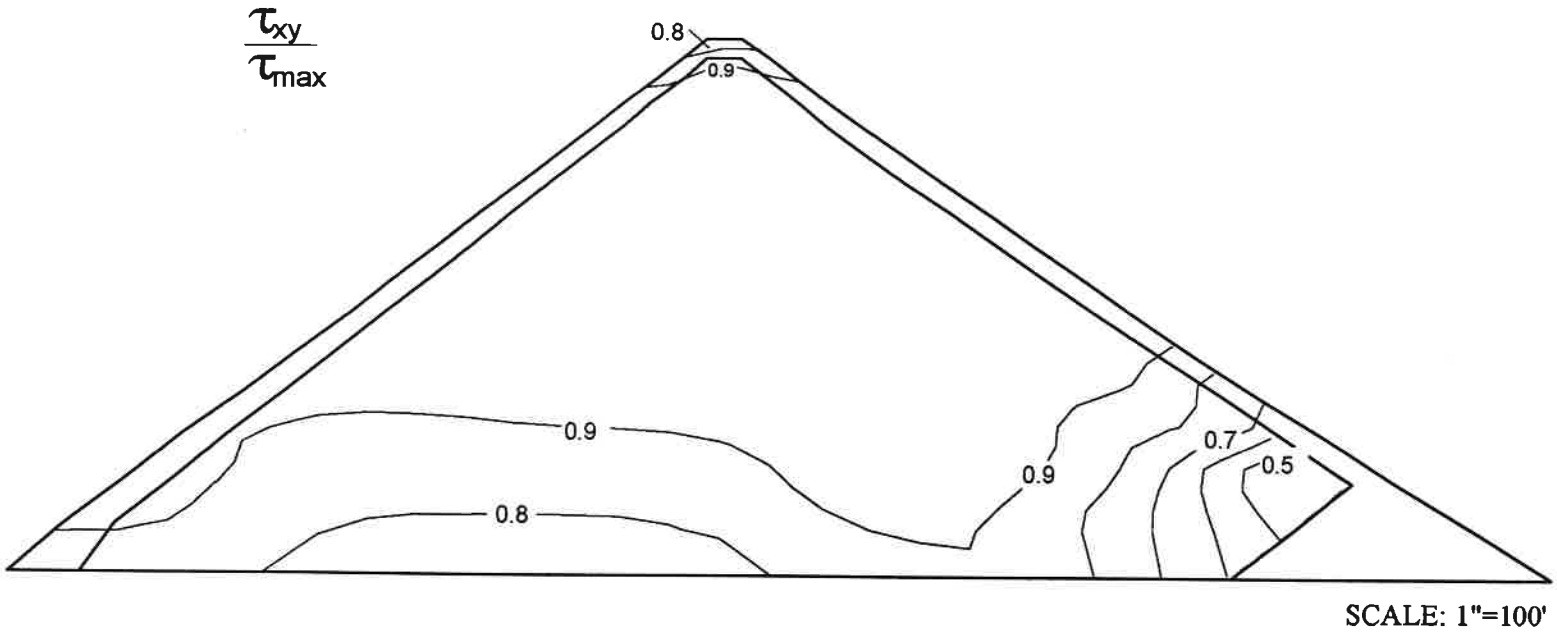

Figure 5-5: Ratio of τ_{xy}/τ_{max} Computed for the Maximum Section of Cogswell Dam: $K_{2,max}$ = 120, Sierra Madre Earthquake

FIG5-6.GRF

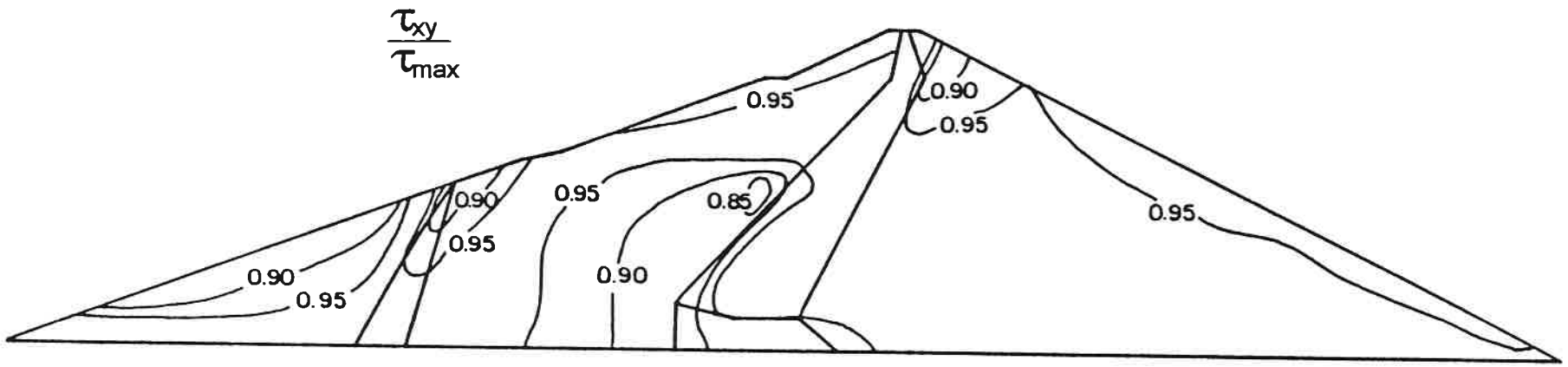

Figure 5-6 (a): Ratio of τ_{xy}/τ_{max} Computed For Maximum Section of Oroville Dam With Length to Height Ratio of 6.8 (after Mejia and Seed, 1981)

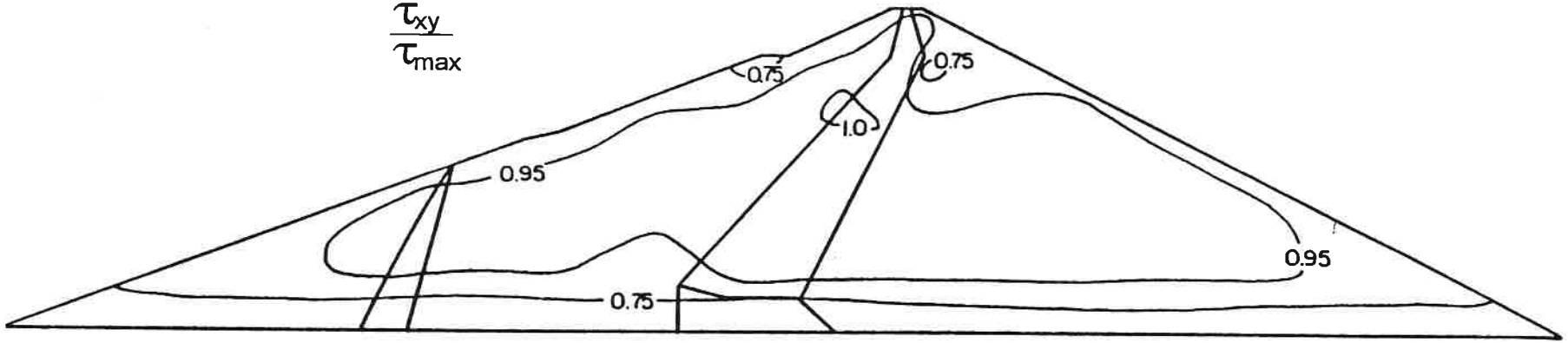

Figure 5-6 (b): Ratio of τ_{xy}/τ_{max} Computed For Maximum Section of Dam With Valley Wall Slopes of 1:1 (after Mejia and Seed, 1981)

5.3 Dynamic Properties of Rockfill

An estimate of the most representative $K_{2,max}$ value for the rockfill comprising Cogswell Dam can be made based on a comparison of the recorded and calculated fundamental periods. Such a comparison could be made using the results of the 2-D analyses, provided that an appropriate allowance is made for the stiffening effect of the actual 3-D geometry. Fig. 5-7 (after Mejia and Seed 1983) summarizes the results of several studies that provide comparisons between the fundamental frequency of 3-D dams with different crest length-to-height (L/H) ratios versus infinitely long dams with the same maximum cross-section and properties. For example, a shear beam analysis (assumes a constant shear wave velocity) of a triangular dam with a L/H ratio of 2.1:1 in a V-shaped canyon indicates that the 2-D (plane-strain) fundamental period is about 1.65 times greater than the 3-D fundamental period. However, a comparison of the 2-D and 3-D dynamic analyses of Cogswell Dam for the same $K_{2,max}$ value indicates that the ratio of the 2-D to 3-D calculated fundamental periods is about 1.4 even though the dam canyon is roughly V-shaped. This lower ratio of 2-D to 3-D fundamental periods results from the nonlinearity of the soil properties: the stiffer 3-D model responds more strongly to the input motions, experiences generally greater shear strains, and thus has slightly smaller shear wave velocities than a 2-D model having the same low strain shear modulus (or $K_{2,max}$ value). For this reason, a certain amount of judgement is needed in selecting an appropriate correction factor from Fig. 5-7 for application to 2-D dynamic response analysis results.

An estimate of the $K_{2,max}$ for the rockfill was obtained by comparing the fundamental period calculated by the 3-D analyses with the recorded values for both the Whittier Narrows and Sierra Madre earthquakes. The appropriateness of such a comparison, however, requires that the FE model correctly reflect the range of shear strains induced in the dam by these earthquakes. As discussed earlier, the 3-D analyses over-predicted the response of the dam and are thus likely to have also over-predicted the induced shear strains. Two approaches were used to approximately compensate for the

FIG5-7.GRF

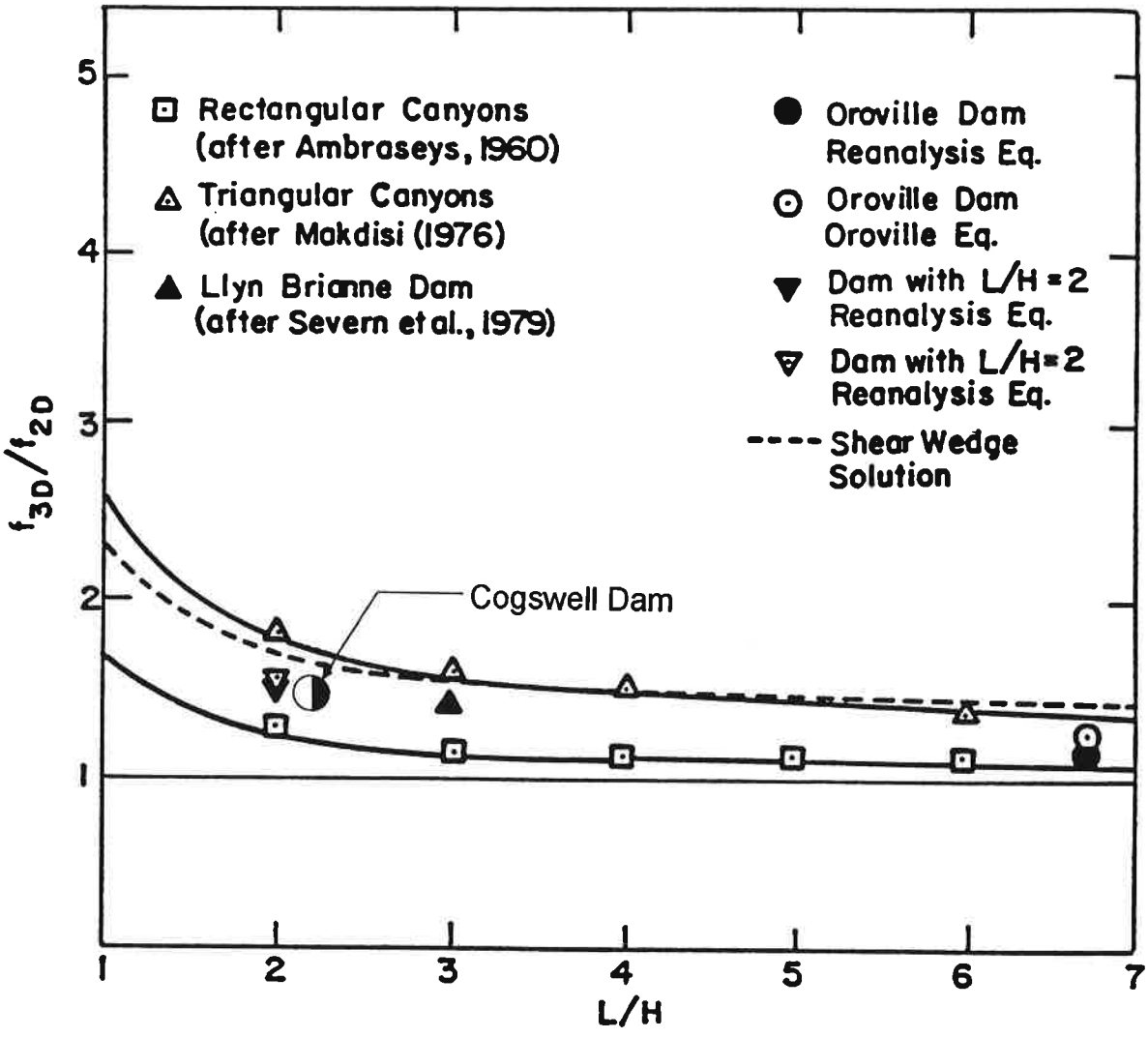

Figure 5-7: Comparison Between Natural Frequencies Computed From 2-D and 3-D Analyses of Dams in Triangular and Rectangular Canyons (after Mejia and Seed, 1981)

apparent over-prediction of dam response. The first approach attempted to compensate for any topographic effects present in the right abutment motion by constructing a pseudo-foundation motion by dividing the recorded crest motions by the Fourier transfer functions provided by the 3-D response analyses. This approach required iterating on one of the crest motions to account for the nonlinearity of the transfer function with respect to the induced shear strains, and thus only one recorded motion can be "deconvolved" at a time. The resulting pseudo-foundation motions corresponding to the "deconvolved" right crest and center crest motions were not very similar in frequency content which indicates that dam-canyon interaction effects were significant in addition to any topographic effects in the recorded abutment motion. Consequently, the second approach was to simply scale the recorded abutment motion by a factor of 0.5 before input to the analysis, and thus reduce the peak crest accelerations to values more closely reflective of recorded values. This approach was considerable less involved, and appears to be just as valid an approximation given the complexity of the problem and the uncertainties involved in any approximate compensation for the over-prediction of dynamic response.

The relationships between the $K_{2,max}$ value (using a gravel curve for modulus degradation) and the calculated fundamental period of the dam for the Whittier Narrows and Sierra Madre earthquakes are presented in the upper two plots of Fig 5.8. For the Whittier Narrows Earthquake, the fundamental period of the dam was estimated to be between 0.37 and 0.42 seconds (Section 3) for which a $K_{2,max}$ of between 120 and 145 would provide the best agreement. For the Sierra Madre Earthquake, the fundamental period of the dam was estimated to between 0.45 and 0.48 seconds for which a $K_{2,max}$ of between 125 and 140 would provide the best agreement. The above estimates of $K_{2,max}$ correspond to different levels of earthquake-induced shear strain, but the difference in strain levels is not sufficient to provide a very broad test of the most appropriate dynamic rockfill properties.

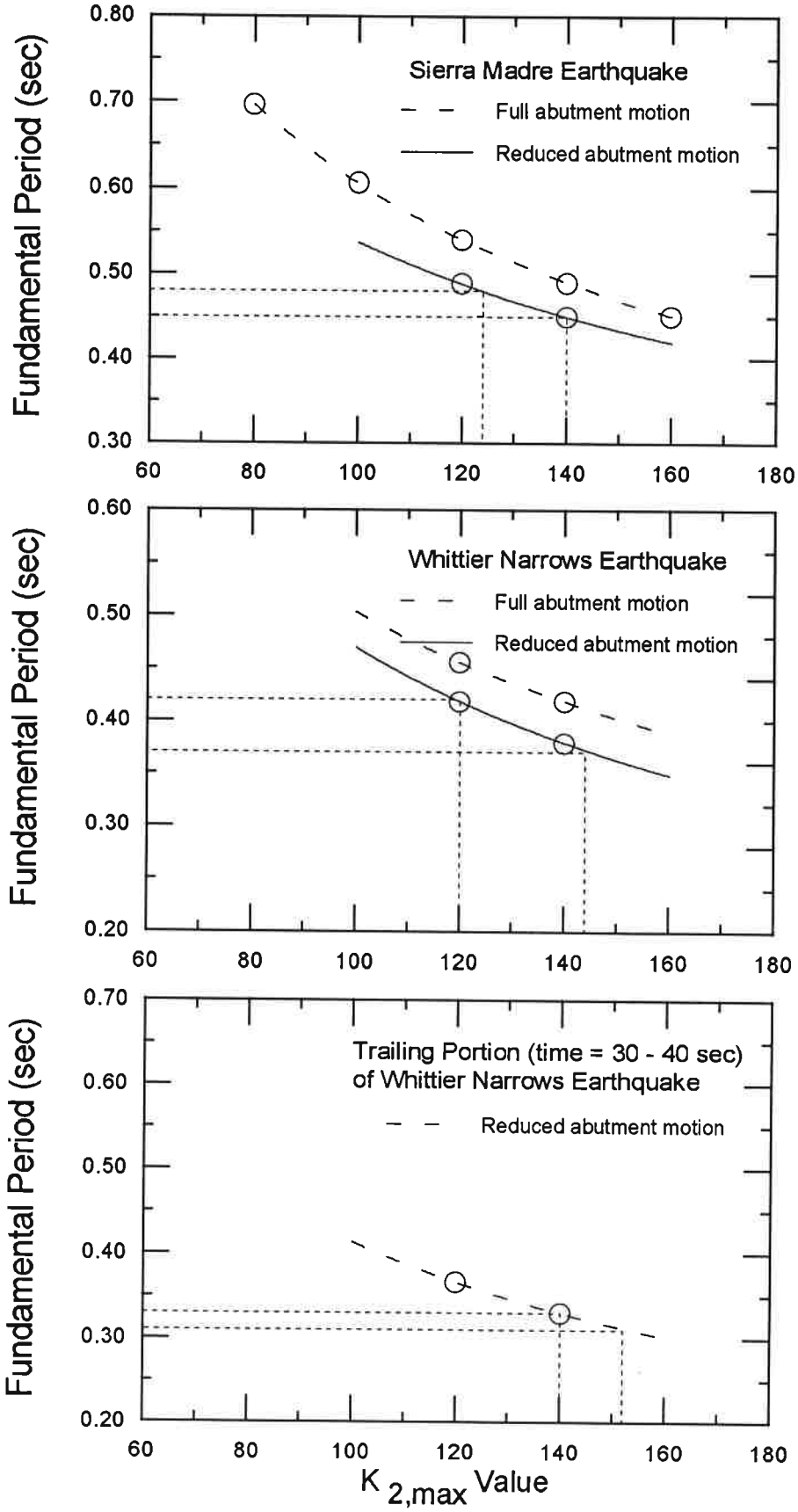

Figure 5-8: Fundamental Period of 3-D FEM Model Versus $K_{2,max}$ Value Using the Median Gravel Modulus Degradation Relationship

K-TP-ALL.GRF

To evaluate the appropriateness of the selected modulus degradation relationship, the trailing portions (times between 20 and 40 seconds after triggering of the instruments) of the Whittier Narrows and Sierra Madre earthquakes were analyzed further. The trailing portions of these earthquake records are of small amplitude, but their amplitudes are still substantially greater than typical SMIP instrumentation noise (Shakal and Ragsdale 1984). The response spectra for the center crest motion and the Fourier amplification ratios from the right abutment to the center crest for the trailing portions (20-40 seconds; 30-40 seconds) of these two earthquakes are presented in Fig. 5-9 and 5-10, respectively. The fundamental period of the dam appears to have been between about 0.31 and 0.33 seconds for the low level vibrations at the ends of these two earthquakes. The lower plot in Fig. 5-8 shows the relationship between the $K_{2,max}$ value and calculated fundamental period of the dam based on 3-D dynamic response analyses using a trailing portion of the Whittier Narrows Earthquake as input. The calculated strain levels are very low under this level of input excitation (a representative effective shear strain of about $3.0 \times 10^{-4}\%$), such that degradation of the modulus is quite small. Based on these data, the appropriate $K_{2,max}$ value would be between 140 and 155 for use with the modulus degradation relationship for gravel. These results are consistent with those obtained for the full earthquake motions.

The choice of modulus degradation relationship directly affects the $K_{2,max}$ value providing the best agreement with the recorded fundamental periods. It is, however, relatively straight-forward to determine equivalent combinations of $K_{2,max}$ values and modulus degradation curves which result in practically identical calculated fundamental periods of the dam. The dynamic analyses calculate effective shear moduli that are consistent with the level of induced shear strain in each element based on the low-strain (maximum) shear moduli (defined by $K_{2,max}$) and the modulus degradation curve. To illustrate this, the effective shear moduli are plotted against the effective shear strains (Fig. 5-11) calculated for individual elements in the 3-D analysis using $K_{2,max} = 120$, the gravel degradation curve,

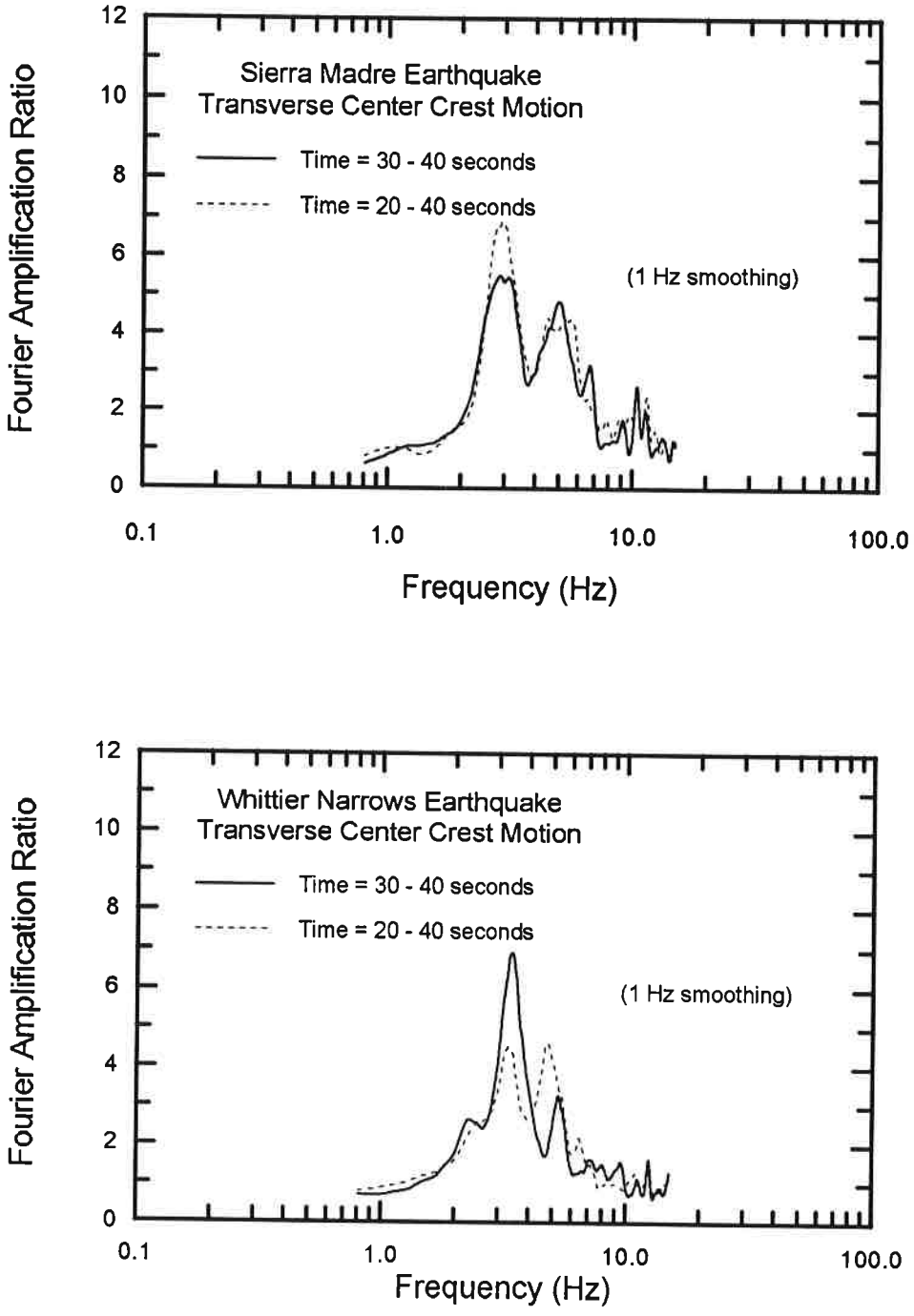

Figure 5-9: Fourier Amplification Ratios for the Trailing Portion of the Transverse Motions Recorded at the Center Crest

FAMPTAIL.GRF

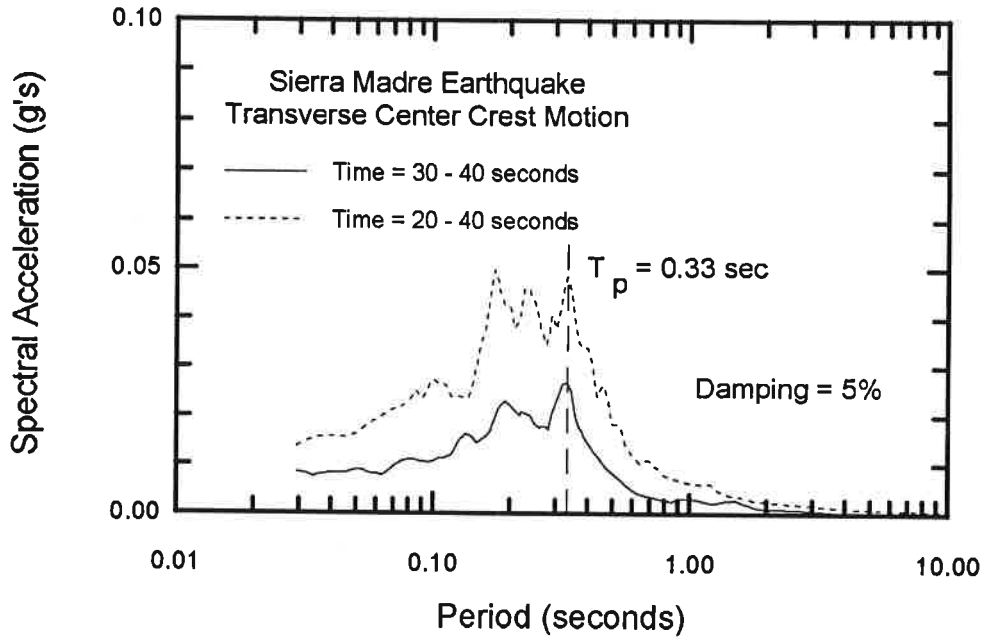

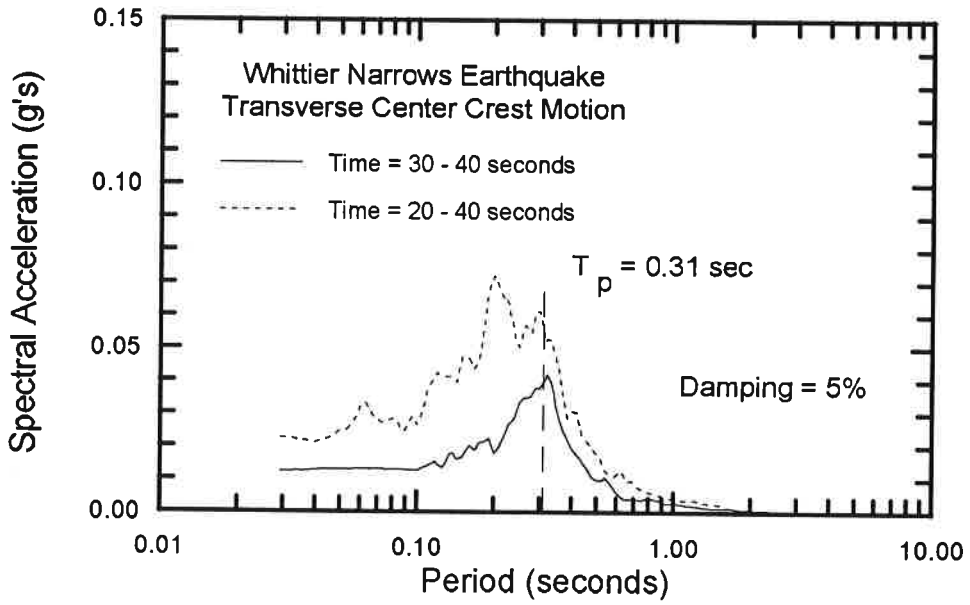

Figure 5-10: Response Spectra for the Trailing Portion of the Transverse Motions Recorded at the Center Crest

and the Sierra Madre Earthquake motion. The open circles in Fig. 5-11 represent all the elements except the highest and lowest 5%. Also shown on Fig. 5-11 are shear modulus versus shear strain curves corresponding to the sand and gravel modulus degradation curves which could satisfactorily reproduce the same analysis result. Boulanger et al. (1993) obtained essentially identical response spectra using such equivalent combinations for 2-D analyses of Cogswell Dam. Thus, equivalent $K_{2,max}$ values for the sand modulus degradation curve can be obtained from diagrams such as shown on Fig. 5-10, or from Tables 4-1 and 4-2 by simply using the typical effective shear strains and then scaling the $K_{2,max}$ value for a gravel curve by the ratio of the corresponding G/G_{max} values for the gravel and sand curves, respectively.

Thus, equivalent agreement between the recorded and calculated 3-D fundamental periods of Cogswell Dam for the Whittier Narrows and Sierra Madre Earthquakes can be obtained using $K_{2,max}$ values of 90 to 105 with the median sand modulus degradation relationship (Seed et al. 1984) or $K_{2,max}$ values of 120 to 140 with the gravel modulus degradation relationship (Seed et al. 1984). For the results obtained using the trailing portions of these earthquakes, however, the appropriate $K_{2,max}$ values would be between 130 and 145 with the median sand modulus degradation relationship and 140 to 155 for the gravel modulus degradation relationship. Thus, the results of these analyses suggest that the gravel modulus degradation relationship is more appropriate because a consistent range of $K_{2,max}$ values was obtained over the full range of induced shear strains, while the sand degradation relationship resulted in inconsistent estimates of $K_{2,max}$. This finding should be further explored, perhaps through the collection of seismic micro-tremor data to confirm the estimated low strain fundamental period of the dam.

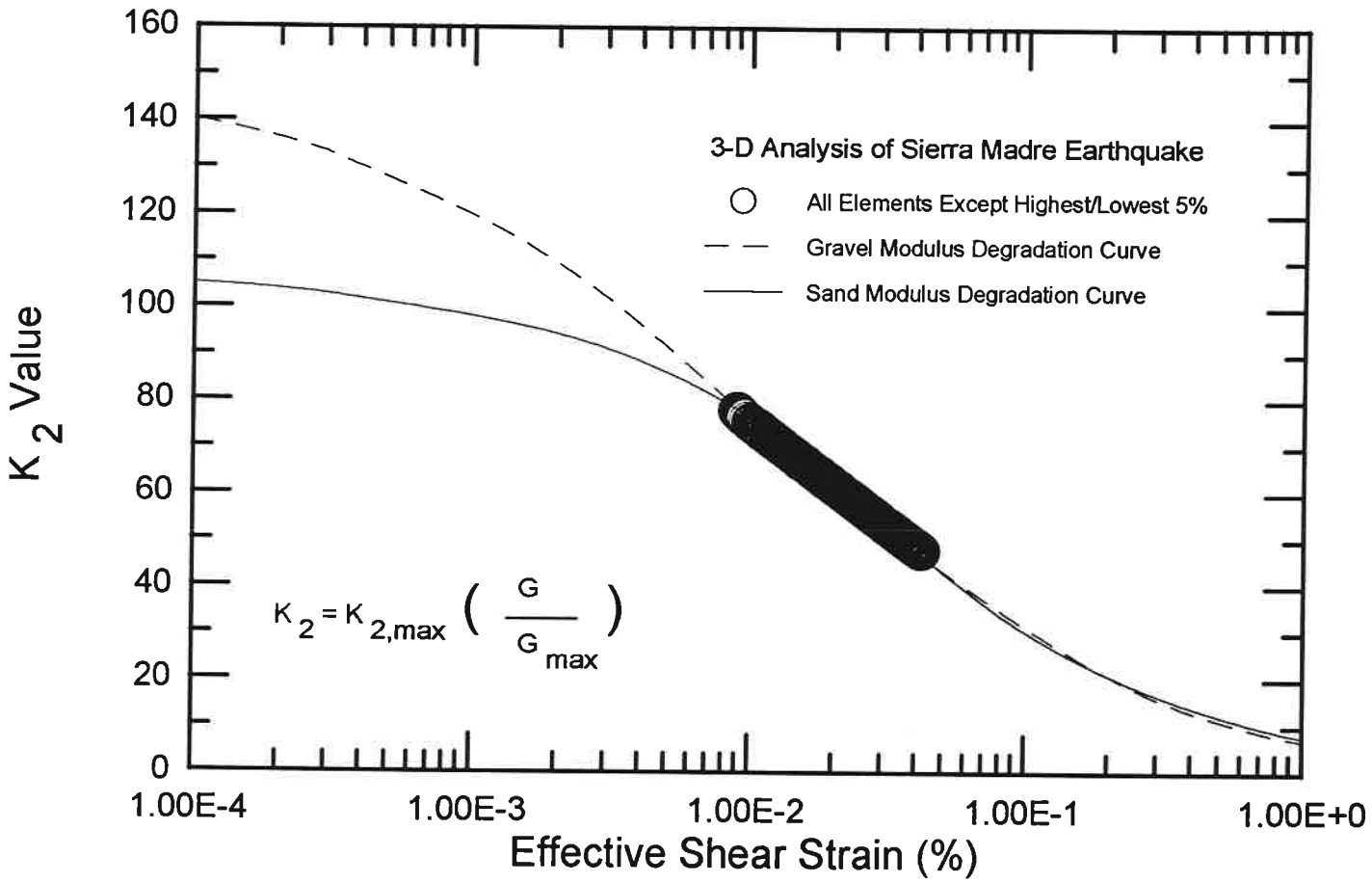

Figure 5-11: Equivalent Combinations of $K_{2,max}$ and Modulus Degradation Curves for 3-D Analysis

GGMAX-1.GRF

6. SEISMICALLY-INDUCED PERMANENT DEFORMATION ANALYSES

The presently available engineering methodologies for estimating seismically-induced permanent deformations in rockfill dams are not well refined and need to be viewed with considerable engineering judgement. It is interesting, however, to perform a deformation analysis using the parameters adopted in previous engineering studies of the dam prior to the Sierra Madre Earthquake. As part of a geotechnical investigation of Cogswell Dam, the LACFCD (1980) estimated that the pseudo-static yield acceleration for potential slip surfaces through the dam is 0.21 g. For the Sierra Madre Earthquake, the maximum average acceleration (k_{max}) for potential sliding masses is estimated to be about 0.3 g based on the recorded motions and the relationships between peak crest accelerations and maximum average accelerations presented by Makdisi and Seed (1978). Thus, the ratio of k_y/k_{max} was 0.7 for which the Makdisi-Seed (1978) procedure for estimating dam and embankment earthquake-induced deformations predicts permanent deformations for a M = 6.5 earthquake to be less than 38 mm. Since the 1991 Sierra Madre event was only a M_L = 5.8 event, the predicted seismically-induced permanent deformations would be less than 25 mm. A Newmark (1965) double-integration of the recorded crest acceleration-time history scaled to a peak acceleration of 0.3 g was also performed. This approach predicted permanent deformations due to the Sierra Madre event to also be less than 25 mm. These estimates are in good agreement with the observed maximum deformations of 41 mm vertical and 16 mm horizontal at the dam crest, and with previous experiences regarding the performance of rockfill dams during earthquake loading. It should be noted that the observed deformations may be partly due to seismically-induced volumetric strains in the rockfill and not due to rigid-body deformation as assumed by a Newmark-type analysis. For this reason, the results of a Newmark-type analysis should be viewed only as a rough indicator of seismic performance.

7. SUMMARY AND CONCLUSIONS

Cogswell Dam, a 85-m high concrete-faced, loosely dumped rockfill dam, experienced a peak transverse crest acceleration of 0.42 g during the 1991 Sierra Madre Earthquake. The dam performed well with a maximum deformation of about 41 mm at the crest and with relatively minor cracking in limited portions of the upstream concrete facing. The good performance of the dam is consistent with previous experiences and with simplified seismically-induced permanent deformation analyses.

Two- and three-dimensional FEM dynamic response analyses of Cogswell Dam during the 1987 Whittier Narrows and 1991 Sierra Madre earthquakes were presented. An assessment of the results indicate that both the 2-D and 3-D dynamic response analyses were limited in their ability to accurately model the observed dam response, and in general, tended to over-predicted the recorded dam response. Dam-canyon interaction effects (nonsynchronous foundation motion, and radiation damping) appear to have had a strong influence on the response of Cogswell Dam, based on estimates of the impedance ratio between the dam and its foundation and using the analytical solutions presented by Dakoulas (1993). These simplified analyses may prove useful for evaluating potential dam-canyon interaction effects, and thus indicate when the available dynamic response analysis programs can reasonably be expected to model prototype response.

It is important to note that dynamic response analyses of dams are most valuable for estimating dynamic shear stresses and strains throughout a dam, whereas the current study has focussed on motion characteristics since these are what the recorded motions provide. Furthermore, the present study has used dynamic response analysis codes which are commonly used in practice (in the case of 2-D) or their equivalent (in the case of 3-D). The over-prediction of the dynamic response of Cogswell Dam in this study, which leads to conservative estimates of induced dynamic shear stresses, illustrates that more sophisticated analysis methods may prove beneficial in certain situations

(such as a marginally stable dam on a compliant foundation).

Estimates of the dynamic rockfill properties were obtained by comparing recorded and calculated 3-D fundamental periods of the dam during the Whittier Narrows and Sierra Madre earthquakes. The insitu rockfill stiffness during the strong shaking of these earthquakes was best represented by: (1) $K_{2,max}$ values of 120 to 140 when using the median modulus degradation curve proposed for gravel by Seed et al. (1984), or (2) $K_{2,max}$ values of 90 to 105 when using the median modulus degradation curve proposed for sands by Seed et al. (1984). The insitu rockfill stiffness during the low strain, trailing portions of these earthquakes was best represented by: (1) $K_{2,max}$ values of 140 to 150 when using the median modulus degradation curve proposed for gravel by Seed et al. (1984), or (2) $K_{2,max}$ values of 130 to 140 when using the median modulus degradation curve proposed for sands by Seed et al. (1984). These analyses indicate that the median modulus degradation curve for gravel provides a more consistent representation of the insitu degradation of the dam's stiffness than is provided by the median modulus degradation curve for sands. Therefore, the insitu dynamic properties of the rockfill comprising the body of Cogswell Dam appear to be reasonably represented by a $K_{2,max}$ value of 120 to 140 with the median modulus degradation relationship proposed for gravels by Seed et al. (1984).

It is recommended that the right crest instrument be relocated to the left (or right) abutment, close to the dam-abutment contact. The new position would allow an evaluation of dam-canyon interaction effects in future earthquakes, including a comparison between the existing right abutment instrument and the new abutment instrument location. This alteration would not require purchase of new equipment. If funding permitted, the evaluation of dam-canyon interaction effects would benefit from an additional instrument located near the downstream toe of the dam.

REFERENCES

Boulanger, R. W., Bray, J. D., Chew, S. H., Seed, R. B., Mitchell, J. K., and Duncan, J. M. (1991). "SSCOMPPC: A Finite Element Analysis Program for Evaluation of Soil-Structure Interaction and Compaction Effects." Geotechnical Engineering Report No. UCB/G/91-02, University of California, Berkeley, April.

Boulanger, R. W., Bray, J. D., and Seed, R. B. (1993). "Response of Two Dams in the 1987 Whittier Narrows Earthquake." Third International Conference on Case Histories in Geotechnical Engineering, St. Louis, MO, June 1-4.

Bray, J. D., Seed, R. B. and Boulanger, R. W. (1990). "Investigation of the Response of Puddingstone and Cogswell Dams in the Whittier Narrows Earthquake of October 1, 1987: Volume I: Puddingstone Dam." Report No. UCB/GT/90-01, Univ. of Calif., Berkeley, June.

Caterpillar (1991). Caterpillar Performance Handbook, 22nd Edition, CAT publication by Caterpillar, Inc., Peoria, Illinois, U.S.A., October.

Dakoulas, P. (1993). "Earth Dam-Canyon Interaction Effects for Obliquety Incident SH Waves." J. Geotechnical Engineering, ASCE, Vol. 119, No. 11, Nov., pp. 1696-1716.

Duncan, J. M., Byrne, P., Wong, K. S., and Mabry, P. (1980). "Strength, Stress-Strain and Bulk Modulus Parameters for Finite Element Analyses of Stresses and Movement in Soil Masses." Geotechnical Engineering Research Report No. UCB/GT/80-01, University of California, Berkeley.

Lefebvre, G. and Duncan, J. M. (1971). "Three Dimensional Finite Element Analyses of Dams." Geotechnical Engrg. Report No. TE 71-5 to U.S. Army Engineers Waterways Experiment Station, University of California, Berkeley, May.

Harder, L. F. Jr. (1992). "Performance of Earth Dams During the Loma Prieta Earthquake." Proc. 2nd International Conference on Recent Advances in Geotechnical Earthquake Engineering and Soil Dynamics, March 11-15, St. Louis, MO. pp. 1613-1629.

Huang, M., Shakal, A., Darragh, R., Ventura, C., Cao, T., Sherburne, R., Fung, P., Wampole, J., DeLisle, M., and Petersen, C. (1991). "CSMIP Strong-Motion Records from the Sierra Madre, California Earthquake of 28 June 1991." Report No. OSMS 91-03, California Dept. Mines and Geology, Sacramento, August.

Kagawa, T., Mejia, L. H., Seed, H. B., and Lysmer, J. (1981). "TLUSH: A Computer Program for the Three-Dimensional Analysis of Earth Dams." Report No. UCB/EERC-81-14, Univ. of California, Berkeley, September.

Konno, T., Suzuki, Y., Tateishi, A., Ishihara, K., Akino, K, Iizuka, S. (1993). "Gravelly Soil Properties by Field and Laboratory Test." Third International Conference on Case Histories in Geotechnical Engineering, St. Louis, MO, June 1-4.

Lai, S. S. (1985). "Analysis of the Seismic Response of Prototype Earth and Rockfill Dams." Ph. D. dissertation, Univ. of California, Berkeley, Dec.

Los Angeles County Flood Control District (1980). "Geotechnical Investigation of Cogswell Dam." An internal report prepared by the LACFCD, October.

Lysmer, J., Udaka, T., Tsai, C.F. and Seed, H. B. (1975). "FLUSH: A Computer Program for Approximate 3-D Analysis of Soil-Structure Interaction Problems." Report No. UCB/EERC-75-30, Univ. of California, Berkeley, November.

Makdisi, F. I., and Seed, H. B. (1978). "Simplified Procedure for Estimating Dam and Embankment Earthquake-Induced Deformations." Journal of the Soil Mechanics and Foundations Division, ASCE, Vol. 104, No. GT7, July, pp. 849-867.

Mejia, L. H. and Seed, H. B. (1983). "Comparison of 2-D and 3-D Dynamic Analyses of Earth Dams." Journal of the Soil Mechanics and Foundation Division, ASCE, Vol. 109, No. GT11, November, pp. 1383-1398.

Mejia, L. H., Sykora, D. W., Hynes, M. E., Fong, K., and Koester, J. P. (1991). "Measured and Calculated Dynamic Response of Rock-Fill Dam." Proc., Second International Conference on Recent Advances in Geotechnical Earthquake Engineering and Soil Dynamics, March 11-15, St. Louis, Missouri.

Mejia, L. H., Sun, J. I., Salah Mars, S., Moriwaki, Y. and Beikae, M. (1992). "Nonlinear Dynamic Response Analysis of Lexington Dam." Proc., CSMIP92 Seminar on Seismological and Engineering Implications of Recent Strong Motion Data, Sacramento, CA, May 21.

Newmark, N. M. (1965). "Effects of Earthquakes on Dams and Embankments." Geotechnique, London, England, Vol. 5, No. 2, June.

Romo, M. P., Ayala, G., Resendiz, D., and Diaz, C. R. (1980). "Response of El Infiernillo and La Villita Dams." Mexican Comision Federal de Electricidad, Report of "Performance of El Infiernillo and La Villita Dams Including the Earthquake of March 14, 1979." pp. 87-108, February.

Seed, H. B., and Idriss, I. M. (1970). "Soil Moduli and Damping Factors for Dynamic Response Analysis." Earthquake Engineering Research Center, Report No. EERC 70-10, University of California, Berkeley, December.

Seed, H. B., Wong, R. T., Idriss, I. M., and Tokimatsu, K. (1984). "Moduli and Damping Factors for Dynamic Analyses of Cohesionless Soils." Earthquake Engineering Research Center,

Report No. EERC 84-14, University of California, Berkeley, September.

Seed, R. B., Bray, J. D., Boulanger, R. W., and Seed, H. B. (1989). "Seismic Response of the Puddingstone and Cogswell Dams in the 1987 Whittier Narrows Earthquake." Proc., CSMIP89 Seminar on Seismological and Engineering Implications of Recent Strong Motion Data, Sacramento, CA, pp. 7-1 through 7-10, May 9.

Shakal, A. F. and Ragsdale, J. T. (1984). "Acceleration, velocity and displacement noise analysis for the CSMIP accelerogram digitization system." Proc. 8th World Conference on Earthquake Engineering, Vol. 2, p. 111-118.

State of California (1986). Cogswell Dam, 32-5, Safety Review Report. Prepared by the Division of Safety of Dams, Department of Water Resources, State of California, June.

Yasuda, N. and Matsumoto, N. (1993). "Dynamic Deformation Characteristics of Sands and Rockfill Materials." Can. Geotech. J., Vol. 30, No. 5, Oct., pp. 747-757.